Master Thesis in Geographical Information Science nr 217

Environmental Determinants of Peatland Degradation in Central Kalimantan:

A GIS-Based Remote Sensing Analysis

Reneé Clarencia Hägglund

2026
Department of
Physical Geography and Ecosystem Science
Centre for Geographical Information Systems
Lund University
Sölvegatan 12
S-223 62 Lund
Sweden

Reneé Clarencia Hägglund (2026). ***Environmental Determinants of Peatland Degradation in Central Kalimantan: A GIS-Based Remote Sensing Analysis***

Master degree thesis, 30 credits in Geographical Information Science (GIS)
Department of Physical Geography and Ecosystem Science, Lund University

Environmental Determinants of Peatland Degradation in Central Kalimantan:

A GIS-Based Remote Sensing Analysis

Reneé Clarencia Hägglund

Master thesis, 30 credits, in Geographical Information Science

Supervisor:

Torbern Tagesson
Department of Physical Geography and Ecosystem Science.
Lund University

Acknowledgement

I would like to express my sincere gratitude to my supervisor, Torbern Tagesson, for his valuable guidance, constructive feedback, and continuous support throughout this thesis. His advice and encouragement greatly contributed to the completion of this work.

I would also like to thank Petter Pilesjö for his support and guidance during the development of this project.

I am also deeply grateful to David Tenenbaum for his continuous support, guidance, advice, and assistance throughout my years of study.

Special appreciation extended to Radjali Amin for his contribution of valuable information and important spatial data from Indonesia, and to Witono and Poppy for support and contribution on illustration and literature.

Finally, I would like to express my deepest gratitude to my husband Jan and my son Simon for their endless patience, encouragement, and support throughout this journey.

This work is dedicated to the memory of my late mother, Elisabeth, whose love, strength and spirit will always remain with me.

Abstract

Tropical peatlands in Central Kalimantan, Indonesia, represent important terrestrial carbon stores and support highly diverse tropical rainforest ecosystems with significant ecological, hydrological, and climatic functions. However, decades of drainage development, deforestation, plantation expansion, land-use change, and recurrent fire have contributed to extensive peatland degradation across the region. Large-scale hydrological disturbance following the Mega Rice Project initiated in the 1990s further accelerated peat drying, vegetation degradation, forest loss, and increased fire vulnerability. This study analysed peatland degradation in south-eastern Central Kalimantan between 2017 and 2025 using remote sensing and GIS-based spatial analysis. Satellite-derived indicators including the Normalized Difference Vegetation Index (NDVI), Normalized Difference Water Index (NDWI), VIIRS active fire detections, annual forest loss data, and supplementary Land Surface Temperature (LST) information were integrated with environmental variables related to hydrology, terrain, drainage infrastructure, and land use. Particular emphasis was placed on NDWI as a proxy indicator of peatland moisture conditions associated with hydrological disturbance. Spatial and statistical analyses were performed using Pearson correlation, hotspot analysis, Ordinary Least Squares (OLS), Geographically Weighted Regression (GWR), Random Forest (RF), and weighted spatial overlay techniques. The results showed that peatland degradation is spatially heterogeneous, with major degradation hotspots concentrated in the southern and central peatland regions where vegetation decline, moisture reduction, forest loss, and fire occurrence overlapped. Drainage-related variables, particularly proximity to drainage canals, consistently emerged as dominant factors influencing peatland moisture dynamics and degradation patterns, while Topographic Wetness Index (TWI) showed weaker and less consistent relationships. The findings further demonstrated that degradation processes vary spatially according to local environmental conditions and disturbance intensity rather than occurring uniformly across the peatland landscape. Although vegetation and moisture indicators showed relatively strong relationships, fire occurrence appeared to be influenced by additional climatic and anthropogenic factors beyond those included in the analysis. Overall, the study highlights the critical role of hydrological disturbance in tropical peatland degradation and emphasises the importance of long-term hydrological restoration and sustainable peatland management, particularly in heavily drained peatland areas. The integration of remote sensing, GIS, and spatial modelling techniques provides a useful framework for identifying degradation hotspots and supporting future peatland restoration and conservation strategies in tropical regions.

Keywords: geography, GIS, remote sensing, tropical peatlands, peatland degradation, drainage canals, hydrological disturbance, Central Kalimantan.

Abstrak

Lahan gambut tropis di Kalimantan Tengah, Indonesia, merupakan penyimpan karbon daratan yang penting serta mendukung ekosistem hutan hujan tropis dengan fungsi ekologis, hidrologis, dan klimatologis yang signifikan. Namun, pembangunan jaringan drainase, deforestasi, ekspansi perkebunan, perubahan penggunaan lahan, dan kebakaran berulang telah menyebabkan degradasi lahan gambut secara luas di wilayah tersebut. Gangguan hidrologis akibat Proyek Lahan Gambut Sejuta Hektar (Mega Rice Project) sejak tahun 1990-an semakin mempercepat pengeringan gambut, degradasi vegetasi, kehilangan hutan, dan meningkatnya kerentanan terhadap kebakaran. Penelitian ini menganalisis degradasi lahan gambut di bagian tenggara Kalimantan Tengah selama periode 2017–2025 menggunakan penginderaan jauh dan analisis spasial berbasis GIS. Indikator berbasis satelit, termasuk Normalized Difference Vegetation Index (NDVI), Normalized Difference Water Index (NDWI), deteksi titik api aktif VIIRS, data kehilangan hutan tahunan, serta informasi Suhu Permukaan Lahan (LST) yang digunakan sebagai indikator pendukung, diintegrasikan dengan variabel lingkungan yang berkaitan dengan hidrologi, topografi, drainase, dan penggunaan lahan. Penelitian ini menempatkan NDWI sebagai indikator proksi kondisi kelembapan gambut yang berkaitan dengan gangguan hidrologis. Analisis dilakukan menggunakan korelasi Pearson, analisis hotspot, Ordinary Least Squares (OLS), Geographically Weighted Regression (GWR), Random Forest (RF), dan teknik weighted spatial overlay. Hasil penelitian menunjukkan bahwa degradasi lahan gambut bersifat heterogen secara spasial, dengan hotspot utama terkonsentrasi di wilayah gambut bagian selatan dan tengah area penelitian. Wilayah tersebut menunjukkan tumpang tindih antara penurunan vegetasi, pengurangan kelembapan, kehilangan hutan, dan kejadian kebakaran. Variabel drainase, terutama kedekatan terhadap kanal drainase, secara konsisten menjadi faktor dominan yang memengaruhi dinamika kelembapan gambut dan pola degradasi, sementara Topographic Wetness Index (TWI) menunjukkan hubungan yang lebih lemah dan kurang konsisten. Hasil penelitian juga menunjukkan bahwa proses degradasi bervariasi sesuai kondisi lingkungan lokal dan intensitas gangguan. Meskipun indikator vegetasi dan kelembapan menunjukkan hubungan yang relatif kuat, kejadian kebakaran tampaknya dipengaruhi oleh faktor iklim dan aktivitas manusia lainnya di luar variabel yang dianalisis. Secara keseluruhan, penelitian ini menyoroti pentingnya gangguan hidrologis dalam degradasi lahan gambut tropis serta menekankan perlunya restorasi hidrologis jangka panjang dan pengelolaan lahan gambut berkelanjutan, terutama pada wilayah dengan drainase intensif. Integrasi penginderaan jauh, GIS, dan pemodelan spasial memberikan kerangka kerja yang berguna untuk mengidentifikasi hotspot degradasi dan mendukung strategi restorasi serta konservasi lahan gambut tropis di masa mendatang.

Kata kunci: geografi, GIS, remote sensing, lahan gambut tropis, degradasi lahan gambut, kanal drainase, gangguan hidrologis, Kalimantan Tengah.

Table of Contents

List of Figures

List of Tables

List of Abbreviations

AWS	Amazon Web Services
BRG	Badan Restorasi Gambut
BRGM	Badan Restorasi Gambut dan Mangrove
CO_2	Carbon dioxide
COP-DEM-GLO-30-DGED	Copernicus Digital Elevation Model Global 30 m DGED
DEM	Digital Elevation Model
ESA	European Space Agency
FIRMS	Fire Information for Resource Management System
GADM	Database of Global Administrative Areas
GFW	Global Forest Watch
GIS	Geographic Information System
GWR	Geographically Weighted Regression
KHG	Kesatuan Hidrologis Gambut
KHG-FEG	Kesatuan Hidrologis Gambut – Fungsi Ekosistem Gambut
KLHK	Kementerian Lingkungan Hidup dan Kehutanan
KDE	Kernel Density Estimation
LST	Land Surface Temperature
MDI	Mean Decrease Impurity
MRP	Mega Rice Project
NASA	National Aeronautics and Space Administration
NDVI	Normalized Difference Vegetation Index
NDWI	Normalized Difference Water Index
OLI/TIRS	Operational Land Imager / Thermal Infrared Sensor
OLS	Ordinary Least Squares
OOB	Out-of-Bag
QA	Quality Assessment
QA_PIXEL	Quality Assessment Pixel Band
RF	Random Forest
RMSE	Root Mean Square Error
R^2	Coefficient of Determination
SCL	Scene Classification Layer
TWI	Topographic Wetness Index
USGS	United States Geological Survey
VIIRS	Visible Infrared Imaging Radiometer Suite
WRI	World Resources Institute
WWF	World Wide Fund for Nature

1 INTRODUCTION

Tropical peatlands are wetland ecosystems formed through the long-term accumulation of partially decomposed organic material under waterlogged conditions (WWF Indonesia, 2009). The peat material mainly consists of plant remains, including trees, roots, and other organic matter that decompose slowly in saturated environments. Over thousands of years, this process forms thick peat deposits that store large amounts of organic carbon. Globally, tropical peatlands are mainly distributed across Southeast Asia, the Congo Basin, and parts of the Amazon, where they function as major carbon stores and important ecological systems (Page et al., 2011; Dargie et al., 2017).

Indonesia, located in Southeast Asia, contains one of the world's largest areas of tropical peatlands, covering approximately 13.4 million hectares mainly distributed across Sumatra, Kalimantan, and Papua (Anda et al., 2021). Although tropical peatlands occupy only a small proportion of the Earth's land surface, they play an important role in the global climate system due to their substantial carbon storage capacity (Page & Baird, 2016). In addition, tropical peatlands support high biodiversity and contribute to regional hydrological regulation by storing and gradually releasing water during wet and dry periods (Page & Baird, 2016). These ecosystems are therefore important for environmental stability, climate regulation, and local livelihoods.

Over recent decades, tropical peatlands across Southeast Asia, including Indonesia, have experienced extensive degradation caused by large-scale land-use change and hydrological disturbance (Mishra et al., 2021). In Central Kalimantan, extensive drainage canal construction, deforestation, agricultural expansion, and recurrent peat fires have significantly altered natural peatland hydrology (Page at al., 2009; Taufik et al., 2019). Much of this disturbance is associated with the Mega Rice Project (Choy & Onuma, 2025) initiated in the mid-1990s, which introduced large-scale drainage networks into peatland areas (Toumbourou et al., 2025). Lowering of the water table has increased peat drying, oxidation, carbon emissions, and fire vulnerability, resulting in long-term environmental impacts (Page et al., 2009; Taufik et al., 2019). Central Kalimantan was selected as the focus of this study because it represents one of the most heavily disturbed tropical peatland regions in Indonesia, where extensive drainage, recurrent fires, and land-use conversion have caused widespread peatland degradation (Page et al., 2009; Toumbourou et al., 2024). The region therefore provides an important case study for understanding peatland degradation processes in Southeast Asia.

Previous studies have identified drainage as a major driver of peatland degradation in Indonesia (Dadap et al., 2021; Salmayenti et al., 2025). Peatlands located closer to drainage canals or within areas of high canal density often experience stronger drying, vegetation stress, and increased fire susceptibility because drainage lowers water tables and creates drier peat conditions that are more vulnerable to burning and degradation (Sinclair et al., 2020; Dadap et al., 2021). In addition, peatland degradation does not occur uniformly across the landscape but varies spatially due to differences in hydrological conditions, drainage intensity, land-cover change, fire frequency, and local environmental characteristics (Sinclair et al., 2020; Mishra et al., 2021).

Peatland restoration efforts, including canal blocking and hydrological rewetting, have been implemented in parts of Central Kalimantan to reduce peat drying and fire risk (WWF Indonesia, 2009). However, due to the spatial variability of degradation processes, it remains difficult to identify priority areas for restoration and environmental management. Spatially explicit analyses are therefore needed to better understand how hydrological disturbance and environmental factors influence peatland degradation, including vegetation decline, moisture reduction, fire occurrence, and forest loss across the region.

Previous studies have examined various aspects of peatland degradation, including vegetation change, fire occurrence, carbon emissions, hydrological disturbance, and deforestation, using different datasets and analytical approaches (Miettinen et al., 2017; Mishra et al., 2021). However, fewer studies have integrated multiple satellite-derived indicators of vegetation condition, surface moisture, fire activity, and temperature together with drainage-related and terrain-based environmental variables within a single spatial framework to examine spatial variability in peatland degradation. In Central Kalimantan, the long-term spatial interactions between drainage networks, environmental conditions, and multiple peatland degradation indicators remain complex and require further investigation.

Tropical peatlands are large, environmentally sensitive, and often difficult to access, GIS and remote sensing provide effective tools for analysing long-term spatial patterns of peatland degradation. Remote sensing data provide spatially continuous observations that can be used to analyse vegetation condition and environment dynamics across large areas (Yan et al., 2025)

1.1 Aim

The aim of this thesis is to analyse how hydrological conditions, drainage patterns, terrain characteristics, and land-use pressures influence peatland degradation in Central Kalimantan between 2017 and 2025. Using remote sensing and GIS, the study maps vegetation stress, surface moisture changes, fire occurrence, and land surface temperature as indicators of peatland condition. By integrating these satellite-derived indicators with hydrological variables and spatial regression analyses, the study seeks to identify the environmental drivers of degradation and highlight areas that are most vulnerable. The results provide spatial evidence that can support peatland management, restoration planning, and climate mitigation efforts.

1.2 Research questions

1. *Spatial patterns:* Spatial patterns: Where are the major areas of peatland degradation, characterized by reduced vegetation greenness (Normalized Difference Vegetation Index, NDVI), reduced moisture conditions (Normalized Difference Water Index, NDWI), increased fire occurrence, forest loss, and increased land surface temperature (LST) in Central Kalimantan between 2017–2025?

2. Indicator relationships: How are satellite-derived indicators (NDVI, NDWI, fire occurrence, and LST) spatially related, and what do these relationships indicate about peatland degradation processes?

3. Environmental drivers: How do hydrological, terrain, and land-use factors including drainage proximity, canal density, elevation, slope, and topographic wetness index (TWI) explain spatial variation in peatland degradation indicators?

1.3 Hypotheses

H1: Hydrological variables, particularly drainage canal proximity and topographic wetness index (TWI) are the strongest predictors explaining spatial variation in satellite-derived peatland degradation indicators (NDVI, NDWI, fire occurrence, and LST).

H2: Relationship between peatland degradation indicators and environmental drivers vary spatially across the peatland area rather than occurring uniformly.

2 THEORETICAL BACKGROUND

2.1 Hydrology of tropical peatlands

Most tropical peatlands in Southeast Asia are raised peat domes that are predominantly rain-fed (ombrotrophic) and highly dependent on stable hydrological conditions (Apers et al., 2022; Ritzema, 2007; Page et al., 2006). These peatlands are mainly distributed in lowland region such as Central Kalimantan, Indonesia, although some ombrotrophic peatlands may also occur in tropical highland areas (Apers et al., 2022; Page at al., 2011). Unlike many temperate and boreal peatlands, tropical peatlands are commonly covered by dense peat swamp forest vegetation, including broadleaf evergreen species and palm-dominated ecosystems (Girkin et al., 2022).

Under natural conditions, peatland hydrology is largely regulated by precipitation inputs, evapotranspiration, and lateral water movement within peat soils, which together help maintain high water-table conditions (Mishra et al., 2021). Because tropical peatlands commonly form dome-shaped systems with strong lateral hydraulic connectivity, changes in water levels in one area may influence hydrological conditions across large portions of the peatland (Hooijer et al., 2010; Taufik et al., 2019). Water tables are normally maintained close to the peat surface, which helps preserve saturated conditions and limits peat decomposition (Morris & Waddington, 2011).

Tropical peatlands are highly sensitive to hydrological disturbance (Nguyen et al., 2016) particularly artificial drainage, which lowers water tables and increases peat drying (Apers et al., 2022), which can enhance peat oxidation, subsidence, vegetation degradation, and carbon loss (Hooijer et al., 2012; Ohkubo et al., 2021). Due to the lateral hydraulic connectivity of peat soils, drainage effects may propagate beyond the immediate canal area, lowering surrounding water tables and contributing to uneven spatial patterns of degradation across the peatland landscape (Sinclair et al., 2020).

As a result, peatland degradation often develops heterogeneously rather than uniformly. Variations in drainage intensity, vegetation cover, local hydrological conditions, and disturbance history contribute to strong spatial variability in peatland degradation patterns (Lampela et al., 2016; Taufik et al., 2019).

2.2 Peat dome structure and hydrological characteristics

Tropical peatlands in Central Kalimantan commonly occur as peat domes formed through the long-term accumulation of organic material under waterlogged conditions. These domes typically have greater peat thickness in their centre and gradually thin toward the margins (Page et al., 2011). Peat dome morphology plays a fundamental role in controlling peatland hydrology, nutrient distribution, and ecosystem functioning (Nguyen et al., 2016).

Under natural conditions, the water table remains close to the surface, limiting decomposition and supporting peat swamp forest vegetation (Page et al., 2006; Mishra et al., 2021). Water movement is typically slow and occurs laterally from the dome centre toward the margins (Page et al., 2006). Saturated conditions and water tables near the peat surface also reduce oxygen diffusion, causing decomposition to proceed slowly under anaerobic conditions (Morris and Waddington, 2011).

This hydrological configuration makes tropical peat domes highly sensitive to drainage disturbance (Saputra et al., 2026), particularly where drainage canals intersect or border peatland systems (Sinclair et al., 2020). Drainage lowers the water table locally but may also propagate drying across large portions of the peat dome due to the strong hydraulic connectivity of peat soils (Hooijer et al., 2010). Prolonged lowering of the water table can increase peat oxidation, subsidence, moisture loss, and vegetation stress.

These hydrological characteristics provide an important framework for understanding peatland drying and degradation processes in tropical peatland systems.

2.3 Drainage canals and peatland degradation

Drainage canals are widely recognized as a key driver of peatland degradation in tropical peatland system (Lampela et al., 2016; Ritzema, 2007). In Southeast Asia, drainage canals networks are commonly constructed to support agricultural expansion, plantation development, logging, and various land conversion activities (Page et al., 2011; Ritzema, 2007). These canals alter natural hydrology system by increasing water outflow and lowering groundwater levels, thereby disrupting the naturally saturated conditions required for peatland stability (Hooijer et al., 2010).

Lowering of the water table exposes peat to aerobic conditions, increasing peat oxidation and accelerating organic matter decomposition (Morris & Waddington, 2011; Hooijer et al., 2012). Prolonged drainage promotes peat drying, moisture decline, and land subsidence, particularly during the first years after drainage establishment (Hooijer et al., 2012; Ritzema et al., 2007). These hydrological changes reduce the capacity of peatlands to retain water and maintain ecological stability.

Due to the strong lateral hydraulic connectivity of tropical peat soils, the impacts of drainage are not restricted to areas immediately adjacent to canals. Drying effects may propagate across large portions of peat domes, extending hydrological disturbance far beyond canal margins (Hooijer et al., 2010; Astiani et al., 2017). Consequently, peatland degradation often develops heterogeneously across the landscape, with stronger drying conditions commonly observed closer to drainage features (Lampela et al., 2016; Taufik et al., 2019).

Field-based studies further demonstrate the substantial hydrological impact of drainage canals. In tropical peatlands, drainage has been shown to increase water table depth from approximately 11.7 cm to 37.3 cm below the peat surface, with drying effects extending up to 500 m from drainage canals (Astiani et al., 2017).

Lowering of the water table also alters peatland microclimatic conditions, including increased soil temperature and reduced moisture content, which together accelerate peat decomposition and increase vegetation stress (Hirano et al., 2009; Dadap et al., 2020). These changes may reduce tree biomass growth, alter forest structure, and decrease ecosystem resilience in degraded peatland landscapes (Astiani et al., 2017). In addition, prolonged drainage can increase CO_2 emissions and gradually transform peatlands from long-term carbon sinks into net carbon sources, thereby contributing substantially to greenhouse gas emissions (Hooijer et al., 2012; Leifeld et al., 2019).

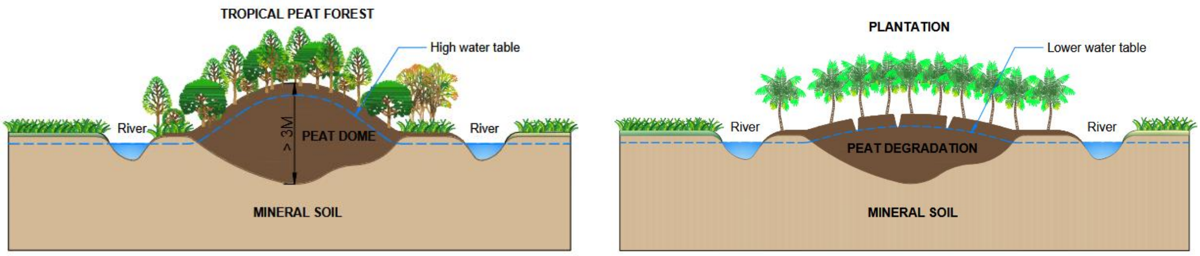

Figure 2.1. Conceptual illustration of tropical peatland degradation following drainage canal construction and land-use conversion (adapted from GRID-Arendal, 2024).

Figure 2.1. illustrates the transition from intact peat dome conditions to drained peatland systems following drainage canal construction and land-use conversion. The figure highlights the lowering of the water table and associated peat drying processes within tropical peatland landscapes.

2.4 Deforestation and land-use change in tropical peatlands

Peatland forest cover in Southeast Asia declined from 76% to 29% between 1990 and 2015 (Mishra et al., 2020). During the early 2000s, deforestation rates in insular Southeast Asia were among the highest globally (Miettinen et al., 2011), with continued peatland conversion occurring in subsequent decades (Miettinen et al., 2016; Horton et al., 2021). In Kalimantan, major drivers of peatland deforestation include agricultural expansion, plantation development, infrastructure growth, and timber harvesting to meet both local and global demands (Curran et al., 1999; Astiani et al., 2017). Large areas of peat swamp forest have been converted to oil palm plantations, pulpwood plantations, and smallholder agricultural land, particularly in Indonesia and Malaysia (Gaveau et al., 2014; Miettinen et al., 2016; Simorangkir, 2007).

Deforestation contributes directly to peatland degradation through the removal of forest cover that helps regulate microclimatic conditions and maintain moist surface environment. Previous studies have shown that disturbance to forest canopy cover can alter peatland microclimatic and hydrological conditions, increasing vulnerability to drying and degradation (Mishra et al., 2021; Choy & Onuma, 2025). Vegetation loss increases solar exposure, raises surface temperatures, and accelerates peat drying, oxidation, and subsidence (Page et al., 2011; Miettinen et al., 2017). In many tropical peatland regions, deforestation is also closely associated with drainage canal construction and land conversion activities, which further intensify hydrological disturbance and ecosystem degradation.

Drained and deforested peatlands are generally more accessible and more vulnerable to repeated disturbance, contributing to continued environmental degradation across peatland landscapes (Field et al., 2016). Understanding these land-use processes is therefore important for interpreting spatial patterns of peatland degradation.

2.5 Anthropogenic disturbance and drainage development in Central Kalimantan

Large-scale peatland disturbance in Central Kalimantan intensified during the Mega Rice Project (MRP) initiated in 1996 (Novitasari et al., 2018; Horton et al., 2021). The project aimed to convert approximately one million hectares of peat swamp forest into rice cultivation areas through the construction of extensive drainage canal networks (Page et al., 2009). These canals rapidly lowered groundwater levels and disrupted the natural hydrological conditions of tropical peat domes.

Although the Mega Rice Project ultimately failed due to unsuitable peat soil conditions and hydrological instability, the drainage infrastructure remained across large parts of the landscape. The lowered water tables contributed to peat oxidation, land subsidence, increased fire vulnerability, and widespread forest degradation (Page et al., 2009; Taufik et al., 2019). Following the collapse of the project, many drained peatland areas were gradually converted into oil palm plantations, acacia pulpwood plantations, and smallholder agricultural land (Gaveau et al., 2014; Austin et al., 2019).

Remote sensing studies have shown that forest loss in Central Kalimantan is strongly associated with drainage canal proximity, logging activities, and plantation expansion (Austin et al., 2019; Gaveau et al., 2022; Horton et al., 2021). Between 2001 and 2023, extensive peatland forest loss was documented across southern Central Kalimantan, particularly within former Mega Rice Project regions (Global Forest Watch, 2024). Recurrent peat fires, many of which are associated with human land-clearing activities and increased accessibility provided by drainage canals, have further reinforced degradation processes by creating feedback between drainage, peat drying, vegetation loss, and burning (Field et al., 2016). In the ex-Mega Rice Project area, Horton et al. (2021) found that fire occurrence was strongly associated with anthropogenic factors, particularly proximity to settlements and drainage canals, highlighting the importance of land accessibility and human disturbance in controlling peatland fire distribution. Drainage-related peat drying has also been identified as an important factor increasing peatland fire susceptibility in Indonesian peatlands (Ruwaimana et al., 2024).

In response to severe peatland fire events, Indonesia established the Peatland Restoration Agency (*Badan Restorasi Gambut*, BRG) in 2016 to coordinate peatland restoration and rewetting initiatives. The agency was later expanded into the Peatland and Mangrove Restoration Agency (*Badan Restorasi Gambut dan Mangrove*, BRGM). Restoration strategies include canal blocking, hydrological rewetting, revegetation, and fire prevention measures aimed at reducing peatland degradation and fire risk. Despite these interventions, legacy drainage infrastructure and ongoing plantation expansion continue to influence peatland hydrology and environmental degradation across Central Kalimantan (Taufik et al., 2019; BRGM, 2026).

2.6 Fire, climate variability in tropical peatland

Fire is a major disturbance process in tropical peatlands and plays a central role in peatland degradation in Southeast Asia, where peatland carbon dynamics are strongly influenced by the balance between peat accumulation and peat loss (Page et al., 2002; Field et al., 2016; Ruwaimana et al., 2024). Unlike fires in mineral soil forests, peat fires can burn both above and below the ground surface. Once ignited, peat can smoulder for extended periods due to its high carbon content, porous structure, and low moisture conditions, making fires difficult to detect and extinguish (Page et al., 2009; Sinclair et al., 2020; Grosvenor et al., 2024). Because combustion may continue beneath the surface even during intermittent rainfall, peat fires often persist longer than surface vegetation fires and can affect extensive areas of peatland ecosystems (Grosvenor et al., 2024).

The occurrence of peatland fire is strongly influenced by the interaction between climatic variability and human activities. In Indonesia, fire is commonly associated with land-clearing practices related to agricultural expansion, plantation development, and smallholder farming activities (Field et al., 2009; Goldstein et al., 2020). Oil palm expansion has been identified as one of the major direct drivers of forest conversion in Indonesia, accounting for approximately one-third of old-growth forest loss between 2001 and 2019 (Gaveau et al., 2022). Fires are frequently intentionally ignited to clear vegetation because burning is considered a rapid and inexpensive land preparation method (Simorangkir, 2007). Under dry conditions, however, these fires can spread uncontrollably into surrounding peatland areas (Ruwaimana et al., 2024; Simorangkir, 2007). Hydrological disturbance substantially increases peatland fire susceptibility by reducing moisture retention and increasing forest vulnerability to burning (Cochrane, 2003; Taufik et al., 2019). Artificial drainage lowers the groundwater table, reduces peat moisture content, and exposes deeper peat layers to oxidation and ignition (Hooijer et al., 2010; Taufik et al., 2019). Declining water levels also reduce conditions necessary for peat accumulation and may accelerate peat decomposition and carbon loss (Ruwaimana et al., 2024).

Drained peatlands therefore become considerably more flammable compared to intact peat swamp forests. Previous studies have shown that fire occurrence is often concentrated near drainage canals, roads, deforested regions, plantation areas, and other accessible disturbed landscapes, reflecting the combined influence of hydrological alteration and human accessibility (Konecny et al., 2016; Goldstein et al., 2020; Gaveau et al., 2022). Recent large-scale analyses further demonstrate that fire occurrence increases significantly with drainage density, particularly in disturbed tropical peatland systems (Salmayenti et al., 2025).

Central Kalimantan has a humid tropical climate characterized by high annual rainfall, relatively stable temperatures, and a seasonal dry period typically occurring between July and September (Aldrian & Susanto, 2003). During El Niño years, reduced precipitation and prolonged drought conditions can substantially lower peat moisture content, increase peat drying, and create favourable conditions for fire ignition and spread across tropical peatlands (Field et al., 2016; Ruwaimana et al., 2024; Grosvenor et al., 2024; Hirano et al., 2024).

Severe fire events in Indonesia, including those in 1997, 2015, and 2019, have been closely associated with ENSO-related drought conditions (Wooster et al., 2012; Field et al., 2016;

Grosvenor et al., 2024). The 2015 peatland fire event alone released an estimated 0.89–1.75 Gt CO_2 equivalent into the atmosphere, contributing substantially to global greenhouse gas emissions (Field et al., 2016).

Repeated burning can further accelerate peatland degradation by removing vegetation cover, reducing peat thickness, altering surface characteristics, and disrupting ecological functioning (Page et al., 2011; Turetsky et al., 2015). Fire therefore acts both as a driver and a consequence of peatland degradation, interacting closely with drainage, deforestation, land-use change, and climatic variability within tropical peatland landscapes. Severe peat fires may remove peat accumulated over long time periods and contribute substantially to carbon emissions from tropical peatlands (Ruwaimana et al., 2024).

2.7 Remote sensing indicators of peatland condition

Remote sensing and GIS provide effective approaches for monitoring peatland conditions across large spatial scales, particularly in tropical regions where field observations are often limited (Kamlun & Phua, 2024). Satellite-derived indicators can be used to assess vegetation condition (Yan et al.,2025), surface moisture, thermal characteristics, land-cover change, and fire activity, which are important components of peatland degradation processes. In tropical peatlands, remote sensing techniques have been widely applied to detect vegetation disturbance, peat drying, land-cover change, and fire occurrence associated with hydrological alteration and anthropogenic activities (Kamlun & Phua, 2024; Mishra et al., 2021).

In this study, peatland degradation is defined as the deterioration of peatland ecological and hydrological functions resulting from drainage, deforestation, land-use change, and recurrent fire. Peatland degradation was assessed using multiple satellite-derived indicators representing different dimensions of ecosystem condition. NDVI, NDWI, and forest loss were treated as primary indicators of vegetation condition. Fire occurrence was included as an indicator of disturbance because recurrent peat fires are both a manifestation and a driver of peatland degradation. Land Surface Temperature (LST) was included as a supplementary environmental indicator reflecting thermal responses associated with peat drying, vegetation loss, and hydrological disturbance. Consequently, LST is interpreted primarily as an environmental response to degradation processes rather than as a direct measure of peatland degradation itself.

2.7.1 Normalized Difference Vegetation Index (NDVI)

The Normalized Difference Vegetation Index (NDVI) is widely used to assess vegetation greenness, biomass, and vegetation condition using the contrast between near-infrared and red spectral reflectance (Rouse et al., 1974; Pettorelli et al., 2005). Higher NDVI values generally indicate dense and healthy vegetation, whereas lower values may reflect vegetation stress, degradation, deforestation, or disturbance (Pettorelli et al., 2005). In tropical peatlands, reductions in NDVI can indicate vegetation loss associated with drainage, fire, land conversion, and declining ecosystem condition.

2.7.2 Normalized Difference Water Index (NDWI)

The Normalized Difference Water Index (NDWI) is widely used to represent vegetation and surface moisture conditions and is sensitive to changes in vegetation water content (Gao, 1996). In tropical peatlands, moisture availability plays an important role in maintaining peat stability and regulating decomposition and fire susceptibility (Page & Baird, 2016). Lower NDWI values generally indicate reduced vegetation moisture and drier surface conditions, whereas higher values reflect greater vegetation water content (Gao, 1996). Prolonged drying can increase peat oxidation, subsidence, and vulnerability to fire, making NDWI a useful indicator for monitoring hydrological conditions and peatland degradation processes.

2.7.3 Land Surface Temperature (LST)

Land Surface Temperature (LST) provides information on surface thermal conditions and energy exchange processes (Weng, 2009). Deforestation and drainage disturbances can alter evapotranspiration and hydrological functioning in tropical peatlands, contributing to enhanced drying and degradation processes (Treby et al., 2024). Drained and disturbed tropical peatlands often exhibit altered surface energy balance and drying associated with vegetation loss and hydrological disturbance (Dommain et al., 2010; Treby et al., 2024). Drained and deforested peatlands often exhibit higher surface temperatures compared to intact peat swamp forests due to reduced canopy cover and lower moisture content (Dommain et al., 2010; Hirano et al., 2024). Although temperature variation in equatorial regions is generally smaller than in temperate regions, spatial differences in LST can still provide useful information on environmental disturbance and drying patterns. In this study, LST was used as a supplementary indicator of thermal responses associated with peatland degradation and environmental change rather than as a direct measure of peatland degradation itself.

2.7.4 Fire occurrence (VIIRS)

Fire occurrence represents an important indicator of peatland disturbance and degradation. Active fire detections derived from the Visible Infrared Imaging Radiometer Suite (VIIRS) provide near-daily observations of thermal anomalies associated with biomass burning and peat fires (Schroeder et al., 2014; Giglio et al., 2016). In tropical peatlands, fire occurrence is closely linked to drainage, drought conditions, land-cover change, and human activities (Field et al., 2016). Because peat fires are strongly associated with degraded and drained peatlands, VIIRS fire detections can provide useful information for identifying spatial patterns of disturbance and fire-prone areas.

2.8 Environmental drivers of peatland degradation

Peatland degradation is controlled by several interacting environmental and human-induced drivers that influence hydrology, vegetation condition, surface moisture, and disturbance intensity. In tropical peatlands, hydrological conditions are particularly important because high water tables limit peat decomposition, while water table lowering exposes peat to oxygen and accelerates oxidation and carbon loss (Morris & Waddington, 2011; Hooijer et al., 2012). Therefore, variables related to drainage, terrain, and forest loss are important for understanding spatial variation in peatland degradation.

The indicator framework adopted in this study differs from the standard UNCCD Good Practice Guidance for SDG Indicator 15.3.1, which assesses land degradation using land cover change, land productivity, and soil organic carbon. However, several indicators used in this thesis are conceptually related to this framework. Forest loss corresponds to land cover change, while NDVI provides information related to vegetation productivity. Because direct measurements of soil organic carbon were unavailable, the study focused on peatland moisture conditions represented by NDWI, which provide information on hydrological degradation processes that are particularly important in tropical peatland ecosystems. Additional indicators including fire occurrence and drainage-related variables were incorporated to capture peatland-specific degradation processes that are not explicitly represented within the SDG 15.3.1 framework. This approach therefore complements established land degradation assessments while addressing the unique characteristics of tropical peatlands.

Drainage proximity and canal density are key drivers of peatland degradation. Drainage canals lower groundwater levels and increase water outflow from peatland areas, leading to peat drying, oxidation, subsidence, and increased carbon emissions (Hooijer et al., 2010; Hooijer et al., 2012; Dadap et al., 2021). Dadap et al. (2021) showed that drainage canals are widespread across Southeast Asian peatlands and that drainage density provides important information for explaining peat subsidence and emissions. Areas closer to canals are often more strongly affected by drying because canal impacts can extend into the surrounding peatland (Astiani et al., 2017). Higher canal density may therefore indicate stronger hydrological disturbance and greater degradation risk.

Terrain characteristics can also influence peatland moisture patterns. Elevation and slope affect water movement, drainage direction, and local water accumulation. Although tropical peatlands often have low relief, small topographic differences can influence hydrological gradients and water-table variation. In peat dome systems, water generally moves laterally from the dome centre toward the margins, and microtopographic differences can create spatial variation in wetness conditions (Lampela et al., 2016). These local differences may affect vegetation condition, peat moisture, and degradation vulnerability.

The Topographic Wetness Index (TWI) is commonly used as a terrain-based indicator of potential moisture accumulation and soil moisture distribution (Kopecký et al., 2021). Higher TWI values generally represent areas with greater potential for water accumulation, while lower values may indicate relatively drier or better-drained conditions. In peatland environments, TWI can provide useful information on relative wetness, although it may not fully capture artificial drainage effects caused by canals (Morris & Waddington, 2011). Therefore, TWI is best interpreted together with drainage variables such as canal proximity and canal density.

Forest loss is another important driver of peatland degradation. Removal of forest cover reduces shading, increases surface exposure, and alters local microclimatic and hydrological conditions, contributing to enhanced peat drying and degradation processes (Dommain et al., 2010; Page et al., 2011). Deforested peatlands may experience higher surface temperatures, reduced moisture retention, and greater vulnerability to drying and fire (Dommain et al., 2010). In Southeast Asian peatlands, forest loss has been strongly associated with plantation expansion, drainage, and land-use conversion (Miettinen et al., 2016). Gaveau et al. (2022) also showed that oil palm expansion has been a major driver of forest conversion in Indonesia, including in Kalimantan.

Together, drainage, terrain conditions, and forest loss influence peatland degradation by altering moisture availability, vegetation condition, and disturbance intensity. These drivers do not act independently but interact across the landscape, creating spatially heterogeneous degradation patterns. This makes them important explanatory variables for analysing variation in peatland moisture decline and degradation processes.

2.9 Spatial statistical and machine learning approaches

Spatial statistical and machine learning approaches are useful for analysing relationships between peatland degradation indicators and environmental drivers. These methods can help identify whether degradation patterns are explained by hydrological, terrain, and land-use variables, and whether these relationships are spatially uniform or vary across the landscape.

Ordinary Least Squares (OLS) regression is a global regression approach used to examine relationships between a dependent variable and a set of explanatory variables across a study area (Majid & Bilal, 2018). In spatial environmental studies, OLS can provide an initial understanding of which environmental variables are statistically associated with degradation indicators. However, OLS assumes that relationships between variables remain spatially constant across space, which may be insufficient for environmentally heterogeneous landscapes such as tropical peatlands (Majid & Bilal, 2018).

Spatial autocorrelation refers to the tendency for nearby locations to exhibit similar values or characteristics rather than being randomly distributed across space (Fotheringham et al., 2002). Moran's I is commonly used to evaluate whether spatial patterns are clustered, dispersed, or random and can also be applied to regression residuals to assess whether unexplained spatial structure remains after modelling (Esri, 2024). In addition, the Koenker (Breusch–Pagan) statistic is used to evaluate whether relationships between explanatory variables and the dependent variable remain stable across the study area. Significant Moran's I and Koenker statistics may indicate spatial non-stationarity, suggesting that relationships vary geographically and that local regression approaches may be more appropriate for analysing spatial environmental processes (Fotheringham et al., 2002).

Geographically Weighted Regression (GWR) is a local regression technique designed to address spatial non-stationarity by estimating separate local regression coefficients for each location, allowing relationships between variables to vary spatially rather than assuming a single global relationship (Brunsdon et al., 1996; Comber et al., 2023). This makes GWR particularly useful for peatland degradation studies, where the influence of drainage, terrain, vegetation, and land-use factors may differ according to local environmental conditions and disturbance intensity. Because GWR produces location-specific parameter estimates, the results can be mapped and interpreted spatially to identify areas where environmental drivers exert stronger or weaker influence across the landscape (Matthews & Yang, 2012).

Hotspot analysis is another spatial statistical approach used to identify areas where high or low values are spatially concentrated. The Getis-Ord Gi* statistic is commonly used to identify statistically significant hotspots and cold spots within spatial datasets (Getis & Ord, 1992). The method uses z-scores and p-values to determine whether clusters of high or low values differ significantly from random spatial patterns (Esri, 2024). In environmental studies, hotspot analysis is useful for identifying areas with concentrated disturbance patterns such as fire occurrence and environmental degradation (Manepalli et al., 2011). In peatland studies, hotspot analysis can help identify areas with recurring fire occurrence and spatially concentrated degradation patterns.

Random Forest (RF) is an ensemble machine-learning method that combines multiple decision trees to improve prediction accuracy and reduce model variance (Breiman, 2001). RF can model complex and non-linear relationships and interactions between predictor variables and response variables without assuming linearity, making it useful for analysing environmental drivers that may not have simple linear relationships with peatland degradation indicators. In this study, Random Forest regression was used to investigate the relative importance of environmental variables influencing peatland moisture change, represented by NDWI slope. Predictor variables included drainage-related, terrain, and land-use factors such as distance to canals, canal density, topographic wetness index (TWI), forest loss, and canal-block proximity. In addition to predictive modelling, RF provides variable importance measures that can be used to evaluate the relative contribution of environmental variables to model performance (Louppe et al., 2013). One of the most commonly used importance metrics is Mean Decrease in Impurity (MDI), which is based on the reduction of node impurity contributed by each predictor variable across the ensemble of decision trees (Scornet, 2021). Model performance can be evaluated using measures such as coefficient of determination (R^2), root mean square error (RMSE), and out-of-bag (OOB) error, which provide information on explanatory power and prediction error.

Together, OLS, Moran’s I, Koenker diagnostics, GWR, and Random Forest provide complementary approaches for understanding peatland degradation. OLS provides a global overview, Moran’s I and Koenker diagnostics indicate whether spatial effects are present, GWR examines local variation in relationships, and Random Forest helps identify important drivers and potential nonlinear patterns.

3 STUDY AREA

3.1 Geographic location

Figure 3.1 shows the location and peatland extent of the study area in south-eastern Central Kalimantan, Indonesia. The study area is located approximately between 113°E–116°E longitude and 2°S–3°S latitude and covers approximately 23,155 km², of which peatlands account for approximately 11,523 km² (49.8%) based on peatland delineation derived from the KHG dataset (KLHK, 2026).

The study area forms part of the broader tropical peatland landscape of Central Kalimantan and is dominated by lowland peat swamp ecosystems characterized by extensive peat swamp forests and large peat dome systems that are highly sensitive to hydrological disturbance (Page et al., 2006; Lampela et al., 2016). In addition to relatively intact peat swamp forest, the landscape also contains extensive drainage canal networks and areas affected by land-use change, plantation expansion, and recurrent fire events (Page et al., 2009; Ritzema, 2007). Over recent decades, these disturbances have altered large portions of the peatland environment, resulting in a heterogeneous landscape consisting of degraded vegetation, agricultural land, disturbed peatlands, and remnant peat swamp forest.

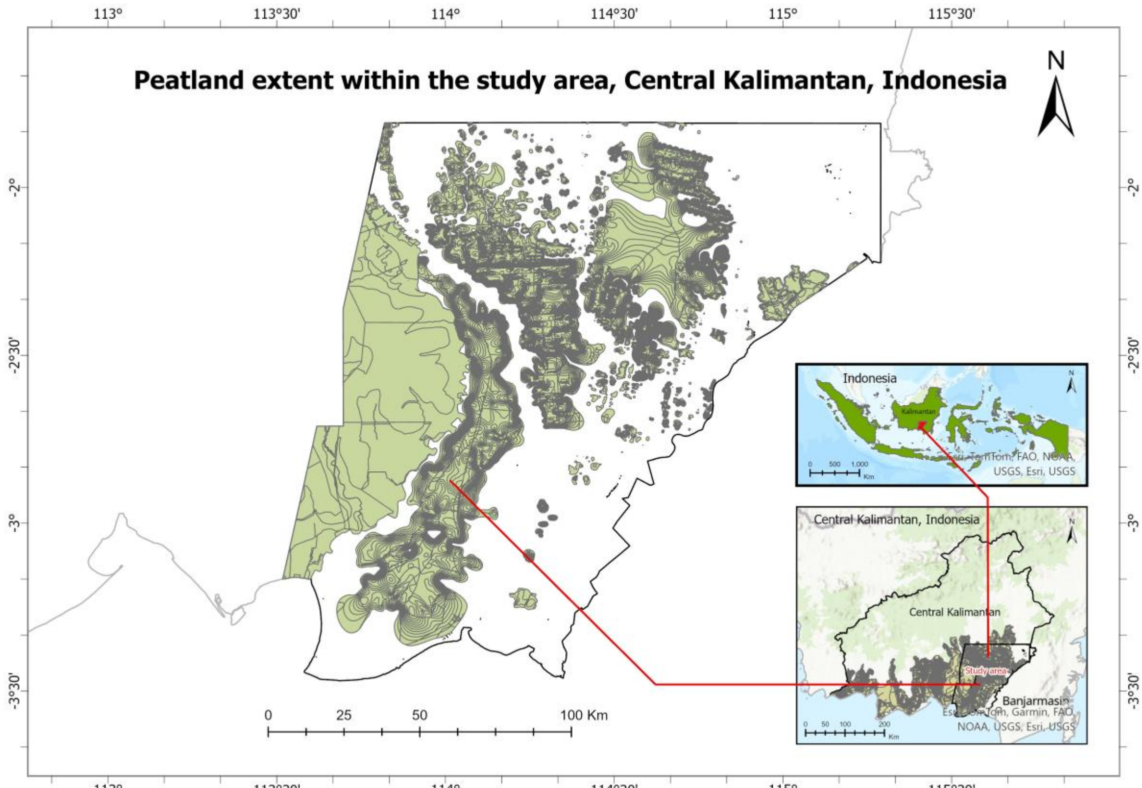

Figure 3.1. Location and peatland extent of the study area in Central Kalimantan, Indonesia. The inset map shows the location of the study area within Indonesia
Source: Peatland data from KLHK (KHG-FEG 2026). Administrative boundaries from GADM (2023). Basemap: Esri, TomTom, Garmin, USGS (accessed 2026).

Peatland areas are concentrated primarily within the southern lowland areas, where low elevation, extensive drainage infrastructure, and seasonal drying contribute to increased vulnerability to peat drying and fire occurrence (Taufik et al., 2019; Ruwaimana et al., 2024). The area experiences a humid tropical climate with high annual rainfall and a seasonal dry period typically occurring between July and September (Aldrian & Susanto, 2003).

These environmental conditions make the study area highly suitable for investigating spatial variation in peatland degradation and moisture dynamics.

4 DATA AND METHODOLOGY

4.1 Methodological workflow

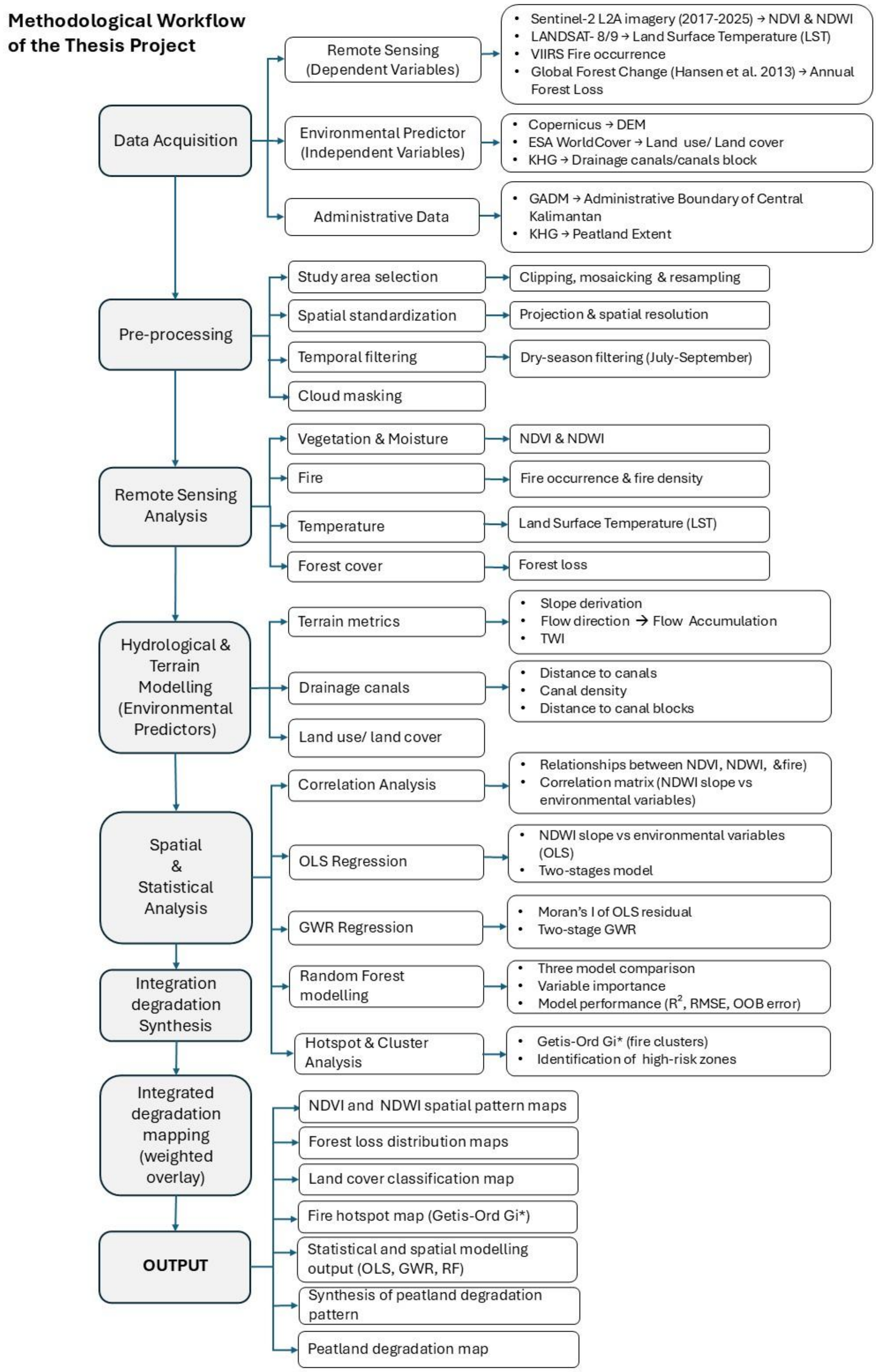

Figure 4.1. Detailed Methodological workflow.

4.2 Data sources

This study integrated satellite remote sensing data, terrain data, and vector datasets describing peatland extent, drainage infrastructure, forest loss, and land cover to analyse spatial pattern of peatland degradation in Central Kalimantan.

4.2.1 Satellite data

Satellite imagery from Sentinel-2 and Landsat platforms was used to analyse peatland environmental conditions between 2017-2025. To improve temporal consistency and minimise seasonal effects, dry-season imagery acquired between July and September was selected, as this period generally has lower rainfall and reduced cloud cover in Central Kalimantan (Aldrian & Susanto, 2003).

Multispectral satellite imagery from Sentinel-2, provided by the European Space Agency (ESA), was downloaded through the Copernicus Open Access Hub (ESA, 2026a). Sentinel-2 provides optical imagery with a spatial resolution of 10–20 m and a revisit frequency of five days at the Equator (ESA, 2026a). During image selection, scenes with cloud cover between 0–40% were used. Multiple images acquired between July and September each year from 2017 to 2025 were used in this study *(Appendix A1).* Annual NDVI and NDWI composite layers were generated from the selected imagery. Cloud and cloud-shadow masking were applied during preprocessing using the Scene Classification Layer (SCL), as described in Section 4.3.2.

Land Surface Temperature (LST) was derived from Landsat 8–9 Operational Land Imager/Thermal Infrared Sensor (OLI/TIRS) Collection 2 Level-2 data obtained from the United States Geological Survey (USGS) EarthExplorer platform (USGS, 2026). The LST has a spatial resolution of 30 m. Dry-season imagery acquired between July and September during 2017–2025 was used to improve temporal consistency and minimise seasonal variability. Scenes with cloud cover greater than 30% were excluded during image selection. Annual LST layers were generated from the selected Landsat imagery and subsequently used to derive both mean LST and LST temporal trends. The Quality Assessment (QA_PIXEL) band included in the Collection 2 Level-2 dataset was used to identify and exclude cloud, cloud-shadow, and other low-quality pixels. Landsat provides a long historical record and thermal infrared bands suitable for estimating surface temperature, which is a relevant indicator of peatland drying and degradation.

Fire activity data was derived from active fire detections obtained from VIIRS downloaded via the NASA Fire Information for Resource Management System (FIRMS) (NASA, 2026). VIIRS detects thermal anomalies associated with active fires at approximately 375 m spatial resolution and provides near-daily observations for the period 2017–2025. Low-confidence detections were removed using attribute filtering, and only detections classified as high confidence (“h”) were retained for analysis to improve detection reliability. All VIIRS active fire detections occurring within the peatland study area were included. No additional filtering was applied to distinguish vegetation fires from other fire types.

Forest-loss data were obtained from the Hansen Global Forest Watch (GFW) platform provided by the World Resources Institute (WRI), based on the Hansen Global Forest Change dataset (Hansen et al., 2013; version 2024 v1.12). The dataset provides annual forest-loss information for the period 2001–2024 at a spatial resolution of approximately 28 m (Hansen et al., 2013; Global Forest Watch, 2026). Because forest-loss data for 2025 were not available at the time of analysis, the most recent available dataset (2024) was used.

4.2.2 Terrain data

Terrain data were derived from the Copernicus Digital Elevation Model (DEM) Global Coverage dataset (COP-DEM-GLO-30-DGED), provided through the Copernicus Programme and accessed via the Amazon Web Services (AWS) Open Data Registry (ESA, 2026b). The DEM has a spatial resolution of 30 m and was used as the basis for terrain analysis in this study.

4.2.3 Peatland hydrological data

Peatland hydrological unit (*Kesatuan Hidrologis Gambut*) data were provided by the Directorate of Peat Ecosystem Protection and Management, Ministry of Environment and Forestry (KLHK), Indonesia (KHLK, 2026). The dataset classifies land based on peat depth, where non-peatland areas contain mineral soils or land with peat depths of 0-0.5 m, while peatland areas contain peat soils with peat depth greater than 0.5 m (KHLK, 2026).

The broader study area included both peatland and non-peatland environments. However, the main statistical and spatial modelling analyses were restricted to mapped peatland areas because peatlands differ substantially from surrounding mineral soil landscapes in their hydrological and ecological characteristics, which could otherwise influence the modelling results. Some descriptive maps and visualisations were nevertheless produced for the broader study area to provide environmental context and illustrate regional spatial patterns.

Drainage canal and canal block datasets were provided by Peatland and Mangrove Restoration Agency (BRGM), Indonesia (BRGM, 2026). The dataset includes the spatial distribution of drainage canals and canal-blockings structures within the peatland area (*Appendix A2)*. The datasets were obtained through academic collaboration and were provided for research purposes in this study (R. Amin, personal communication, 2026).

4.2.4 Land-use/land cover data

Land-cover information was obtained from the ESA WorldCover 2021 dataset, provided by the European Space Agency (ESA), with a spatial resolution of 10 m (ESA, 2021). The dataset provides a standardized global land-cover classification derived from Sentinel-1 and Sentinel-2 satellite imagery and includes 11 land-cover classes.

Within the tropical peatland study area, nine land-cover classes were present: tree cover, shrubland, grassland, cropland, built-up areas, bare or sparse vegetation, permanent water bodies, herbaceous wetlands, and mangroves *(Figure 4.2).* Detailed information on the proportional coverage of each original ESA WorldCover class is provided in *Appendix A3.*

The dataset was used to characterize environmental conditions within the study area and served as the basis for the land-cover reclassification described in Section 4.4.6.

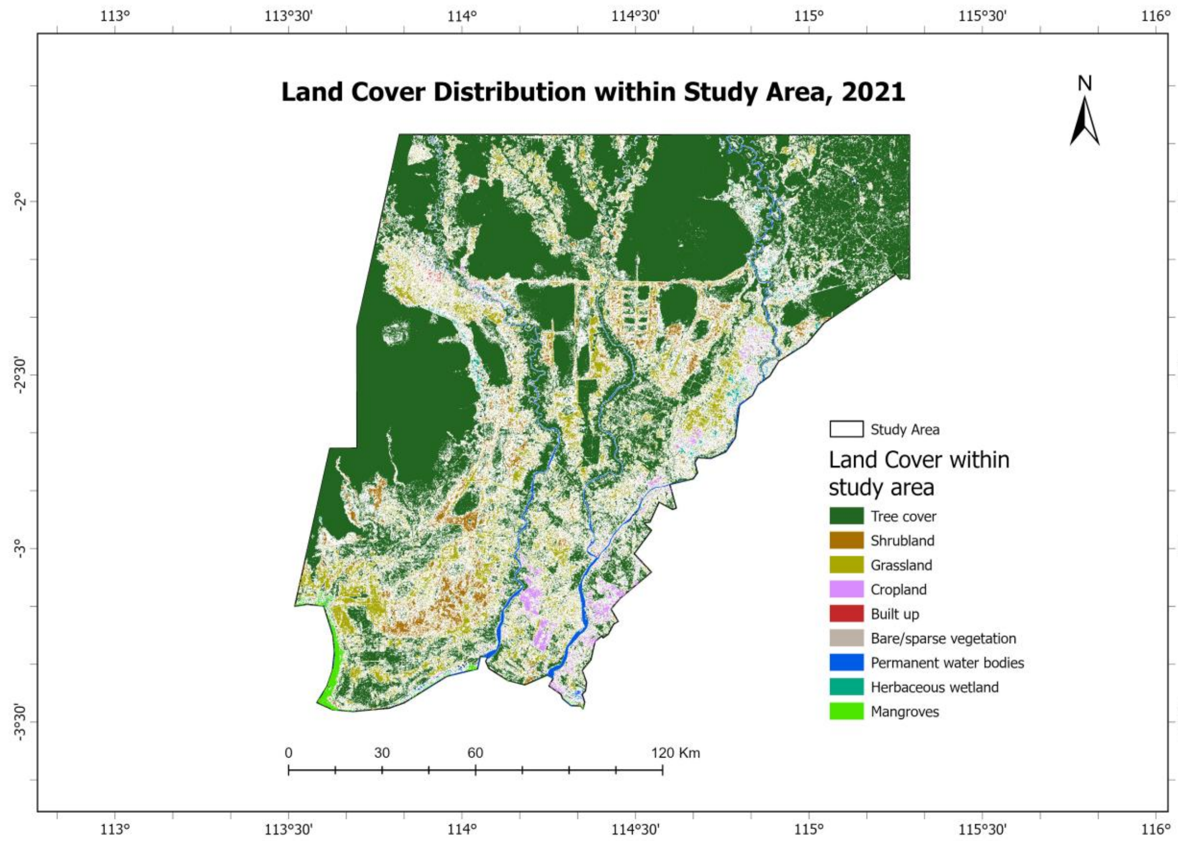

Figure 4.2. Land-Cover distribution within the study area in 2021 based on ESA WorldCover data.

4.3 Data preprocessing and indicator generation

4.3.1 Spatial data preprocessing

Selected satellite imagery covering the study area was mosaicked, reprojected to WGS 1984 UTM Zone 49S, and clipped to the study area boundary. Datasets were subsequently clipped using the peatland mask. Continuous raster datasets were resampled using bilinear interpolation, whereas categorical datasets such as land cover were resampled using nearest neighbour interpolation during reprojection to ensure spatial consistency among datasets. Spatial resolution varied depending on the original dataset and analytical purpose. Resampling was primarily applied to analyses related to NDWI slope. A summary of the spatial resolution and temporal coverage of derived variables is provided in *Appendix A4*.

4.3.2 Vegetation and moisture indices (NDVI and NDWI)

Vegetation condition was assessed using NDVI, calculated at 10 m spatial resolution from Sentinel-2 imagery as:

$$\text{NDVI} = \frac{B8-B4}{B8+B4}$$

Where B8 is the near-infrared band (NIR) and B4 is red band of Sentinel-2 imagery.

Surface moisture conditions were assessed using NDWI, calculated at 20 m spatial resolution as:

$$\text{NDWI} = \frac{B8A - B12}{B8A + B12}$$

Where B8A is narrow near-infrared band and B12 is the shortwave infrared (SWIR) band of Sentinel-2 imagery.

Annual NDVI composite layers were generated using the maximum value of cloud-filtered Sentinel-2 scenes acquired between July and September for each year of the study period to represent peak vegetation greenness conditions. In contrast, annual NDWI composite layers were generated using the mean value of cloud-filtered Sentinel-2 scenes to represent average surface moisture conditions.

Temporal trends in NDVI and NDWI were calculated using a pixel-wise linear trend analysis applied to the annual composite layers between 2017 and 2025. The slope was calculated in Raster Calculator using the standard least-squares slope formula:

$$\text{Slope} = \frac{(n\sum(t_i\, x_i) - (\sum t_i)(\sum x_i)}{(n\sum(t_i{}^2) - (\Sigma \text{t}_\text{i})^2}$$

where $x_i$represents the annual NDVI or NDWI raster value for year i, $t_i$represents the corresponding year, and n is the number of annual observations ($n = 9$) for the period 2017–2025. The resulting slope represents the average annual rate of change in NDVI or NDWI over the study period.

Positive slope values indicate increasing vegetation greenness or moisture conditions, whereas negative slope values indicate declining vegetation greenness or moisture conditions. The trend calculation includes an intercept and therefore does not constrain the fitted relationship to pass through the origin. In this study, NDVI and NDWI slopes were interpreted as indicators of vegetation and moisture change rather than direct measures of peatland degradation. Potential degradation patterns were identified by evaluating these trends together with forest loss, fire occurrence, and drainage-related variables.

4.3.3 Land Surface Temperature (LST) derivation

LST was calculated at 30 m spatial resolution from Landsat 8-9 TIRS Band 10 data. Filtered thermal data were converted to degrees Celsius to generate annual LST layers for the period 2017-2025. Mean LST layers were subsequently calculated to represent average surface temperature conditions during the study period, whereas LST trends were derived to represent long-term temporal changes in surface temperature. Temporal trends in LST were calculated using the same pixel-wise linear slope approach described in Section

4.4 Derivation of environmental variables

4.4.1 Distance to canal

A distance raster with 10 m spatial resolution was generated from the drainage canal network using Distance Accumulation tools in ArcGIS Pro. The raster represents the distance from each raster cell to the nearest drainage canal and is subsequently used as an explanatory variable in the statistical analyses.

4.4.2 Canal density

Canal density was calculated from the drainage canal network using Line Density tool in ArcGIS Pro with a 10 m output resolution The analysis generated a continues raster surface representing the spatial concentration of drainage canals across the peatland areas. Higher density values indicate areas with more intensive drainage infrastructure.

4.4.3 Distance to canal blocks

Canal blocks are structures designed to restrict water flow and increase water retention in drained peatlands. A distance-to-canal-block raster with 10 m spatial resolution was generated using the Distance Accumulation tool in ArcGIS Pro. The raster represents the distance from each raster cell to the nearest canal block and was included as an explanatory variable in the Random Forest analysis to assess the potential influence of restoration efforts on peatland moisture conditions. Shorter distances may indicate a greater potential influence of canal-blocking structures on nearby peatland moisture conditions, although the effect may depend on the direction of water flow and hydrological connectivity within the canal network.

4.4.4 Topographic Wetness Index (TWI)

TWI was derived from the Copernicus DEM using flow accumulation, flow direction, slope, and specific catchment area (SCA). TWI represents the spatial distribution of potential surface moisture and wetness based on terrain characteristics and was calculated as:

$$TWI = ln\left(\frac{a}{tan\beta}\right)$$

Where a represents the specific catchment area (SCA) and β represents the slope angle in radians.

Higher TWI values indicate areas with greater potential moisture retention, whereas lower values represent relatively drier areas. The TWI raster was used as an explanatory variable to assess the influence of topography on peatland moisture conditions and degradation patterns.

4.4.5 Fire density

Fire density was derived from VIIRS active fire detections for the period 2017–2025. Fire data were downloaded as point-based detections representing fire occurrences within the study area. The datasets were subsequently clipped to peatland areas to retain only fire detections occurring within mapped peatlands.

The point-based fire detections were converted into a continuous raster surface using Kernel Density Estimation (KDE) in ArcGIS Pro. KDE was applied using a 2 km search radius and a 10 m output cell size to represent the spatial distribution and intensity of fire occurrence. Density values were expressed as fire detections per square kilometre. The KDE approach was primarily used to describe the general spatial concentration and intensity of fires across the peatland areas. The resulting fire density raster was included as an explanatory variable in the statistical analysis.

4.4.5 Forest loss

Forest-loss data from Global Forest Watch were available annually for the period 2001–2024. For visualisation of long-term forest-loss patterns, cumulative forest loss was grouped into three periods (2001-2008, 2009-2016, and 2017-2024). These periods were used to illustrate the historical progression of forest loss within the study area.

For analyses related to recent peatland degradation, forest loss occurring during the study period was examined separately using the periods 2017-2020 and 2021-2024. This subdivision was intended to distinguish earlier and more recent forest-loss patterns that may influence current peatland condition. Because forest-loss data for 2025 were not available at the time of analysis, the most recent available data from 2024 were used in the statistical analyses.

4.4.6 Land cover

To improve the interpretability of the land-cover data, the original ESA WorldCover classes were reclassified into five broader land-cover categories:

1. *Intact forest*: tree cover
2. *Degraded vegetation:* shrubland, grassland, and bare/sparse vegetation
3. *Agriculture:* cropland
4. *Built-up areas*
5. *Wet area:* permanent water bodies, herbaceous wetlands, and mangroves

The reclassification was performed in ArcGIS Pro using the Reclassify tool. The resulting land-cover layer was used to characterize land-cover patterns within peatland areas and was included as an explanatory variable in the Random Forest modelling.

Although the ESA WorldCover dataset represents land-cover conditions in 2021 only, historical tree-cover data from the Hansen Global Forest Change dataset indicate that large portions of the peatland landscape were forested in 2000 *(Appendix A5).* Therefore, shrubland, grassland, and sparse vegetation classes were interpreted as potentially disturbed land-cover types within a historically forested peatland environment. However, these classes were not assumed to represent degradation independently and were interpreted together with forest-loss, NDVI, NDWI, and fire-occurrence indicators when assessing peatland degradation.

4.5 Spatial and statistical analyses

4.5.1 Fishnet generation and zonal statistics

A regular fishnet grid consisting of 1 km x 1 km cells was created to divide the peatland area into equal spatial units for analysis. The fishnet approach was used to integrate environmental variables and remote sensing indicators derived from datasets with different spatial resolutions and formats, including raster and point-based data. Summarising data within fishnet cells also reduced spatial noise and improved comparability among variables during statistical analyses

A 1 km × 1 km grid size was selected to provide a practical balance between spatial detail and regional-scale analysis across the large peatland study area. Although the original datasets had spatial resolutions ranging from approximately 10 m to 30 m, the larger grid facilitated integration of multiple datasets within a common analytical framework. While some fine-scale information may have been lost during the aggregation process, the selected grid size was considered appropriate for identifying broader spatial patterns of peatland degradation and environmental drivers.

Zonal statistics were applied to summaries raster values within each fishnet cell. Mean values of NDVI slope, NDWI slope, TWI, fire density, canal density, distance to canal, and forest loss, were extracted for each grid cell. Additional variables, including land cover and distance to canal blocks, were also incorporated for use in the Random Forest modelling.

The resulting fishnet-based dataset was used as input for subsequent statistical and spatial modelling analyses.

4.5.2 Hotspot analysis of fires

Spatial hotspot analysis was performed using the Getis-Ord Gi* statistic in ArcGIS Pro to identify statistically significant spatial clusters of fire occurrence within the peatland area. Unlike the Kernel Density fire analysis, which describes the general spatial concentration and intensity of fire detections, the Getis-Ord Gi* statistic identifies statistically significant spatial clusters of high and low fire occurrence. The analysis was applied to annual VIIRS active fire detections to distinguish areas with significantly high concentrations (hotspots) and low concentrations (coldspots) of fire activity.

The Getis-Ord Gi* statistic calculates a z-score and p-value for each spatial feature based on the concentration of neighbouring fire detections within a defined spatial neighbourhood. Statistically significant positive z-scores indicate fire hotspots, whereas statistically significant negative z-scores represent coldspots.

The years 2019 and 2023 were selected for hotspot analysis because they represented periods with relatively high fire activity within the VIIRS active fire detection dataset, whereas limited fire detections were observed during 2020-2022.

Hotspot analysis was performed using the Euclidean distance method with a fixed distance band of 500 m to define the spatial neighbourhood between fire detections. Confidence levels of 90%, 95%, and 99% were used to classify statistically significant hotspots.

4.5.3 Integrated peatland degradation map

An integrated peatland degradation map was developed for peatland areas only using indicators representing key degradation processes, including vegetation decline (NDVI slope), moisture reduction (NDWI slope), TWI, fire density, forest loss, and distance to drainage canals. LST was not included in the integrated degradation map due to its relatively weak relationships with peatland moisture dynamics and limited spatial variability compared with the other indicators.

Prior to overlay analysis, all variables were individually reclassified into three ordinal classes representing low (1), moderate (2), and high (3) degradation influence using the Natural Breaks (Jenks) classification method in ArcGIS Pro. The Jenks method was selected because it identifies natural groupings within the data by minimizing within-class variance and maximizing between-class variance, thereby improving the representation of spatial differences in peatland degradation intensity. The resulting class thresholds and interpreted relationship of each indicator to peatland degradation processes are provided in *Appendix A6.*

For NDVI and NDWI slope, strong negative trends were classified as high degradation influence, whereas weak negative or positive trends were classified as low degradation influence.

For fire density and forest loss, higher values represented higher degradation influence. Forest-loss areas during 2017–2024 were grouped into two temporal periods (2017-2020 and 2021-2024) *(Appendix A6)*. The classification was based on the relative extent of forest loss within peatland areas, where the period with larger mapped forest-loss extent was assigned a higher degradation influence class, whereas areas without detected forest loss were classified as low degradation influence.

Shorter distances to drainage canals were classified as higher degradation influence due to the stronger potential impact of drainage on peatland hydrological conditions. Detailed threshold values and forest loss classifications used for degradation reclassification are provided in *Appendix A6*.

Intermediate values between the low and high classes were assigned to the moderate degradation class. Subsequently, all reclassified layers were aligned to a common spatial resolution (20 m) and spatial extent before being combined using the Weighted Overlay tool in ArcGIS Pro. Equal weights were assigned to all indicators to produce the composite peatland degradation index.

Table 4.1. Peatland degradation reclassification.

Indicators	Degradation influence	
	High	Low
NDVI slope	Strong negative trend	Weak or positive trend
NDWI slope	Strong negative trend	Weak or positive trend
TWI	Low values	High values
Fire density	High values	Low values
Forest loss	High forest loss	Limited (no forest loss)
Distance to drainage canal	Short distance	Long distance

The resulting composite raster values ranged from 6 to 18 and were subsequently grouped into three final degradation classes representing low, moderate, and high peatland degradation.

4.5.4 Relationship between peatland degradation indicators

Pearson correlation was applied to examine the strength and direction of linear relationships among degradation indicators. The analysis focused on indicators representing different aspects of peatland degradation processes, including vegetation condition (NDVI slope), surface moisture dynamics (NDWI slope), fire disturbance (fire density) and thermal condition (LST slope).

4.5.5 Baseline relationship between peatland moisture conditions and environmental variables

Ordinary Least Squares (OLS) multiple linear regressions were applied to examine the global relationship between NDWI slope and selected explanatory variables across peatland areas.

Two model stages were developed to examine the influence of different environmental variable groups:

- *Stage I* included distance to drainage canal, canal density, TWI, and fire density to assess the influence of *hydrological and disturbance-related factors* on peatland moisture conditions.
- *Stage II* additionally incorporated forest loss as *a land-use disturbance* factor to evaluate whether vegetation removal improved the explanation of peatland moisture degradation patterns identified in *Stage I.*

OLS was used as a baseline global regression model prior to spatial modelling. Model diagnostics, including coefficient determination (R^2), Akaike Information Criterion (AIC), Koenker (BP) statistics, Variance Inflation Factor (VIF), and Moran's I of residuals, were used to evaluate model performance, assess multicollinearity, and examine spatial characteristics of regression residuals.

4.5.6 Spatially varying relationships between changes in peatland moisture conditions and environmental variables

Based on OLS diagnostics indicating spatial non-stationarity, Geographically Weighted Regression (GWR) was applied to examine spatially varying relationships between NDWI slope and selected explanatory variables across peatland areas. GWR was used to capture spatial variation in these relationships, as the significant Koenker (BP) statistic and spatial autocorrelation in the OLS residuals indicated that the relationships were not spatially stable.

Several explanatory variables initially tested in the GWR analysis were based on the variables included in the OLS models. However, some variable combinations produced unstable or unsuccessful outputs during the GWR process in ArcGIS Pro. Therefore, a reduced set of explanatory variables was selected for the final GWR models based on model performance and successful implementation.

Two models were developed:

- *Stage I* included canal density and TWI to assess the influence of *hydrological and terrain-related* factors on NDWI slope.

- *Stage II* included distance to drainage canals, TWI, and forest loss to evaluate the combined influence of *drainage proximity, terrain conditions, and land-use disturbance* on NDWI slope.

Model performance was evaluated using local R^2 values, AIC, and spatial patterns of residuals. Moran's I of residuals was used to assess spatial autocorrelation and compare residual spatial patterns between OLS and GWR models.

4.5.7 Importance of environmental variables determining changes in peatland moisture change

Random Forest (RF) modelling was applied as a machine-learning approach to assess variable importance and to capture non-linear relationships between NDWI slope and environmental drivers. A stepwise modelling approach was used to evaluate the contribution of different groups of explanatory variables.

Three RF models were developed to evaluate the incremental contribution of different variable groups to peatland moisture modelling:

- *Model I* included core environmental variables, including distance to drainage canal, canal density, TWI, fire density, and forest loss, to assess the influence of hydrological and disturbance-related factors on NDWI slope.
- *Model II* additionally incorporated land-cover information evaluate whether vegetation and surface-condition variables improved the explanation of peatland moisture variability identified in Model I
- *Model III* further included distance to drainage canal blocks to assess the potential contribution of peatland restoration structures to moisture conditions and determine whether restoration-related variables improved model performance

This stepwise approach allows comparison of model performance and helps identify which variables significantly improve explanatory power, rather than relying on a single full model.

The RF analysis was implemented in Python using the RandomForestRegressor algorithm from the Scikit-learn package (Pedregosa et al., 2011). Prior to modelling, records containing missing values were removed. The dataset was randomly divided into training (80%) and testing (20%) subsets.

RF models were developed using 500 decision trees with bootstrap aggregation and out-of-bag (OOB) validation. Model performance was evaluated using coefficient of determination (R^2), root mean square error (RMSE), and OOB score. Variable importance was evaluated using the Mean Decrease in Impurity (MDI) metric to identify the most influential predictors of peatland moisture change.

5 RESULTS

5.1 Spatial patterns of peatland degradation

5.1.1 Patterns of land cover distribution

The land-cover composition within mapped peatland areas in 2021 was illustrated in *Figure 5.1*. Intact forest remains the dominant land-cover type, accounting for approximately 71.6% of the peatland area. However, a substantial proportion (26%) is classified as degraded vegetation, indicating extensive disturbance within peat soils. Agriculture, built-up areas, and wet areas represent minor proportions of the peatland landscape.

The spatial distribution shows that degraded vegetation is concentrated in southern and central peat zones, whereas intact forest dominates the northern and western peat area. This land-cover pattern provides important context for interpreting the spatial distribution of vegetation decline, moisture change, fire occurrence, and surface temperature. The percentages represent proportional coverage within mapped peat soils.

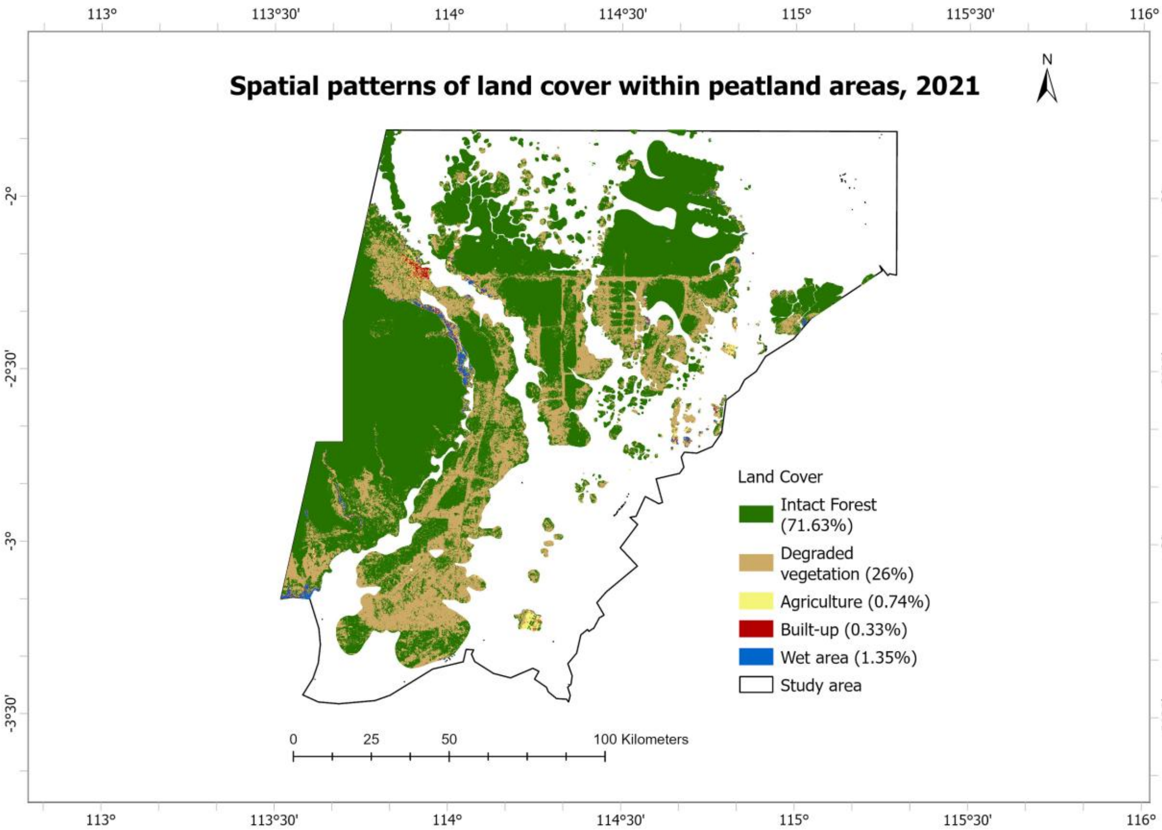

Figure 5.1. Spatial patterns of land-cover distribution within peatland areas, 2021.

5.1.2 Vegetation greenness and moisture dynamics

Mean NDVI and NDVI temporal trends during 2017-2025 showed substantial spatial variability across peatland areas (*Figure 5.2*). Areas with high mean NDVI did not always correspond to areas with stable or increasing NDVI trends. Mean NDVI represents the long-term distribution of vegetation cover, whereas NDVI slope indicates areas of increasing or decreasing vegetation over time.

Mean NDVI values ranged from approximately -0.08 to 0.70, indicating substantial spatial variability across peatland areas. Higher mean NDVI values were concentrated in remaining forested peatlands and along river corridors, whereas lower values were more common in parts of the southern and central peatland areas. Overall, the spatial pattern showed considerable heterogeneity in long-term vegetation cover across the peatland landscape.

NDVI temporal trend values ranged from approximately −0.16 to 0.09 per year, showing both negative and positive vegetation trends across peatland areas. Negative trends were widespread across northern, central, and southern peatland regions, whereas positive trends were more localized and scattered. Overall, the spatial distribution indicated heterogeneous vegetation dynamics across the peatland landscape between 2017 and 2025.

In addition to the mean NDVI and NDVI temporal trends analyses, annual maximum NDVI trends were also examined to assess peak vegetation greenness during the study period. The spatial pattern of maximum NDVI trends generally showed similar heterogeneous vegetation dynamics across the peatland landscape and is presented in *Appendix A7*.

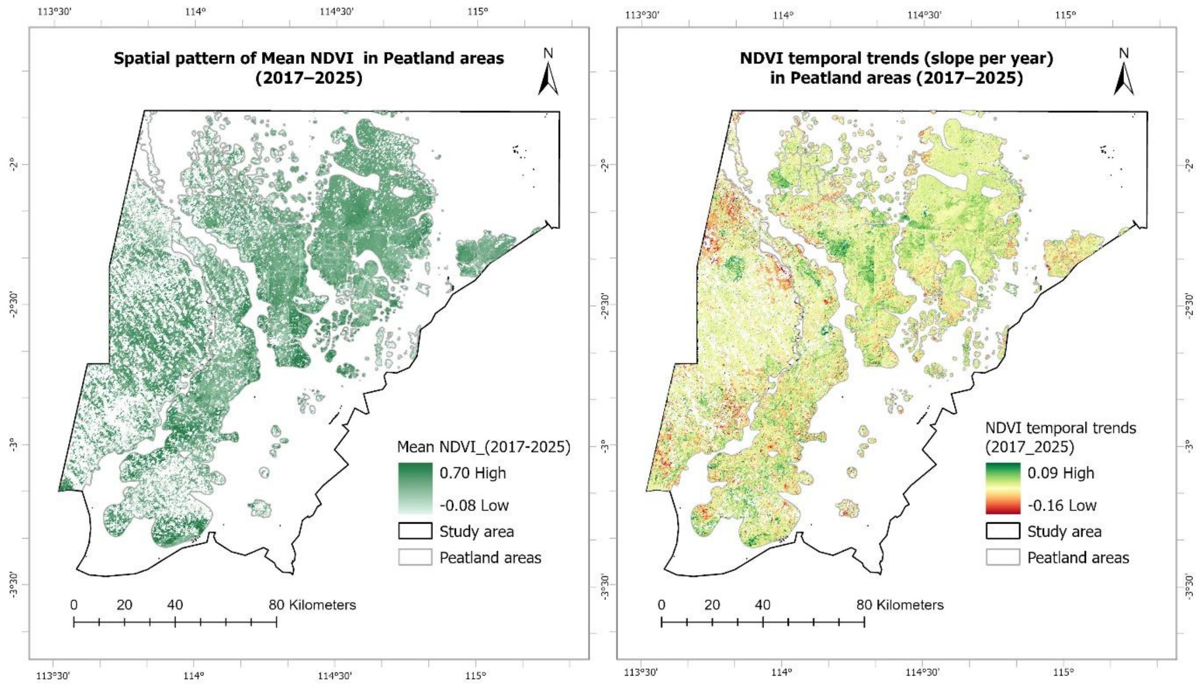

Figure 5.2. Spatial patterns of mean NDVI and NDVI temporal trends in peatland areas.

Mean NDWI and NDWI temporal trends showed substantial spatial variability across peatland areas between 2017 and 2025 (*Figure 5.3*). Mean NDWI represents long-term surface moisture conditions, whereas NDWI slope reflects the direction and magnitude of moisture change over time.

Mean NDWI values ranged from approximately -0.33 to 0.64, indicating substantial spatial variability in surface moisture conditions across peatland areas. Higher mean NDWI values dominated much of the peatland landscape, indicating generally wet surface conditions across central, northern, and several western peatland regions. In contrast, lower mean NDWI values were more localized and scattered, particularly along peripheral peatland zones and other localized areas of reduced moisture conditions.

NDWI temporal trend values ranged from approximately -0.10 to 0.08, showing both decreasing and increasing moisture trends across peatland areas. Most values were close to zero, indicating relatively limited overall moisture change during the study period. Negative trends occurred throughout the peatland landscape but were generally scattered rather than forming large continuous zones. Positive trends were similarly patchy and spatially dispersed. Overall, the spatial pattern indicated heterogeneous moisture dynamics across peatland areas between 2017 and 2025.

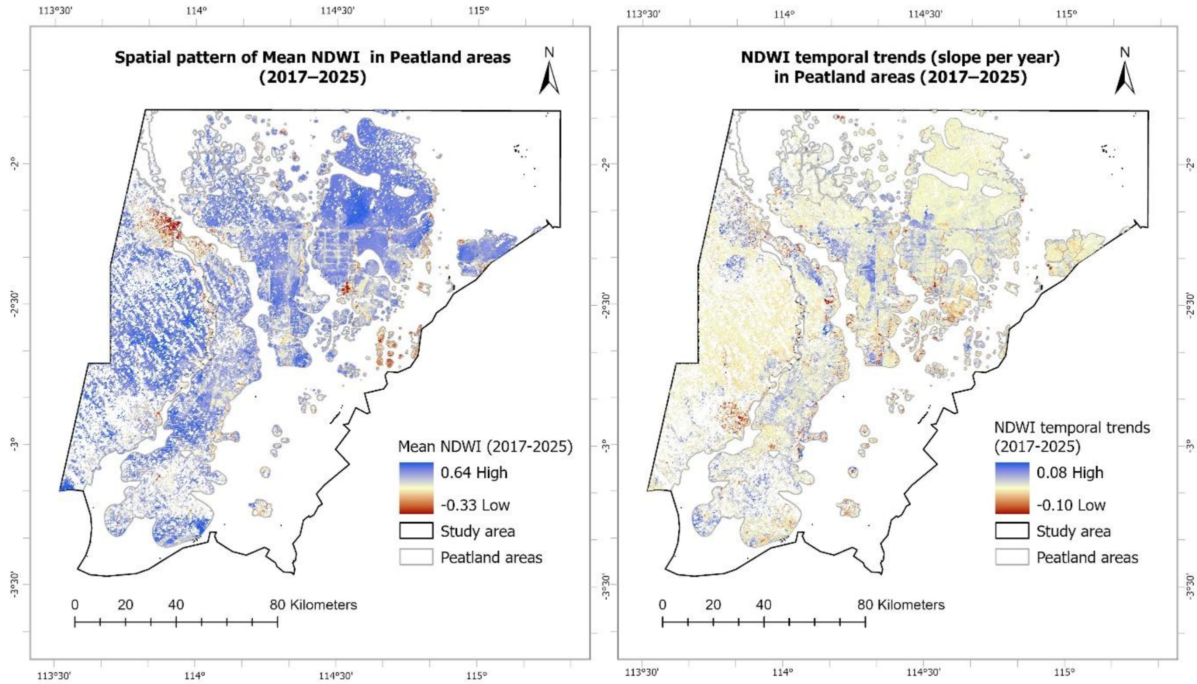

Figure 5.3. Spatial patterns of mean NDWI and NDWI temporal trends in peatland areas.

Land Surface Temperature (LST) was analysed to characterise surface thermal conditions across the peatland areas for the period 2017-2025. Mean LST values range from approximately 24.2 °C to 50.8 °C, with an overall mean of 32.7 °C (standard deviation ≈ 2.8 °C), indicating moderate spatial variability in surface temperature. However, valid LST observations were spatially limited as it occurred only in scattered patches across peatland areas. The LST slope shows generally weak and spatially limited changes, with values ranging from approximately -2.8 °C to +2.6 °C over the study period. Warming trends are present but occur mainly in localized clusters, particularly in southern and some eastern parts of the peatland areas, while most areas show minimal change.

5.1.3 Fire occurrence, density and hotspot patterns

Overall fire activity was relatively low across most peatland areas *(Figure 5.4)*, with a mean fire density of approximately 0.09 fire detections per km². However, localized hotspot areas reached substantially higher density values of up to approximately 6.38 fire detections per km². Most peatland areas showed no or very few detected fire events, while higher fire densities were concentrated primarily in the southern and some central parts of the study area.

The spatial pattern of fire occurrence points was consistent with the density results, indicating that fire activity was unevenly distributed and concentrated in specific locations. Fire density was therefore included as an explanatory variable in subsequent analyses of peatland degradation.

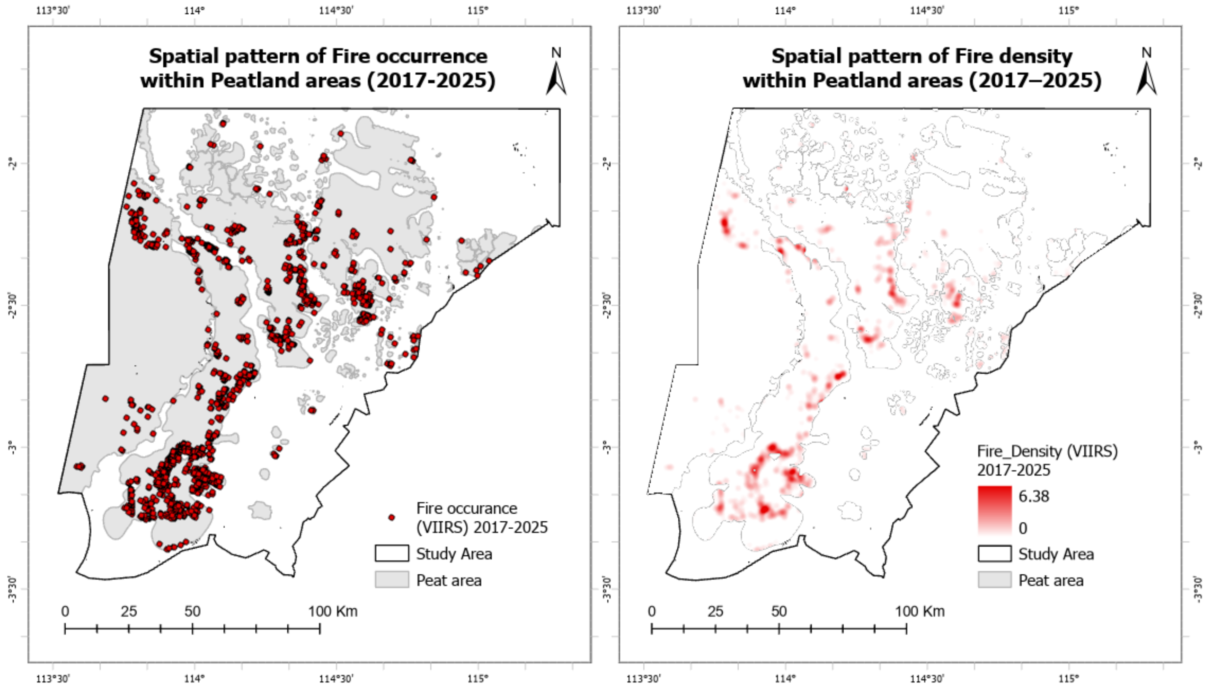

Figure 5.4. Spatial patterns of fire occurrence and fire density within peatland areas.

Forest loss shows a clear spatial pattern across the study area *(Figure 5.5)*. The cumulative forest loss map (2001-2024) indicates intensive areas of forest removal, particularly in the southern and central parts of the study area. These areas form relatively continuous zones of long-term forest loss.

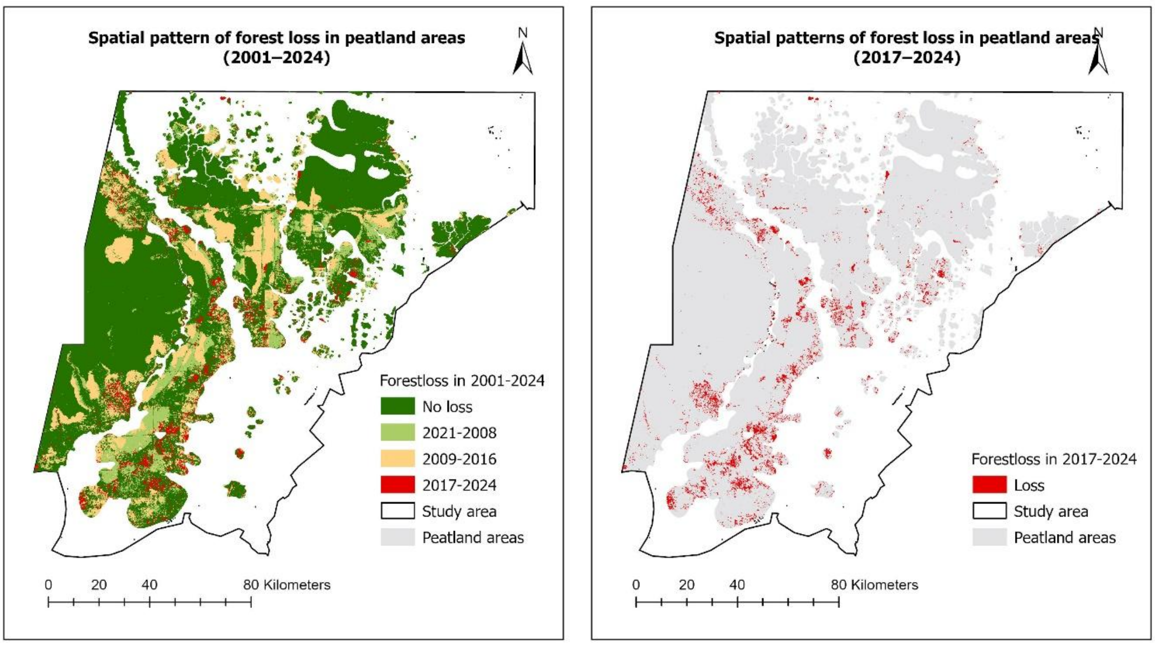

Figure 5.5. Spatial patterns of forest loss in peatland areas.

In contrast, forest loss during the study period (2017-2024) appears more fragmented and spatially dispersed. It occurs in scattered clusters across study area, particularly in southern, central regions (indicated with red colours in *Figure 5.5*), with additional smaller patches in the north. By comparison, northern and western areas show comparatively lower levels of forest loss than the more affected southern and central regions.

Overall, the comparison between long-term and recent forest loss indicates that forest removal has occurred over extended periods, whereas more recent loss appeared more spatially fragmented.

To complement the spatial analysis, annual fire occurrence and forest loss were compared for the period 2017-2024 (*Figure 5.6*). Fire activity showed strong interannual variability, with a major peak in 2019 and a smaller increase in 2023. Forest loss also varied between years, with relatively high values observed during 2018-2020. Although some years with elevated fire activity coincided with higher forest loss, the temporal patterns were not consistent across all years.

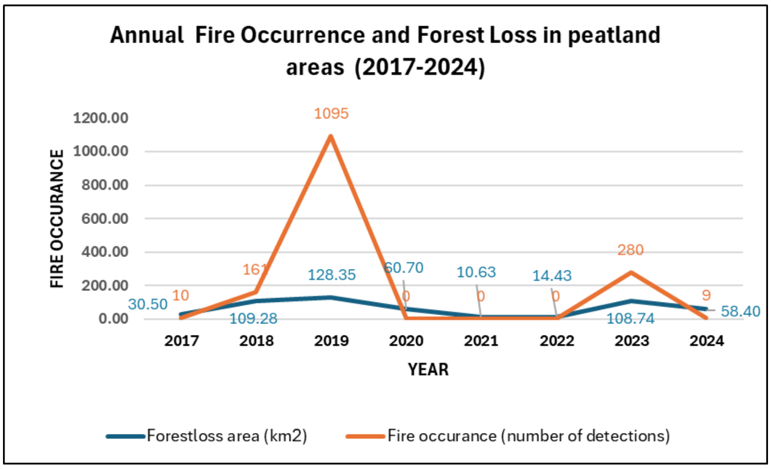

Figure 5.6. Annual fire occurrence and forest loss in peatland areas (2017-2024).

Overall, peak fire years tend to coincide with higher forest loss, although this relationship is not consistent across all years.

The Hotspot analysis of peat degradation is illustrated in *Figure 5.7.* The results reveal clear spatial clustering, with high-confidence hotspots (99%) concentrated in the southern and central parts of the study area, whereas northern areas showed fewer hotspots (*Figure 5.7*). Hotspots are primarily located in the southern and central peatland regions, with similar spatial patterns observed in both years.

A comparison between 2019 and 2023 indicates that although hotspot extent varies, they consistently occur in similar regions.

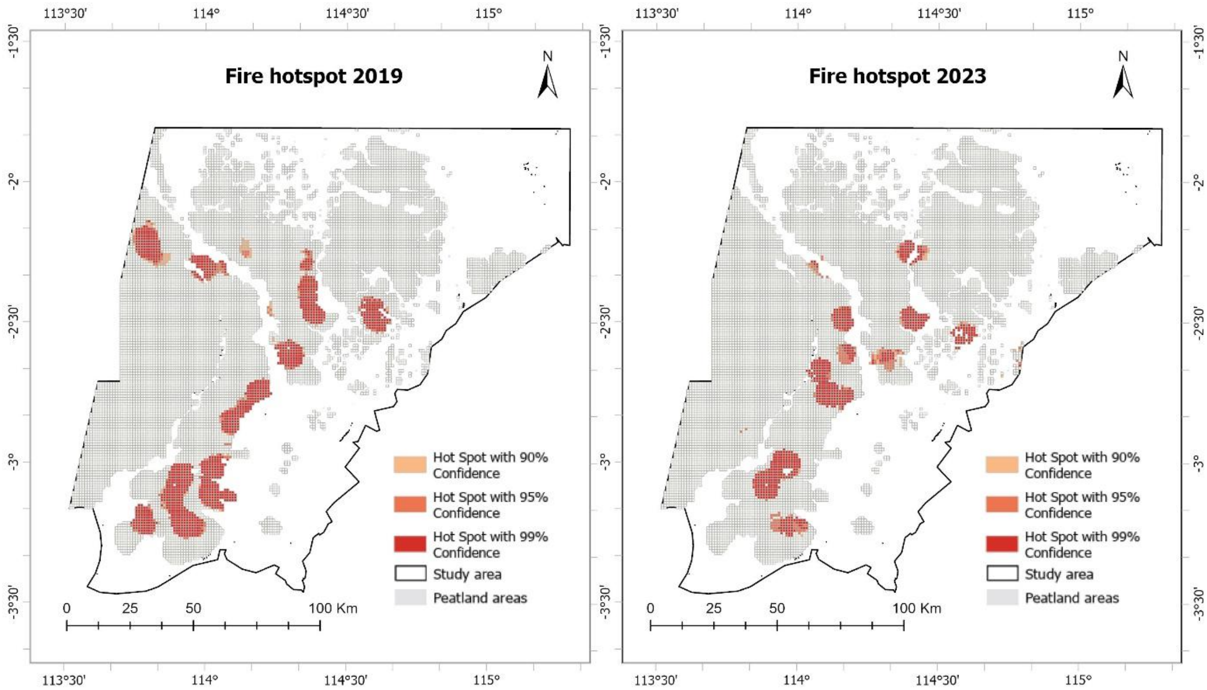

Figure 5.7. Spatial patterns of statistically significant fire hotspots in 2019 and 2023.

5.1.4 Peatland degradation map

The peatland degradation map *(Figure 5.8)* shows a heterogeneous spatial pattern of degradation across the study area. Most of the peatland areas are classified as having low to moderate degradation levels, indicating generally stable or moderately disturbed condition.

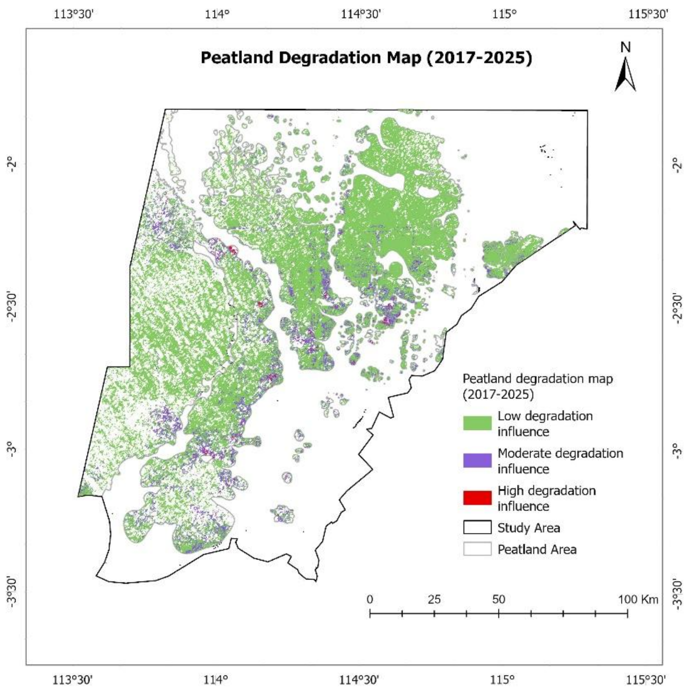

Figure 5.8. Peatland degradation map (2017-2025).

Areas of moderate to high degradation were primarily concentrated in the southern and central peatland regions. These zones represent locations where multiple degradation indicators overlap, including close proximity to drainage canals, higher fire density, increased forest loss, and areas of reduced surface moisture and vegetation condition.

In contrast, northern and western peatland regions are predominantly characterized by low to moderate vulnerability, indicating relatively stable hydrological conditions and lower levels of disturbance.

5.2 Relationships between satellite-derived peatland degradation indicators

5.2.1 Relationship between NDVI, NDWI and Fire

The correlation matrix (*Table 5.1*) shows a moderate positive relationship between NDVI slope and NDWI slope (r = 0.653). In contrast, fire density was not significantly correlated with either NDVI (r = −0.058) or NDWI (r = −0.012).

Table 5.1. Pearson correlation (r) between NDVI slope, NDWI slope, and fire density (n=7040).

Indicators	NDVI slope	NDWI slope	Fire density
NDVI slope	1.000	0.653*	-0.058
NDWI slope	0.653*	1.000	-0.012
Fire density	-0.058	-0.012	1.000

** Significant Correlation ($p < 0.05$)*

5.2.2 Relationship between NDWI and LST

Due to limited spatial coverage of valid LST observations, temperature-related correlations were not included in the main correlation matrix. Instead, the relationship between NDWI slope and LST slope was examined separately using scatter plots *(Figure 5.9).*

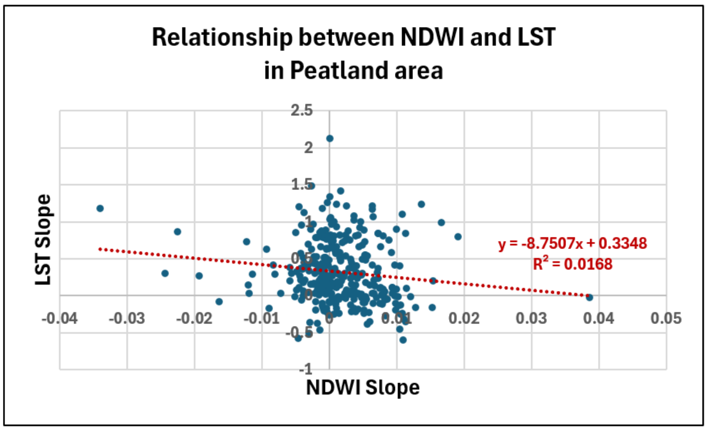

Figure 5.9. Scatter plot showing the Relationship between NDWI slope and LST slope in peatland areas (2017-2025).

The scatter plot shows a weak negative relationship between NDWI slope and LST slope (r = −0.130; R^2 = 0.016), indicating that areas with decreasing moisture trends tended to show slightly higher warming trends. However, the relationship was weak and highly variable across peatland areas, suggesting that additional environmental factors may influence LST variation.

5.3 Environmental drivers of peatland degradation

This section examines how environmental variables explain the spatial variation in peatland degradation indicators across the study area. The analysis is restricted to peatland areas only (11,523 km²) which cover approximately 50% of the total study area to ensure consistency with the study objective.

Building on the spatial patterns (Section 5.1) and the relationships between indicators (Section 5.2), the analysis focuses on key drivers, including drainage proximity, canal density, terrain characteristics (derived from DEM), and land-use factors.

Multiple approaches are used to assess these relationships. Correlation analysis provides an initial overview of how variables are related, while OLS is used to assess their overall influence at the global scale.

5.3.1 Spatial pattern of drainage variables

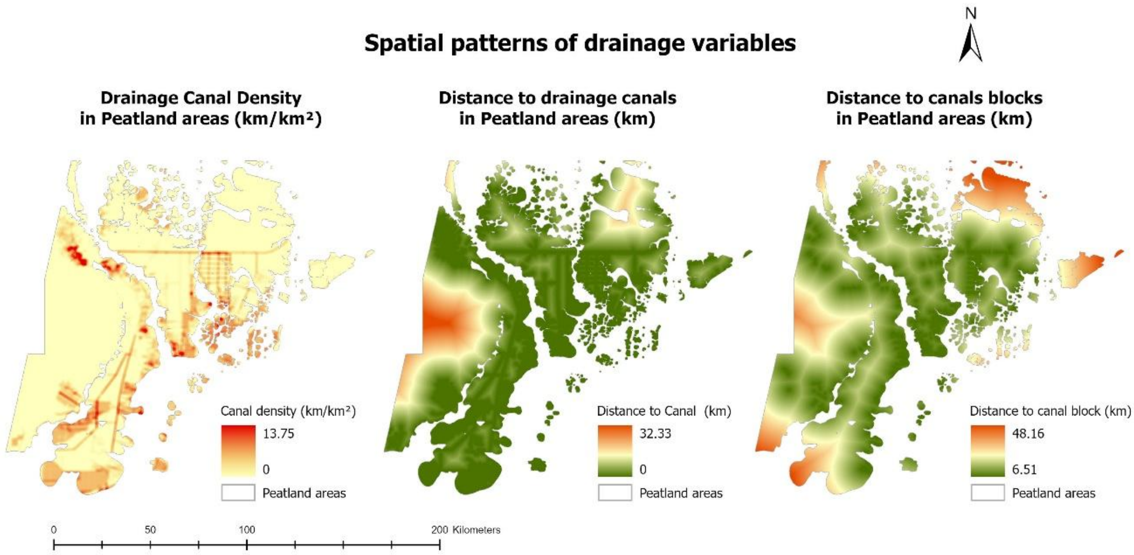

Figure 5.10. Spatial patterns of drainage variables within peatland areas, including canal density, distance to drainage canals, and distance to canal blocks in peatland areas (2017-2025).

Canal density ranged from 0 to 13.75 km/km², with the highest values concentrated in the southern and central peatlands, as well as several localized hotspots in the western peatland areas (*Figure 5.10*). These areas indicate intensive drainage infrastructure and a high degree of hydrological modification. Lower canal density values were observed across more fragmented northern peatlands, where canal networks appeared less developed or less continuous (*Figure 5.10*).

The distance-to-canal map highlights the widespread influence of drainage infrastructure across peatland areas (*Figure 5.10*). Distances ranged from 0 to 32.33 km, although large parts of the peatland landscape were located relatively close to drainage canals. Areas situated farther from canals were more limited and occurred mainly in western and peripheral peatland zones, suggesting that only a smaller proportion of peatlands remain relatively isolated from drainage disturbance.

Distance to canal blocks ranged from 6.51 to 48.16 km across peatland areas. Shorter distances to canal blocks were concentrated in central and southern peatlands (*Figure 5.10*), indicating a greater presence of restoration and water-management interventions in these regions. In contrast, larger distances occurred mainly in northern and peripheral peatlands, suggesting that some peatland zones remain relatively far from canal-blocking measures.

Overall, the drainage-related variables show a clear spatial concentration of canal infrastructure and restoration measures in southern and central peatlands, whereas northern and peripheral peatlands are generally less connected to both drainage canals and canal-block interventions.

5.3.2 Drainage influence on peatland moisture

The relationship between drainage proximity and peatland moisture was analysed using mean NDWI slope values across distance classes from drainage canals within peatland areas *(Figure 5.11).* NDWI slope values generally increase with distance from canals between 0-250 m and 1001-2000 m, indicating that areas closer to canals experience stronger drying trends, while areas further away show more stable or slightly increasing moisture conditions. However, the farthest distance class (>2000 m) shows a lower mean value, suggesting local variability and indicating that the relationship is not strictly linear across all distances.

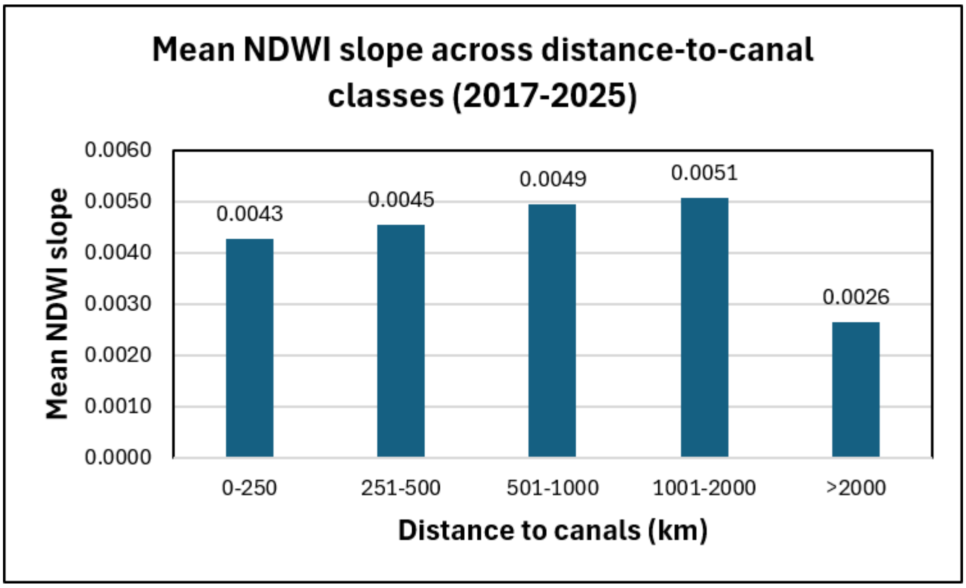

Figure 5.11. Mean NDWI slope across distance-to-canal classes in peatland areas.

5.3.3 Correlation analysis of environmental drivers

Pearson correlation analysis was applied within peatland areas to examine the relationships between NDWI slope and environmental variables, including distance to canal, canal density, TWI, fire density, and forest loss. The correlation analysis was used as an exploratory assessment of linear relationships among variables, while statistical significance and predictor importance were evaluated through the subsequent OLS, GWR, and Random Forest analyses.

The results indicate generally weak linear relationships among the analysed variables. NDWI slope showed a weak negative relationship with distance to canals (r = -0.217). In comparison, canal density showed only a very weak relationship with NDWI slope (r = 0.083), suggesting limited linear associations between drainage variables and moisture trends at the spatial scale analysed.

Table 5.2. *Pearson correlation (r) between NDWI slope and the analysed environmental variables.*

Variables	NDWI slope	Distance to canal	Canal density	TWI	Fire density	Forest loss (%)
NDWI slope	1	-0.217	0.083	0.034	0.037	0.049
Distance to canal	-0.217	1	-0.42	-0.192	-0.203	0.065
Canal density	0.083	-0.42	1	0.3	0.177	0.013
TWI	0.034	-0.192	0.3	1	0.08	0.037
Fire density	0.037	-0.203	0.177	0.08	1	0.104
Forest loss (%)	0.049	0.065	0.013	0.037	0.104	1

The relationship between NDWI slope and terrain conditions (TWI) was negligible (r = 0.034), indicating limited influence of topographic wetness on moisture change. Similarly, NDWI slope showed very weak correlations with fire density (r = 0.037) and forest loss (r = 0.049), suggesting no strong linear relationships between these variables.

5.3.4 Global regression analysis (OLS)

Ordinary Least Squares (OLS) regression was applied to assess the influence of environmental variables on NDWI slope within peatland areas. Two models were tested: Stage I, including distance to canals, canal density, TWI, and fire density. Stage II includes forest loss as a potential land-use disturbance.

Table 5.3. OLS regression results for NDWI slope.

OLS Variables	Stage I		Stage II	
	Coefficient	p-value	Coefficient	p-value
Distance to canals	-0.000000	0.000000***	-0.000000	0.000000***
Canal density	-0.000033	0.464665	0.000103	0.024590*
TWI	-0.000013	0.68854	0.000022	0.469726
Fire density	-0.000082	0.690306	0.000784	0.000282***
Forest loss	-	-	-0.001158	0.000000***

Note: *p < 0.05, ***p < 0.001.

Table 5.3. presents the OLS regression coefficients and their statistical significance for both model stages. In Stage I, distance to canal is the only significant variable ($p < 0.01$). showing a negative relationship with NDWI slope. Other variables, including canal density, TWI and fire density, are not statistically significant. In Stage II, distance to canal, fire density, and forest loss are highly significant ($p < 0.01$). while canal density being statistically significant at the 0.05 level. TWI remains non-significant in both models.

Comparison between Stage I and Stage II

Table 5.4. OLS model diagnostics for NDWI slope.

OLS statistics	Value	
	Stage I	Stage II
Adjusted R^2	0.0467	0.0778
AIC	-82,965	-83,344
Koenker (BP) statistic	357.7871	722.6975
Moran's I (residual)	0.4424	0.4441
Moran's z-score	154.6589	155.2284

The OLS models show low explanatory power, with adjusted R^2 values of 0.0467 in Stage I and 0.0778 in Stage II, indicating that the inclusion of forest loss only slightly improved model performance.

The Koenker (BP) statistic is statistically significant in both stages, indicating that the relationships between NDWI slope and explanatory variables are not spatially stationary. Residual Moran's I values are 0.4424 in Stage I and 0.4441 in Stage II, showing positive spatial autocorrelation, suggesting that the OLS model does not fully capture spatial patterns in NDWI slope. These results indicate that a local spatial modelling approach such as GWR, may be more appropriate. Detailed OLS regression coefficients and diagnostic statistics for Stage I and Stage II models are provided in *Appendix A8.*

5.3.5 Spatial variability of drivers (GWR)

GWR was applied to capture spatial variation in these relationships, as the significant Koenker (BP) statistic and spatial autocorrelation in the OLS residuals indicate that relationships are not spatially stable.

Different combinations of explanatory variables were tested, but models including all variables showed instability. Therefore, a reduced set of variables was used to ensure stable model estimation. Two models were examined. Stage I includes distance to canal and TWI, representing hydrological and terrain conditions. Stage II additionally includes forest loss to account for land-use influence.

Table 5.5. GWR result for NDWI slope.

GWR Statistics	Value	
	Stage I	Stage II
Adjusted R^2	0.2383	0.3040
AIC	29,409	28,398
Moran's I (residual)	0.303827	0.283290
Moran's z-score	106.217934	99.038590
Moran's p-value	0.000000	0.000000

The Stage II model is presented here, as it showed improved performance. Model performance is assessed using local R^2 values, which indicate how well the model explains NDWI slope at each location.

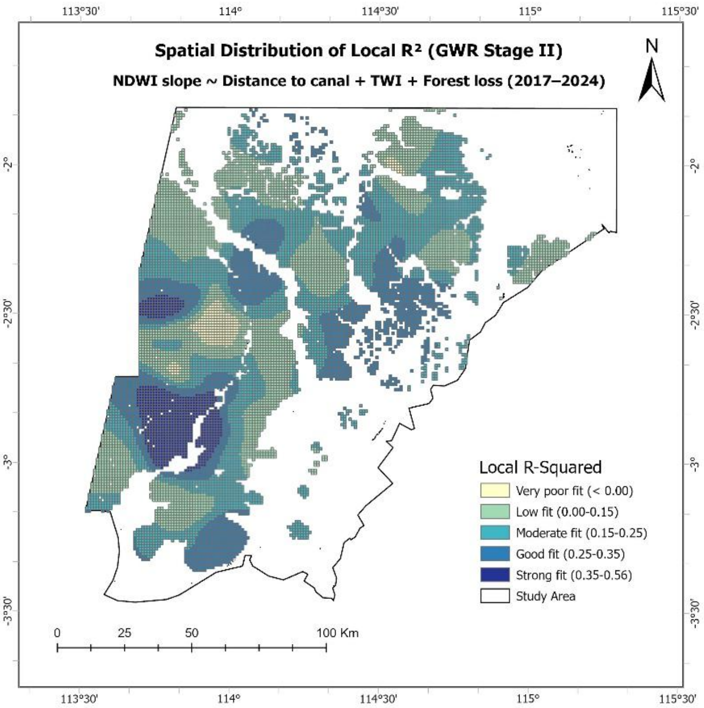

Figure 5.12. Spatial distribution of local R^2 values in peatland areas (GWR Stage II).

The local R^2 values show clear spatial variation in model performance. Higher values are observed in the southern and western parts of the study area, indicating that the selected variables explain NDWI slope better in these areas.

The lower values in other areas suggest that additional factors not included in the model may influence moisture dynamics.

Spatial variation of the Local Effect of Distance to Canals

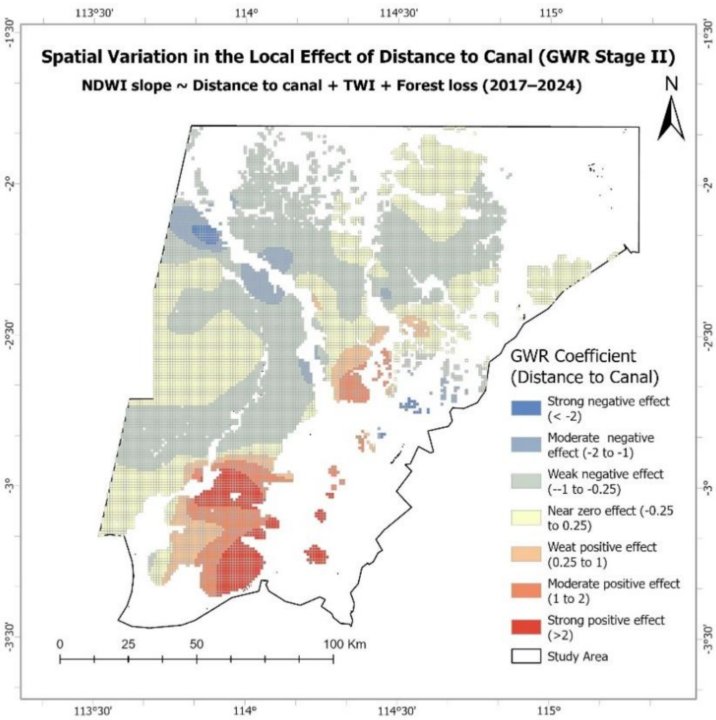

Figure 5.13. Spatial variation of the local effect to distance to canals in peatland areas (GWR Stage II).

Areas with stronger negative coefficients are observed mainly in the southern and central parts of peatland area, indicating that proximity to canal is associate with stronger drying effects in these regions.

In contrast, weaker or near-zero relationships are observed in other area, suggesting that the influence of drainage varies spatially across the peatland.

Spatial variation of the Local Effect of Forest loss

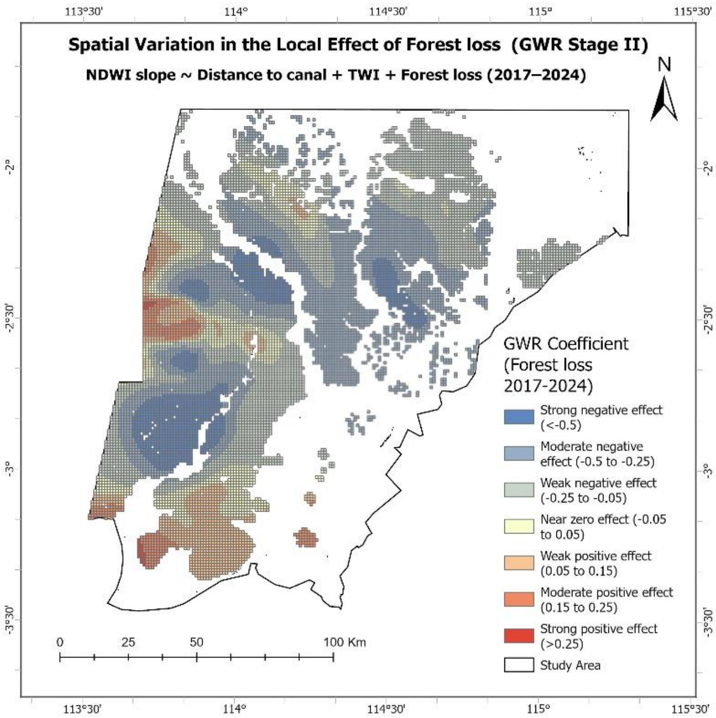

Figure 5.14. Spatial variation of the local effect to forest loss in peatland areas (GWR Stage II).

Forest loss shows a spatially variable relationship with NDWI slope. In several areas, particularly in the southern and central part of the study area, negative coefficients (blue) indicate that higher forest loss is associated with drying trends,

In other area, positive or near-zero coefficient (red to yellow) suggest weaker or inconsistent relationship, indicating that the influence of land-use change on moister dynamic is not uniform across the peatland.

The influence of TWI is generally weaker and more spatially variable *(Appendix A9).* In some areas, higher wetness is associated with reduced drying, but the relationship is not consistent across the study area.

Spatial distribution of GWR Standardized Residual (Stage II)

The spatial distribution of GWR residuals (*Figure 5.15*) represents the unexplained variation in NDWI slope after taking into account the selected variables. Compared to the OLS model, the residuals show a more spatially dispersed, indicating improved representation of spatial variability. However, some clustering remains, suggesting that additional environmental or local factors not included in the model may influence peatland moisture dynamics.

The GWR model shows improved performance compared to OLS, with higher R^2 values and lower AIC, indicating a better model fit. Residual spatial autocorrelation (Moran's I) is reduced compared to OLS but remains positive, suggesting that although GWR captures spatial variability more effectively, some spatial structure is still not fully explained.

Overall, the GWR results confirm that peatland degradation is influenced by spatially varying processes, with drainage and land-use factors having stronger effects in certain areas rather than uniformly across the study area.

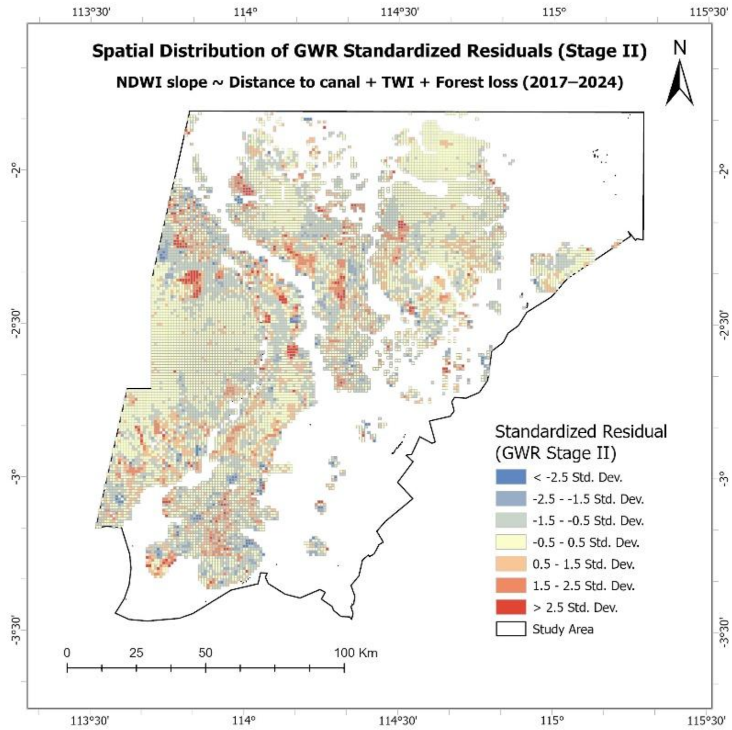

Figure 5.15. Spatial distribution of GWR Standardized Residual in peatland areas (GWR Stage II).

5.3.6 Random forest modelling

Model performance improved across the three RF models. The baseline model (Model I), containing hydrological and disturbance-related variables (distance to canals, canal density, TWI, fire density, and forest loss), produced an R^2 value of 0.123. Model II, which additionally included land-cover information, showed a slight improvement in performance ($R^2 = 0.146$). The highest performance was observed in Model III, which further incorporated distance to canal blocks and achieved an R^2 value of 0.271. A similar trend was observed for OOB accuracy, while RMSE decreased slightly, indicating improved predictive performance.

Table 5.6. Comparison of random forest model performance.

Model	Variables	R^2	OOB	RMSE
Model 1	Hydrology + disturbance	0.123	0.15	0.00603
Model 2	Model 1 + Land cover	0.146	0.177	0.00595
Model 3	Model 2 + Distance to canal block	0.271	0.27	0.0055

These results suggest that land-cover contributed only minor improvements, whereas restoration-related variables associated with canal blocks substantially improved explanatory power.

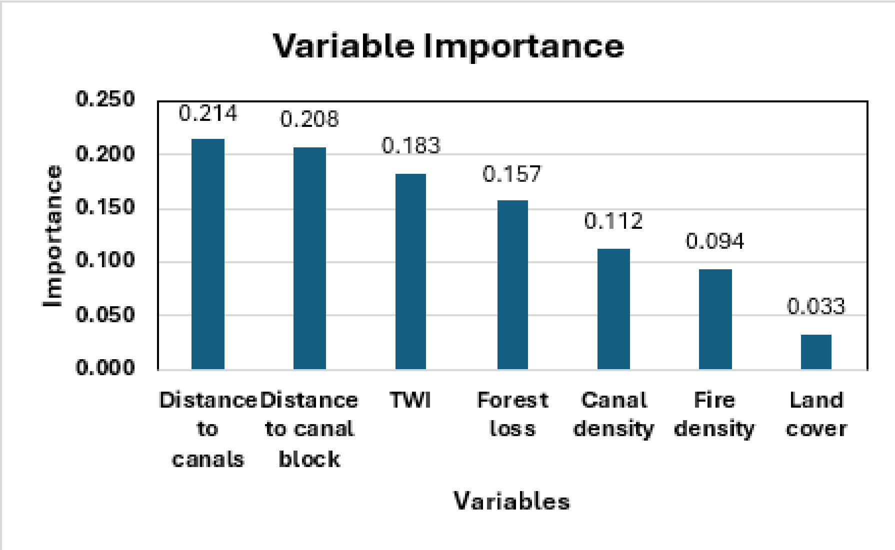

Figure 5.16. Variable importance from the Random Forest (Model 3) in peatland areas.

Variable importance results (*Figure 5.16*) show that distance to canal and distance to canal blocks are the most influential variables, followed by TWI and forest loss. Canal density and fire density have lower importance, while land cover contributes very little to the model.

6 DISCUSSION

6.1 Major hotspots of peatland degradation

The spatial distribution of peatland degradation is not uniform across the peatland areas. It is particularly concentrated in the southern and central regions. These areas show a combination of higher forest loss, clustered fire activity, reduced vegetation condition, and localized moisture decline, indicating more intense degradation processes. In contrast, northern peatland areas appear relatively stable, with lower levels of disturbance and more consistent vegetation conditions. Similar spatial heterogeneity in tropical peatland condition has been reported in previous studies, where drainage intensity, land-use disturbance, and peatland accessibility varied considerably across peatland landscapes (Lampela et al., 2016; Horton et al., 2021; Dadap et al., 2021; Taufik et al. 2019).

The integrated peatland degradation map further supports these spatial patterns by combining multiple indicators into a single framework. As shown in *Figure 5.8,* the map highlights that the major degradation is concentrated in the southern and central peatland regions, where drainage proximity, fire activity, forest loss, and reduced moisture conditions overlap. This suggests that peatland degradation is spatially clustered and shaped by the interaction of multiple environmental and anthropogenic drivers rather than a single factor (Taufik et al., 2019; Ruwaimana et al., 2024).

The limited spatial variation in land surface temperature (LST) observed in this study can be partly explained by the equatorial location of the study area, where temperatures remain consistently high throughout the year. However, previous field studies have shown that LST can vary by approximately 3-4 °C between dry and wet seasons and may increase significantly following drainage (Astiani et al., 2017). This suggests that while broad-scale temperature differences are relatively small, local variations in LST are strongly influenced by environmental conditions such as surface moisture, vegetation cover, and land-use disturbances. Similar relationships between land surface temperature, vegetation cover, and moisture availability have also been observed in degraded tropical peatlands (Ohkubo et al., 2021; Miettinen et al., 2017).

The temporal pattern of fire occurrence, with a major peak in 2019 and a smaller increase in 2023, is consistent with previous studies linking ENSO-related drought and reduced rainfall to increased fire activity in Southeast Asian peatlands and tropical forests (Lam et al., 2026; Zheng et al., 2023). El Niño is typically associated with reduced rainfall and prolonged dry periods, increasing the susceptibility of peatlands to fire (Field et al., 2016; Gaveau et al., 2022). ENSO events typically occur at intervals of approximately 3–5 years and often lead to significant moisture deficits across regions such as Kalimantan. During these periods, reduced precipitation lowers water tables and decreases surface moisture, creating conditions that enhance the likelihood of peat ignition and the persistence of fires (Field et al., 2016; Ruwaimana et al., 2024; Zheng et al.,2023).

In peatland areas, these climatic effects are further amplified by drainage, which lowers the water table and accelerates drying (Apers et al., 2022). Peatland fires in Indonesia are largely human-induced and are commonly used for land clearing (Simorangkir, 2007; Cochrane, 2003), but under dry conditions they can spread uncontrollably and burn into underlying peat layers and root systems, resulting in prolonged burning, increased carbon emissions, and regional haze events (Page et al., 2002; Mishra et al., 2020; Grosvenor et al., 2024; Page & Hooijer, 2016).

Recurrent fire may further reinforce peatland degradation through feedback processes in which previously degraded and fire-affected areas become increasingly susceptible to repeated burning (Webb & Jamaludin, 2024). Previous studies have also shown that drainage canals can influence peat hydrology over large spatial areas and substantially increase peatland fire susceptibility (Ritzema et al., 2014; Dadap et al., 2021).

These findings indicate that peatland degradation hotspots are shaped by the combined influence of hydrological disturbance, land-use change, and climatic variability, with these factors interacting to concentrate degradation in specific areas.

6.2 Relationship between degradation indicators

The analysed relationships showed that vegetation and moisture indicators were more strongly related to each other than to fire occurrence or land surface temperature. The strong positive relationship between NDVI and NDWI (*Table 5.1*) indicates that areas with higher vegetation cover generally also maintained higher surface moisture conditions. This suggests that vegetation condition in the peatland areas is closely linked to peatland moisture availability, which is consistent with previous studies showing that tropical peatland vegetation productivity and ecosystem functioning depend strongly on shallow water-table conditions and stable hydrology (Page et al., 2011; Ritzema et al., 2014; Apers et al., 2022).

In contrast, fire occurrence showed weak relationships with both vegetation and moisture indicators. This suggests that fire activity was not directly controlled by long-term average environmental conditions at the spatial scale analysed. Instead, fire events are more likely influenced by short-term drought, ignition sources, drainage disturbance, and human land-use activities such as land clearing and agricultural burning (Field et al., 2016; Gaveau et al., 2014; Konecny et al., 2016; Horton et al., 2021). Similar patterns have been reported in Southeast Asian tropical landscapes where fire occurrence is often more strongly associated with land degradation and anthropogenic disturbance than with stable long-term vegetation conditions alone (Webb & Jamaludin, 2024; Mishra et al., 2021). Studies in Central Kalimantan have shown that peatland fires are strongly associated with anthropogenic disturbance (Ruwaimana et al., 2024), particularly drainage canals and land accessibility, which increase peat drying and fire susceptibility (Horton et al., 2021; Dadap et al., 2021).

Land surface temperature (LST) patterns were spatially uneven and less distinct compared to vegetation and moisture indicators, suggesting that temperature variation is influenced by local land-surface conditions rather than broad-scale environmental gradients (Weng, 2009; Miettinen et al., 2017). The weak inverse relationship between NDWI slope and LST slope *(Figure 5.8)* suggests that peatland drying may contribute to increased surface warming. Reduced moisture availability can lower evaporative cooling and increase heat absorption, particularly in disturbed peatlands with sparse vegetation cover (Ohkubo et al., 2021). However, the low explanatory power indicates that land surface temperature is also influenced by several additional factors, including vegetation structure, exposed soil surfaces, fire history, drainage intensity, and local atmospheric conditions.

The interpretation of LST as a degradation indicator should be treated with caution. To improve consistency between years, all satellite observations were restricted to the July-September dry season. Although this observation period reduces seasonal variation, it may increase the influence of interannual climatic variability. In Indonesia, rainfall patterns and drought conditions are strongly influenced by large-scale climate oscillations such as the El Niño-Southern Oscillation (ENSO), particularly during the dry season (Aldrian & Susanto, 2003). El Niño events are often associated with lower rainfall and drier conditions, which can contribute to peat drying and increased fire risk (Field et al., 2016; Taufik et al., 2022).

Therefore, some of the observed LST patterns may reflect short-term climatic conditions rather than peatland degradation alone. In addition, satellite-derived LST data may be influenced by cloud contamination, atmospheric effects, and differences in incoming solar radiation between image acquisition dates. Thermal infrared observations are also limited to cloud-free conditions, which can cause data gaps and uncertainty in temporal analyses (Reiners et al., 2023). These factors may partly explain why LST showed weaker and less consistent relationships with the other indicators analysed in this study, particularly NDVI, NDWI, and fire occurrence.

The results suggest that LST is better interpreted as a supplementary indicator of environmental change rather than a direct measure of peatland degradation. Higher surface temperatures may reflect peat drying, vegetation loss, forest canopy removal, and hydrological disturbance, but they may also be influenced by short-term climatic conditions. Therefore, in this study, NDVI, MDWI, forest loss, and fire occurrence were considered the primary indicators of peatland degradation, while LST provided supporting information on environmental responses associated with degradation processes. Future studies could improve the interpretation of LST by incorporating longer time series, climate and precipitation data, drought indices, groundwater observations, and additional validation data to better distinguish climatic variability from degradation-related changes

Taken together, these findings indicate that hydrological change was the most consistent signal of peatland degradation in the study area. Vegetation decline appeared strongly linked to moisture loss, whereas fire occurrence and temperature patterns were influenced by additional short-term and local factors. Overall, the results support previous studies emphasizing that peatland hydrology is a key controlling factor in peatland ecosystem stability, vegetation condition, peat decomposition, and fire vulnerability (Ritzema et al., 2014; Taufik et al., 2019; Apers et al., 2022; Morris & Waddington, 2011).

6.3 Environmental drivers of peatland degradation

The results indicate that hydrological disturbance associated with drainage infrastructure is a major factor influencing peatland degradation in the study area (Dadap et al., 2021). Across multiple analyses, distance to drainage canals consistently emerged as one of the dominant explanatory variables (Astiani et al., 2017). Areas located closer to drainage canals generally showed stronger drying trends, reflected by lower NDWI slope values, while canal density was highest in the southern and central peatlands where degradation vulnerability was also concentrated.

These findings support previous studies showing that drainage lowers peat water tables, increases peat oxidation and subsidence, and enhances susceptibility to vegetation stress and fire (Hooijer et al., 2010; Taufik et al., 2019; Dadap et al., 2021). Previous studies have also shown that drainage canals can influence peat hydrology over large spatial areas, extending hundreds of meters from the canal network (Dadap et al., 2021).

The OLS results further support the importance of drainage proximity. Distance to canals remained significant in both model stages, while forest loss became significant when included in Stage II. However, the relatively low R^2 values and significant spatial autocorrelation in the residuals indicate that OLS alone was insufficient to fully explain the spatial complexity of peatland moisture change. Although distance-to-canal classes suggested slight variation in NDWI trends across peatland areas, the Pearson correlation between NDWI slope and distance to canals remained weak ($r = -0.217$). Together, these findings suggest that peatland degradation is not controlled by a single uniform process across the peatland landscape but instead varies according to local environmental conditions and disturbance intensity. Peatland moisture dynamics are influenced not only by drainage proximity but also by rainfall variability, vegetation cover, peat characteristics, restoration activities, and local hydrological connectivity (Hooijer et al., 2010; Taufik et al., 2019). In addition, NDWI slope represents temporal moisture change rather than absolute wetness conditions, meaning that positive NDWI trends near canals do not necessarily indicate undisturbed hydrological conditions. The grouped distance analysis further suggests that drainage effects may vary locally rather than following a simple linear relationship. Similar heterogeneity in peatland processes has been reported in previous studies emphasizing the importance of local hydrological variability and drainage effects (Belyea & Baird, 2006; Lampela et al., 2016).

The weak Pearson correlation between NDWI slope and distance to canals does not necessarily contradict the regression and Random Forest results, where drainage proximity remained an important explanatory variable. Pearson correlation only measures simple linear pairwise relationships and does not account for spatial variability, interactions among variables, or non-linear processes. In contrast, OLS, GWR, and Random Forest incorporate multiple environmental variables simultaneously and are therefore better able to capture the complex hydrological and spatial interactions influencing peatland conditions. This suggests that the influence of drainage canals on peatland degradation is spatially heterogeneous and may operate indirectly through interactions with vegetation disturbance, land-use change, and local hydrological conditions (Taufik et al..2019; Ritzema et al., 2007).

Forest loss was also associated with stronger drying trends in several parts of the peatland areas. This is consistent with previous studies showing that vegetation removal reduces canopy shading, increases surface exposure, and often occurs together with drainage expansion and agricultural conversion (Goldstein et al., 2020; Gaveau et al., 2022). The combined influence of drainage and forest loss likely reinforces peatland degradation processes, particularly in previously disturbed areas.

Previous studies have further shown that degraded peatlands are more vulnerable to recurrent burning and prolonged hydrological disturbance (Miettinen et al., 2016; Horton et al., 2021), potentially creating feedback loops in which repeated fire further accelerates degradation processes (Webb & Jamaludin, 2024).

Random Forest provided additional insight by capturing more complex and non-linear relationships between peatland moisture dynamics and environmental variables. While OLS and GWR identified distance to drainage canals as the most consistent predictor, Random Forest additionally highlighted distance to canal blocks and TWI as important variables. This does not contradict the regression analysis but instead suggests that these variables may influence peatland moisture dynamics through localized interactions and non-linear processes that are less effectively captured by linear regression models. Previous studies have noted that impurity-based variable importance measures in Random Forest may be influenced by correlated predictor variables and variable distributions (Scornet, 2021).

The importance of distance to canal blocks may also indicate that restoration infrastructure and water-management interventions influence peatland moisture conditions (Suwito et al., 2022), although canal blocks are spatially clustered and unevenly distributed across peatland areas. Previous studies have further shown that the effectiveness of canal blocking and peatland rewetting can vary depending on local hydrological conditions, canal spacing, restoration design, rainfall variability, and spatial differences in water-table dynamics (Suryadi et al., 2021; Mishra et al., 2021). Nevertheless, Suwito et al. (2022) demonstrated that even relatively small-scale canal blocking interventions can contribute to maintaining higher groundwater levels and reducing peatland drying and fire vulnerability in degraded tropical peatlands.

The land-cover analysis further supports this interpretation. Degraded vegetation areas showed the highest fire density and forest loss, indicating that previously disturbed peatlands remain vulnerable to recurrent burning and continued land-cover change. Built-up and agricultural areas also showed drying tendencies. Similar associations between recurrent fire and degraded forest conditions have also been observed in Southeast Asian tropical landscapes, where disturbed forests become increasingly susceptible to repeated burning over time (Webb & Jamaludin, 2024). However, the relatively high NDWI slope observed in degraded vegetation areas should not necessarily be interpreted as healthier peatland conditions. NDWI reflects changes in vegetation and surface moisture rather than direct groundwater levels (Gao, 1996). In degraded peatlands, drainage, vegetation removal, fire disturbance, exposed surfaces, shallow inundation, and vegetation regrowth mosaics can create heterogeneous moisture signals (Page et al., 2011; Miettinen et al., 2017; Taufik et al., 2019).

Taken together, the combined modelling results indicate that peatland degradation in Central Kalimantan is primarily driven by hydrological disturbance, with land-use change acting as an additional reinforcing factor. Drainage-related variables consistently showed stronger explanatory influence than vegetation class alone, highlighting the dominant role of hydrological disturbance in controlling peatland moisture dynamics. Drainage proximity appears more influential than vegetation class alone, supporting previous studies showing that peatland degradation processes intensify near drainage canals where water-table drawdown, vegetation disturbance, and fire occurrence are more pronounced (Ritzema et al., 2014; Sinclair et al., 2020; Dadap et al., 2021). These findings highlight the importance of hydrological management for peatland conservation and restoration. Effective restoration strategies should therefore prioritise hydrological recovery, particularly in heavily drained and previously deforested peatland areas.

6.4 Hypotheses assessment

H1 proposed that hydrological variables, particularly drainage canal proximity and Topographic Wetness Index (TWI), would be the strongest predictors explaining spatial variation in satellite-derived peatland degradation indicators (NDVI, NDWI, fire occurrence, and LST).

This hypothesis was partially supported**.** Drainage canal proximity consistently emerged as one of the dominant predictors across multiple analyses, confirming the importance of hydrological disturbance in explaining peatland degradation patterns. In contrast, TWI showed relatively weak and inconsistent influence across peatland areas. Fire occurrence showed only weak relationships with the analysed environmental variables, while LST was not included in the integrated degradation assessment due to data limitations and its relatively weak relationship with peatland moisture dynamics. These findings are consistent with previous studies showing that drainage strongly alters peatland hydrology and contributes to peat drying, vegetation stress, and fire susceptibility (Hooijer et al., 2010; Taufik et al., 2019; Dadap et al., 2021).

H2 proposed that relationships between peatland degradation indicators and environmental drivers would vary spatially across peatland areas rather than occurring uniformly.

This hypothesis was supported**.** OLS diagnostics indicated spatial non-stationarity, while GWR results demonstrated that the strength and influence of environmental variables differed between locations. This suggests that peatland degradation processes are spatially heterogeneous and influenced by local environmental conditions, hydrological connectivity, and disturbance intensity. Similar spatial variability in peatland hydrology and degradation processes has been reported in previous studies of tropical peatlands (Lampela et al., 2016; Morris & Waddington, 2011).

6.5 Limitations and Future Research

6.5.1 Remote Sensing Indicators and Data Limitations

Several limitations should be considered when interpreting the results of this study. The analysis primarily relied on satellite-derived indicators and spatial datasets rather than direct field measurements. Variables such as NDVI, NDWI, LST, fire detections, and forest loss are useful for identifying landscape-scale spatial patterns of peatland condition, but they do not directly measure key hydrological processes such as groundwater levels, peat moisture content, peat thickness variation, or peat subsidence. In addition, detailed climatic variables such as rainfall variability were not included within the scope of this study.

The indicators used in this study represent proxy measures of peatland degradation derived from remotely sensed observations. NDVI reflects vegetation condition, NDWI represents vegetation and surface moisture conditions, forest loss indicates canopy removal, and fire occurrence reflects disturbance events. Although these indicators cannot directly measure peat oxidation, carbon loss, groundwater dynamics, or peat subsidence, they capture important manifestations of peatland degradation and are widely used in tropical peatland monitoring. Therefore, the results should be interpreted as indirect assessments of peatland degradation rather than direct measurements of the underlying ecological and hydrological processes.

Land cover was represented using the ESA WorldCover 2021 dataset, which provides a snapshot of land-cover conditions during a single year. Although this dataset was useful for characterising landscape conditions within the study area, it does not directly capture land-cover transitions over time. Consequently, the interpretation of degraded vegetation classes was supported by historical tree-cover information from the Hansen Global Forest Change dataset (*Appendix A5*) and forest-loss patterns rather than relying solely on the 2021 land-cover classification.

6.5.2 Temporal and Climatic Uncertainty

Although multi-year satellite data were used for the period 2017–2025, image availability in tropical regions is strongly affected by persistent cloud cover. While cloud masking and dry-season image selection were applied to improve consistency, cloud contamination and data availability still affected the spatial coverage of some datasets, particularly Land Surface Temperature (LST), resulting in fewer valid observations in certain peatland areas.

In addition, NDVI and NDWI trends were derived using pixel-based linear trend analysis for the period 2017–2025. This approach assumes that vegetation and moisture changes follow approximately linear trends through time. However, peatland ecosystems may experience rapid changes, recovery periods, or short-term climatic fluctuations that are not fully captured by a linear trend. Consequently, the calculated trend values should be interpreted as general long-term trends rather than precise representations of interannual variability. Similar limitations apply to LST, where observed temperature patterns may reflect both environmental disturbance and interannual climatic variability.

6.5.3 Model and Degradation Map Uncertainty

The statistical models explained the observed spatial variation to a low degree, particularly in the global OLS models. This indicates that additional factors not included in the study may influence peatland moisture dynamics. Possible missing variables include rainfall variability, groundwater depth, peat thickness, water-management practices, canal condition, and local land-use history. These factors may help explain part of the remaining unexplained variation.

Although precipitation is an important variable of tropical peatland hydrology and influences peat moisture conditions, the present study focused primarily on drainage-related hydrological disturbance, terrain characteristics, and land-use factors. Future research could incorporate precipitation data, drought indices, and climate variability associated with ENSO events to better evaluate their influence on peatland moisture dynamics, fire occurrence, and degradation processes.

The peatland degradation map was produced by combining multiple indicators using a weighted overlay approach. Although the selected indicators were supported by previous literature, the assigned weights and classification thresholds may influence the final results. Different weighting choices could produce slightly different degradation patterns. Therefore, the map should be interpreted as a relative indication of peatland degradation within the study area rather than providing an exact measure of degradation.

The statistical analyses identified several relationships between degradation indicators and environmental variables. However, these relationships do not necessarily mean that one factor directly caused another. For example, moisture decline was associated with proximity to drainage canals, but other factors such as land-use history, restoration activities, and climatic variability may also contribute to the observed patterns. The results should therefore be interpreted as evidence of relationships between environmental factors and peatland degradation rather than direct proof of causation.

6.5.4 Canal Block Limitations and Future Research

The canal block dataset was used as a spatial proxy for restoration influence based on distance to canal-blocking structures. However, the presence of a canal block does not necessarily indicate functionality or successful hydrological restoration. The hydrological influence of canal blocks may vary spatially and is often limited to nearby or upstream areas. Some structures may be damaged, inactive, or vary in effectiveness depending on local maintenance and landscape conditions. In addition, although previous studies have shown that even relatively small-scale canal blocking interventions may contribute to maintaining higher groundwater levels and reducing peatland drying (Suwito et al., 2022), restoration effectiveness remains spatially heterogeneous and may differ considerably across peatland landscapes depending on local hydrological and environmental conditions.

Future research could further evaluate the effectiveness of canal-blocking restoration by conducting more focused comparative analyses between restored peatland areas and similar non-restored areas without canal blocking. An important limitation of the present study is that information on the construction dates and maintenance history of canal-blocking structures was not available. Canal blocks were therefore treated as static spatial features, and it was not possible to distinguish between older and more recently established restoration interventions. Integrating field-based hydrological measurements, rainfall data, peat-depth information, restoration history, and long-term monitoring could improve understanding of how restoration interventions influence peatland moisture dynamics, vegetation recovery, and fire vulnerability under different environmental conditions. In addition, the use of higher temporal resolution satellite data, groundwater monitoring, and hydrological modelling could provide better insight into how drainage and restoration influence peatland dynamics over time. Similar integrated approaches combining remote sensing, field observations, and hydrological modelling have also been recommended in previous tropical peatland restoration studies (Mishra et al., 2021).

7 CONCLUSION

This study analysed how hydrological conditions, drainage patterns, terrain characteristics, and land-use disturbances influence peatland degradation in Central Kalimantan between 2017 and 2025 using remote sensing and GIS-based approaches. The results showed that peatland degradation is spatially heterogeneous, with major hotspots concentrated in the southern and central peatland regions where vegetation decline, moisture reduction, forest loss, and fire occurrence overlapped.

The findings consistently highlight the critical role of hydrological disturbance in shaping peatland degradation patterns. Areas located closer to drainage canals generally showed stronger drying trends and higher degradation vulnerability, indicating that drainage strongly influences peatland functioning. The results further suggest that peatland degradation is driven by interacting hydrological and land-use processes rather than by a single uniform factor, with relationships varying spatially, across the peatland landscape according to local environmental conditions and disturbance intensity.

The study also showed that vegetation dynamics and moisture-related conditions were closely linked, while fire occurrence appeared to be influenced by additional climatic and anthropogenic factors beyond long-term vegetation and moisture trends alone.

From a management perspective, the findings emphasise the importance of hydrological restoration, particularly in heavily drained peatland areas and identified degradation hotspots. Restoration measures such as canal blocking, peatland rewetting, and revegetation are important for improving peatland resilience and reducing further degradation.

Overall, this study demonstrates the usefulness of integrating remote sensing and spatial modelling techniques to analyse tropical peatland degradation in data-limited regions. Understanding the spatial patterns and environmental drivers of peatland degradation is essential for effective peatland management, restoration, and long-term conservation in Central Kalimantan.

REFERENCES

Aldrian, E., & Dwi Susanto, R. (2003). Identification of three dominant rainfall regions within Indonesia and their relationship to sea surface temperature. *International Journal of Climatology, 23*(12), 1435–1452. https://doi.org/10.1002/joc.950

Anda, M., Ritung, S., Suryani, E., Sukarman, Hikmat, M., Yatno, E., Mulyani, A., Subandiono, R. E., Suratman, Husnain, Suratman, & Husnain. (2021). Revisiting tropical peatlands in Indonesia: Semi-detailed mapping, extent and depth distribution assessment. *Geoderma, 402,* 115235. https://doi.org/10.1016/j.geoderma.2021.115235

Apers, S., De Lannoy, G. J. M., Baird, A. J., Cobb, A. R., Dargie, G. C., del Aguila Pasquel, J., Gruber, A., Hastie, A., Hidayat, H., Hirano, T., Hoyt, A. M., Jovai-Sancho, A. J., Katimon, A., Kurnain, A., Koster, R. D., Lampela, M., Mahanama, S. P. P., Melling, L., Page, S. E., Reichle, R. H., Taufik, M., Vanderborght, J., & Bechtold, M. (2022). Tropical peatland hydrology simulated with a global land surface model. *Journal of Advances in Modeling Earth Systems*, *14*(3). Article e2021MS002784. https://doi.org/10.1029/2021MS002784

Astiani, D., Burhanuddin, Curran, L. M., Mujiman; Salim, R. (2017). Effect of Drainage ditches on water table level, soil condition and tree growth of degraded peatland forests in West Kalimantan. *Indonesian Journal of Forestry Research, 4*(1). https://doi.org/10.20886/ijfr.2017.4.1.15-25

Belyea, L. R., & Baird, A. J. (2006). Beyond "The limits to peat bog growth": Cross-scale feedback in peatland development. *Ecological Monographs, 76*(3), 299–322. https://doi.org/10.1890/0012-9615(2006)076[0299:BTLTPB]2.0.CO;2 (esajournals.onlinelibrary.wiley.com)

Breiman, L. (2001). Random forests. Machine Learning, 45(1), 5–32. https://doi.org/10.1023/A:1010933404324

Brunsdon, C., Fotheringham, A. S., & Charlton, M. E. (1996). Geographically Weighted Regression: A Method for Exploring Spatial Nonstationarity. *Geographical Analysis, 28*(4), 281–298. https://doi.org/10.1111/j.1538-4632.1996.tb00936.x

Badan Restorasi Gambut dan Mangrove (BRGM). (2026). Drainage canal and canal block dataset. Peatland and Mangrove Restoration Agency, Indonesia.

Chai, T., & Draxler, R. R. (2014). Root mean square error (RMSE) or mean absolute error (MAE)? Arguments against avoiding RMSE in the literature. *Geoscientific Model Development, 7,* 1247–1250. https://doi.org/10.5194/gmd-7-1247-2014

Choy, Y.K. & Onuma, A. (2025). The Tropical Peatlands in Indonesia and Global Environmental Change: A Multi-Dimensional System-Based Analysis and Policy Implications. *Reg. Sci. Environ. Econ., 217*. https://doi.org/10.3390/rsee2030017

Cobb, A. R., Hoyt, A. M., Gandois, L., Eri, J., Dommain, R., Salim, K. A., Kai, F. M., Su'ut, N. S. H., Harvey, C. F. (2017). How temporal patterns in rainfall determine the geomorphology and carbon fluxes of tropical peatlands. *Proceedings of the National Academy of Sciences, 114*(26), Article E5187–E5196. https://doi.org/10.1073/pnas.1701090114

Cochrane, M. (2003). Fire science for rainforests. *Nature 421*, 913–919. https://doi.org/10.1038/nature01437

Comber, A., Brunsdon, C., Charlton, M., Dong, G., Harris, R., Lu, B., Lu, Y., Murakami, D., Nakaya, T., Wang, Y., & Harris, P. (2023). The GWR route map: A guide to the informed application of geographically weighted regression. *International Journal of Geographical Information Science, 37*(3), 588–630. https://doi.org/10.1080/13658816.2022.2161739

European Space Agency (ESA). (Year). *Sentinel-2 data*. Copernicus Open Access Hub. https://scihub.copernicus.eu/

Curran, L. M., Trigg, S. N., McDonald, A. K., Astiani, D., Hardiono, Y. M., Siregar, P., Caniago, I., & Kasischke, E. (1999). Impact of El Niño and logging on canopy tree recruitment in Borneo. *Science, 286*(5447), 2184–2188. https://doi.org/10.1126/science.286.5447.2184

Dadap, N. C., Hoyt, A. M., Cobb, A. R., Oner, D., Kozinski, M, Fua, P. V., Harvey, C. F., Konings, A. G. (2021). Drainage canals in Southeast Asian peatlands increase carbon emissions. *AGU Advances, 2*, Article e2020AV000321. https://doi.org/10.1029/2020AV000321

Dargie, G. C., Lewis, S. L., Lawson, I. T., Mitchard, E. T. A., Page, S. E., Bocko, Y. E., & Ifo, S. A. (2017). Age, extent and carbon storage of the central Congo Basin peatland complex. *Nature, 542*(7639), 86–90. https://doi.org/10.1038/nature21048

Dommain, R., Joosten, H., & Couwenberg, J. (2010). Hydrological self-regulation of domed peatlands in south-east Asia and consequences for conservation and restoration. *Mires and Peat, 6*, 1–17. https://doi.org/10.19189/001c.128357

European Space Agency (ESA). (2021). *ESA WorldCover 2021 Land Cover Map*. https://worldcover2021.esa.int/

European Space Agency (ESA). (2026a). *Copernicus Sentinel-2 Level-2A imagery*. Copernicus Data Space Ecosystem. https://dataspace.copernicus.eu/

European Space Agency (ESA). (2026b). *Copernicus DEM GLO-30 digital elevation model*. Copernicus Programme. https://registry.opendata.aws/copernicus-dem/

ESRI. (2023). *Ordinary Least Squares (OLS)* tool documentation.

Esri. (2024). *How Hot Spot Analysis (Getis-Ord Gi*) works*. ArcGIS Pro Documentation. https://pro.arcgis.com/en/pro-app/latest/tool-reference/spatial-statistics/h-how-hot-spot-analysis-getis-ord-gi-spatial-stati.htm

Esri. (2024). *How Spatial Autocorrelation (Global Moran's I) works*. ArcGIS Pro Documentation. https://pro.arcgis.com/

Esri. (2026). *World Topographic Map* [basemap]. Sources: Esri, TomTom, Garmin, FAO, NOAA, USGS.

European Commission. (2021). *Copernicus Digital Elevation Model (COP-DEM-GLO-30)*. Retrieved from https://registry.opendata.aws/copernicus-dem/

Field, R. D., van der Werf, G. R., & Shen, S. S. P. (2016). Human amplification of drought-induced biomass burning in Indonesia since 1960. *Nature Geoscience, 9*, 443–447. DOI: https://doi.org/10.1038/ngeo2686

Fotheringham, A. S., Brunsdon, C., & Charlton, M. (2002). Geographically weighted regression: The analysis of spatially varying relationships. Wiley. https://doi.org/10.1111/j.1538-4632.2003.tb01114.x

GADM. (2023). *Global Administrative Areas database*. https://gadm.org/

Gallant, J. C., & Hutchinson, M. F. (2011). A differential equation for specific catchment area. *Water Resources Research, 47*, Article W05535. https://doi.org/10.1029/2010WR009859

Gao, B-C. (1996). NDWI-A normalized difference water index for remote sensing of vegetation liquid water from space. *Remote Sensing of Environment, 58*(3), 257–266. DOI: https://doi.org/10.1016/S0034-4257(96)00067-3

Gaveau, D. L. A., Locatelli, B., Salim, M. A., Husnayaen, Manurung, T., Descals, A., Angelsen, A., Meijaard, E., & Sheil, D. (2022). *Slowing deforestation in Indonesia follows declining oil palm expansion and lower oil prices*. PLOS ONE, 17(3), Article e0266178. https://doi.org/10.1371/journal.pone.0266178

Getis, A., & Ord, J. K. (1992). The analysis of spatial association by use of distance statistics. *Geographical Analysis, 24*(3), 189–206. https://doi.org/10.1111/j.1538-4632.1992.tb00261.x

Global Forest Watch. (2026) Global Forest Change dataset. *World Resource Institute.* http;//www.globalforestwatch.org/

Giglio, L., Schroeder, W., & Justice, C. O. (2016). The collection 6 MODIS active fire detection algorithm and fire products. *Remote Sensing of Environment, 178*, 31–41. DOI: 10.1016/j.rse.2016.02.054

Girkin, N. T., Cooper, H. V., Ledger, M. J., O'Reilly, P., Thornton, S. A., Åkesson, C. M., Cole, L. E. S., Hapsari, K. A., Hawthorne, D., & Roucoux, K. H. (2022). Tropical peatlands in the Anthropocene: The present and the future. *Anthropocene*, 40, Article 100354. https://doi.org/10.1016/j.ancene.2022.100354

Goldstein, J. E., Graham, L., Ansori, S., Vetrita, Y., Thomas, A., Applegate, G., Vayda, A. P., Saharjo, B. H. & Cochrane, M. A, (2020). Beyond slash-and-burn: The roles of human activities, altered hydrology and fuels in peat fires in Central Kalimantan, Indonesia. *Singapore Journal of Tropical Geography*, *41*, 190-208. doi:10.1111/sjtg.12319

Google. (2021). *Google Earth imagery of south-eastern Central Kalimantan, Indonesia* [Satellite image]. Google Earth Web. Retrieved April 23, 2026, from https://earth.google.com/

GRID-Arendal, 2024. *Peatland drainage and degradation conceptual illustration*. Available at: https://www.grida.no/resources/12535 [Accessed 11 May 2026].

Grosvenor, M. J., Ardiyani, V, Wooster, M. J., Gilott, S., Green, D C., Lestari, P., Suri, W. (2024). Catastrophic impact of extreme 2019 Indonesian peatland fires on urban air quality and health. *Communications Earth & Environment*, 5, Article 649. https://doi.org/10.1038/s43247-024-01813-w

Hansen, M. C., Potapov P. V., Moore, R., Hancher, M., Turubanova, S. A., Tyukavina, A., Thau, D., Stehman, S. V., Goetz, S. J., Loveland, T. R., Kommareddy, A., Egorov, A., Chini, L., Justice, C. O., & Townshend, J. R. G. (2013). High-resolution global maps of 21st-century forest cover change. *Science, 342*(6160), 850–853. https://doi.org/10.1126/science.1244693

Hirano, T., Ohkubo, S., Itoh, M., Tsuzuki, H., Sakabe, A., Takahashi, H., Kusin, K., & Osaki, M. (2024). Large variation in carbon dioxide emissions from tropical peat swamp forests due to disturbances. *Communications Earth & Environment, 5* (1), 1–9. https://doi.org/10.1038/s43247-024-01387-7

Hooijer, A., Page, S., Jauhiainen, J., Lee, W. A., Lu, X. X., Idris, A., & Anshari, G. (2012). Subsidence and carbon loss in drained tropical peatlands. *Biogeosciences, 9*(3), 1053–1071.https://doi.org/10.5194/bg-9-1053-2012

Horton, A. J., Virkki, V., Lounela, A., Miettinen, J., Alibakhshi, S., & Kummu, M. (2021). Identifying key drivers of peatland fires across Kalimantan's ex-Mega Rice Project using machine learning. *Earth and Space Science, 8*, e2021EA001873. https://doi.org/10.1029/2021EA001873

Justice, C. O., Román-Cuesta, R. M., Roy, D. P., et al. (2011). The satellite-based active fire detection record of tropical forest fires. *Remote Sensing of Environment, 115,* 272–285.

Kamlun, K. U., & Phua, M. H. (2024). Anthropogenic influences on deforestation of a peat swamp forest in Northern Borneo using remote sensing and GIS. *Forest Systems, 33*(1), Article eSC02. https://doi.org/10.5424/fs/2024331-20585

KLHK. 2026. *KHG-FEG Dataset*. Directorate of Peat Ecosystem Protection and Management, Ministry of Environment and Forestry, Indonesia.

Konecny, K., Ballhorn, U., Navratil, P., Jubanski, J., Page, S. E., Tansey, K., Hooijer, A., Vernimmen, R., & Siegert, F. (2016). Variable carbon losses from recurrent fires in drained tropical peatlands. *Global Change Biology, 22*(4), 1469–1480. https://doi.org/10.1111/gcb.13186

Kopecký, M., Macek, M., & Wild, J. (2021). Topographic Wetness Index calculation guidelines based on measured soil moisture and plant species composition. *Science of the Total Environment, 757.* Article 143785. https://doi.org/10.1016/j.scitotenv.2020.143785

Lam, T., Catto, J.L., Kay, G., Dunstone, N., Barciela, R. & Harper, A. B. (2026). Major fires in Indonesian Borneo are possible under all ENSO phases. *npj Nat. Hazards 3*(46). https://doi.org/10.1038/s44304-026-00209-4

Lampela, M., Jauhiainen, J., Kämäri, I., Koskinen, M., Tanhuanpää, T., Valkeapää, A. & Vasander, H. (2016). Ground surface microtopography and vegetation patterns in a tropical peat swamp forest. *CATENA, 139,*1 27-136. https://doi.org/10.1016/j.catena.2015.12.016

Langner, A., Miettinen, J., & Siegert, F. (2007). Land cover change 2002–2005 in Borneo and the role of fire derived from MODIS imagery. *Global Change Biology, 13,* 2329–2340. https://doi.org/10.1111/j.1365-2486.2007.01442.x

Leifeld, J., Wüst-Galley, C., & Page, S. (2019). Intact and managed peatland soils as a source and sink of GHGs from 1850 to 2100. *Nature Climate Change, 9*(12), 945–947. https://doi.org/10.1038/s41558-019-0615-5

Lindsay, R. (2018). *Peatlands and carbon: A critical synthesis*. Royal Society of Edinburgh.

Louppe, G., Wehenkel, L., Sutera, A., & Geurts, P. (2013). Understanding variable importances in forests of randomized trees. *Advances in Neural Information Processing Systems, 26*, 431–439.

Manepalli, U. R. R., Bham, G. H., & Kandada, S. (2011). Evaluation of hotspots identification using Kernel Density Estimation (K) and Getis-Ord (Gi) on I-630*. *Paper presented at the 3rd International Conference on Road Safety and Simulation, Indianapolis, USA.*

Matthews, S. A., & Yang, T.-C. (2012). Mapping the results of local statistics: Using geographically weighted regression. *Demographic Research, 26*, 151–166. https://doi.org/10.4054/DemRes.2012.26.6

Miettinen, J., Shi, C., & Liew, S. C. (2011). *Deforestation rates in insular Southeast Asia between 2000 and 2010*. Global Change Biology, *17*(7), 2261–2270. https://doi.org/10.1111/j.1365-2486.2011.02591.x

Miettinen, J., Shi, C., & Liew, S. C. (2017). Fire distribution in peninsular Malaysia, Sumatra and Borneo in 2015 with special emphasis on peatland fires. *Environmental Management, 60,* 747–757.

Miettinen, J., Shi, C., & Liew, S. C. (2016). Land cover distribution in the peatlands of Peninsular Malaysia, Sumatra and Borneo in 2015 with changes since 1990. *Global Ecology and Conservation*, 6, 67–78. https://doi.org/10.1016/j.gecco.2016.02.004

Ministry of Environment and Forestry (KLHK). (2026). *Peatland Hydrological Unit (KHG-FEG 2026) dataset*. Indonesia.

Mishra, S., Page, S. E., Cobb, A. R., Lee, J. S. H., Jovani-Sancho, A. J., Sjögersten, S., Jaya, A., Aswandi, & Wardle, D. A. (2021). Degradation of Southeast Asian tropical peatlands and integrated strategies for their better management and restoration. *Journal of Applied Ecology, 58*(7), 1370–1387. https://doi.org/10.1111/1365-2664.13905

Morris; P. J. & Waddington, J. M. (2011). Groundwater residence time distributions in peatlands: Implication for peatland decomposition and accumulation. *Water Resource Research, 47.* Article W02511. doi:10.1029/2010WR009492

NASA. (2026). *FIRMS; Fire Information for Resource Management System.* https://firms.modaps.eosdis.nasa.gov/

Nazeer, M., & Bilal, M. (2017). Evaluation of Ordinary Least Square (OLS) and Geographically Weighted Regression (GWR) for Water Quality Monitoring: A Case Study for the Estimation of Salinity. *Journal of Ocean University of China, 17*(2). 305-310. 10.1007/s11802-018-3380-6

Novitasari, N., Sujono, J., Harto, S., Maas, A., & Jayadi, R. (2018). Restoration of peat dome in ex-Mega rice project area in Central Kalimantan. *AIP Conf. Proc. (1977).* Article 040008. https://doi-org.ludwig.lub.lu.se/10.1063/1.5042978

Nguyen, H.T., Hutyra, L. R., Hardiman, B.S., & Raciti, S. M. (2016). Characterizing forest structure variations across an intact tropical peat dome using field samplings and airborne LiDAR. *Ecological Applications, 26*(2), 587–601. https://doi.org/10.1890/15-0017

Ohkubo, S., Hirano, T., & Kusin, K. (2021). Influence of fire and drainage on evapotranspiration in a degraded peat swamp forest in Central Kalimantan, Indonesia. *Journal of Hydrology, 603,* Article 126906. https://doi.org/10.1016/j.jhydrol.2021.126906

Page, S. E., Siegert, F., Rieley, J. O., Boehm, H-D. V., Jaya, A., & Limin, S. (2002). The amount of carbon released from peat and forest fires in Indonesia during 1997. *Nature, 420,* 61–65.

Page, S. E., Rieley, J. O., & Wüst, R. (2006). Chapter 7 Lowland tropical peatlands of Southeast Asia. *In I. P. Martini, A. Martínez Cortizas, & W. Chesworth (Eds.), Peatlands: Evolution and records of environmental and climate changes*, *Elsevier,* 145–172. https://doi.org/10.1016/S0928-2025(06)09007-9

Page, S., Hoscilo, A., & Wösten, H. (2009). Restoration Ecology of Lowland Tropical Peatlands in Southeast Asia: Current Knowledge and Future Research Directions. *Ecosystem. 12*(6), 888-905. https://doi.org/10.1007/s10021-008-9216-2

Page, S. E., & Baird, A. J. (2016). Peatlands and global change: Response and resilience. *Annual Review of Environment and Resources, 41*, 35–57. DOI: https://doi.org/10.1146/annurev-environ-110615-085520

Page, S. E., Rieley, J. O., & Banks, C. J. (2011). Global and regional importance of the tropical peatland carbon pool. *Global Change Biology, 17*, 798–818. DOI:10.1111/j.1365-2486.2010. 02279.x

Peatland and Mangrove Restoration Agency (BRGM). (2022). *Drainage canal dataset*. Indonesia.

Pedregosa, F., Varoquaux, G., Gramfort, A., Michel, V., Thirion, B., Grisel, O., Blondel, M., Prettenhofer, P., Weiss, R., Dubourg, V., Vanderplas, J., Passos, A., Cournapeau, D., Brucher, M., Perrot, M., & Duchesnay, É. (2011). Scikit-learn: Machine learning in Python. *Journal of Machine Learning Research, 12*, 2825–2830.

Pettorelli, N., Vik, J. O., Mysterud, A., Gaillard, J-M., Tucker, C. J., & Stenseth, N. C. (2005). Using the satellite-derived NDVI to assess ecological responses to environmental change. *Trends in Ecology & Evolution, 20*(9), 503–510. DOI: https://doi.org/10.1016/j.tree.2005.05.011

Reiners, P., Sobtrino. J., & Kuenzer. C. (2023). Satellite-Derived Land Surface Temperature Dynamics in the Context of Global Change-A Review. Remote Sens.15, 1857. https://doi.org/10.3390/rs15071857

Ritzema, H. (2007). The role of drainage in the wise use of tropical Peatlands. Proceedings of the International Symposium and Workshop on Tropical Peatland, Yogyakarta, Indonesia, 27–29 August 2007.

Rouse, J. W., Haas, R. H., Schell, J. A., & Deering, D. W. (1974). Monitoring vegetation systems in the Great Plains with ERTS. *NASA Special Publication,* 351,309-317.

Ruwaimana; M., Gavin, D. G., & Anshari, G. (2024). Interplay of Climate, Fire, Floods, and Anthropogenic Impact on Peat Formation and Carbon dynamic of Coastal and Inland Tropical Peatlands in West Kalimantan, Indonesia. *Ecosystem, 27*, 361–375. https://doi.org/10.1007/s10021-023-00882-w

Salmayenti, R., Baird, A. J., Holden, J., & Spracklen, D. V. (2025). Drainage density and land cover interact to affect fire occurrence in Indonesian peatlands. *Environmental Research Letters, 20,* Article 054036. https://doi.org/10.1088/1748-9326/adc755

Saputra, A. D., Irfan, M., Khakim, M. Y. N., & Iskandar, I. (2026). Impact of Tropical Climate Anomalies on Land Cover Changes in Sumatra's Peatlands, Indonesia. *Sustainability, 18* (2) Article 919. https://doi.org/10.3390/su18020919

Schroeder, W., Oliva, P., Giglio, L., & Csiszar, I. A. (2014). The New VIIRS 375 m active fire detection data product: Algorithm description and initial assessment. *Remote Sensing of Environment, 143*, 85–96. https://doi.org/10.1016/j.rse.2013.12.008

Scornet, E. (2021). Trees, forests, and impurity-based variable importance [Preprint]. *HAL Open Science*. HAL Id: hal-02436169v3. https://hal.science/hal-02436169v3

Simorangkir, D. (2007). Fire use: Is it really the cheaper land preparation method for large-scale plantations? *Mitig Adapt Strat Glob Change, 12*, 147–164. DOI: 10.1007/s11027-006-9049-2

Sinclair, A. L., Graham, L. L. B., Putra, E. I., Saharjo, B. H., Applegate, G., Grover, S. P. & Cochrane, M.A. (2020). Effect of distance from canal and degradation history of peat bulk density in a degraded tropical peatland. *Science of The Total Environment* (699), Article 134199. https://doi-org.ludwig.lub.lu.se/10.1016/j.scitotenv.2019.134199

Suryadi, Y., Soekarno, I., & Humam, I. A. (2021). Effectiveness Analysis of Canal Blocking in Sub-peatland Hydrological Unit 5 and 6 Kahayan Sebangau, Central Kalimantan, Indonesia. *Eng. Technol. Sci., 53*(2), Article 210205. DOI: 10.5614/j.eng.technol.sci.2021.53.2.5

Suwito, E., Marpaung, E. J., Dharmawan, I. W. S., Wibisono, I. T. C., Dohong, A., & Jaya, A. (2022). The effectiveness of canal blocking for peatland restoration in ex-burnt peat swamp forest in Central Kalimantan, Indonesia. *Biodiversitas, 23*(3), 1485–1494. https://doi.org/10.13057/biodiv/d230339

Taufik, M., Setiawan, B. I., & Van Lanen, H. A. J. (2019). Exploring the importance of physical properties of tropical peat soils in determining fire vulnerability. *Geoderma, 347***,** 17–28. https://doi.org/10.1016/j.geoderma.2019.04.001

Toumbourou, T. D., Lestari, S., Yuwati, T. W., Treby, S., Winarno, B., Rachmanadi, D., Idrus, N. I., Sakuntaladewi, N., Budiningsih, K., Grover, S. P. P., &

Rawluk, A. (2024). Principles for equitable and resilient tropical peatland restoration in Central Kalimantan, Indonesia. *Restoration Ecology, 32*(7). Article e14221. https://doi.org/10.1111/rec.14221

Treby, S., Jayasekara, C., Idrus, N. I., Ningsih, S. N. A., Graham, L. L. B., Hutley, L., Beringer, J., & Grover, S. (2024). Evapotranspiration from a drained tropical peatland undergoing restoration [Preprint]. https://doi.org/10.22541/au.173400323.34938181/v1

Tucker, C. J. (1979). Red and photographic infrared linear combinations for monitoring vegetation. *Remote Sensing of Environment, 8,* 127–150. http://dx.doi.org/10.1016/0034-4257(79)90013-0

Turetsky, M. R., Benscoter, B., Page, S., et al. (2015). Global vulnerability of peatlands to fire and carbon loss. *Nature Geoscience, 8*, 11–14. DOI: 10.1038/ngeo2325

United States Geological Survey (USGS). (2026). *Landsat 8–9 Operational Land Imager/Thermal Infrared Sensor (OLI/TIRS) Collection 2 Level-2 data*. U.S. Geological Survey. https://earthexplorer.usgs.gov/

Webb, E. L., & Jamaludin, J. (2024) Fire is associated with forest degradation and economic land concessions, but not land conversion in the rapidly transforming Cambodian landscape. *Environmental Research Letters 19*(9), Article 094005. https://doi.org/10.1088/1748-9326/ad6678

Weng, Q. (2009). Thermal infrared remote sensing for urban climate and environmental studies: Methods, applications, and trends. *ISPRS Journal of Photogrammetry and Remote Sensing, 64*(4), 335–344. https://doi.org/10.1016/j.isprsjprs.2009.03.007

Yan, K., Gao, S., Yan, G., Ma, X., Chen, X., Zhu, P., Li, J., Gao, S., Gastellu-Etchegorry, J-P., Myneni, R. B. & Wang, Q. (2025). A global systematic review of the remote sensing vegetation indices. *International Journal of Applied Earth Observation and Geoinformation, 139,* Article 104560. http://doi.org/10.1016/j.jag.2025.104560

Zheng, H., Xue, L., Ding, K., Lou, S., Wang, Z., Ding, A., & Huang, X. (2023). Enso-Related Fire Weather Change in Southeast and Equatorial Asia: A Quantitative Evaluation Using Fire Weather Index. *Journal of Geographical Research: Atmospheres, 128*(21). Article e2023JD039688. https://doi.org/10.1029/2023JD039688

APPENDICES

Appendix A1

Sentinel-2 Data Acquisition and Tile Coverage (2017–2025)

Sentinel-2 Level-2A imagery used in this study was acquired during the dry-season period (July–September) for each year between 2017 and 2025. Images were selected based on cloud conditions and temporal consistency. Four Sentinel-2 Military Grid Reference System (MGRS) tiles were required to cover the study area: T49MGS, T49MHS, T49MHT, and T50MKC. Multiple scenes per year were mosaicked and processed to generate annual composites for NDVI and NDWI analysis.

Table A1- Sentinel data acquisition and Tile Coverage (2017-2025)

YEAR	July	August	September	Tiles used			
2017*	20170720	0	0	T49MGS	T49MHS	T49MHT	T50MKC
	20170725			T49MGS	T49MHS	T49MHT	T50MKC
2018	20180720	20180814	20180923	T49MGS	T49MHS	T49MHT	T50MKC
2019	20190725	20190829	20190928	T49MGS	T49MHS	T49MHT	T50MKC
2020	20200714	20200729	20200823	T49MGS	T49MHS	T49MHT	T50MKC
2021	20210724	20210808	20210927	T49MGS	T49MHS	T49MHT	T50MKC
2022	20220729	20220808	20220922	T49MGS	T49MHS	T49MHT	T50MKC
2023	20230729	20230818	20230922	T49MGS	T49MHS	T49MHT	T50MKC
2024	20240718	20240728	20240911	T49MGS	T49MHS	T49MHT	T50MKC
2025	20250725	20250802	20250923	T49MGS	T49MHS	T49MHT	T50MKC

* An exception occurred in 2017, when persistent cloud covers limited image availability during August and September.

Sentinel-2 Level-2A imagery provided the spectral bands used for NDVI (B4, B8), NDWI (B8A, B12), and Scene Classification Layer (SCL) cloud masking.

Appendix A2

Drainage canal and canal blocks in Peatland area

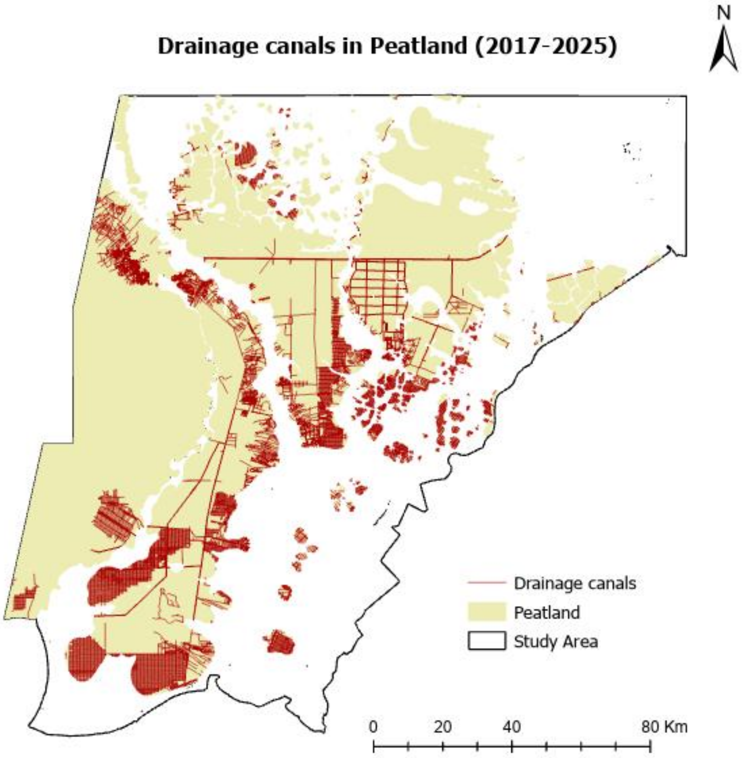

Figure A2a. Spatial distribution of mapped drainage canals within peatland areas

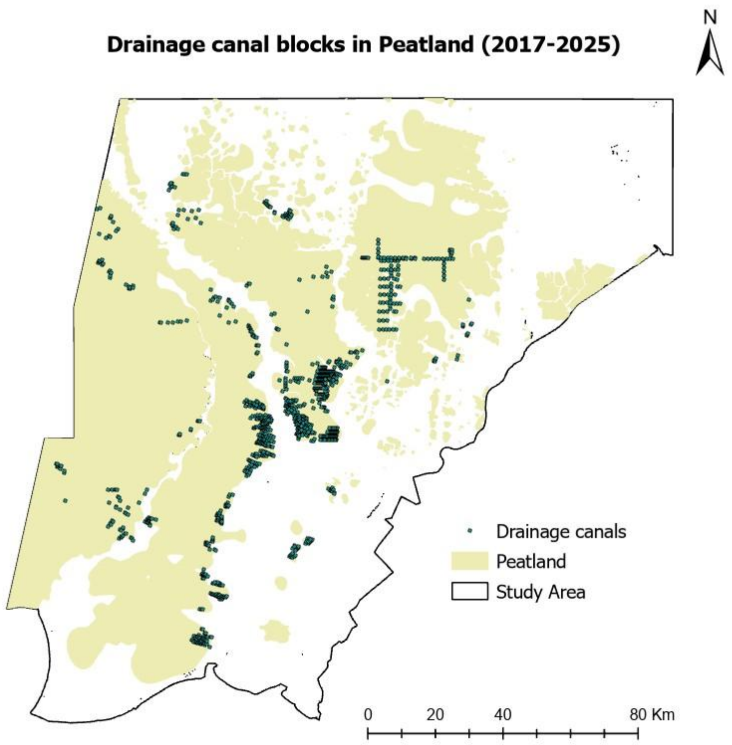

Figure A2b. Spatial distribution of mapped canal blocking structures within peatland areas

Appendix A3

Original ESA WorldCover 2021 land-cover composition within the study area

The land-cover distribution within the study area in 2021 is shown in *Figure 4.2.*

The landscape is dominated by tree cover (69.04%), indicating that large portions of the region remain covered by forest vegetation. Grassland (14.54%) and shrubland (9.28%) also occupy substantial areas, particularly within disturbed and partially degraded peatland regions. Smaller proportions of the study area consist of cropland (2.65%), herbaceous wetlands (1.75%), permanent water bodies (1.69%), mangroves (0.59%), and built-up areas (0.34%) *(Figure 3.2).*

Wetlands and mangrove areas are mainly concentrated along river corridors and coastal zones, whereas cropland and built-up areas are more localized and associated with human land-use activities (Figure 4.2).

The spatial distribution of land-cover classes reflects the heterogeneous environmental conditions and varying levels of disturbance across the peatland landscape in Central Kalimantan.

Appendix A4

Descriptive statistics of Peatland indicators and environmental variables (2017–2025)

Table A4a. Descriptive statistics of Peatland indicators and environmental variables (2017–2025)

Variables	Mean	Min	Max	Std Dev	Resolution	Period
NDVI MAX Trend	-0.054	-2.407	2.858	0.225	10 m	2017–2025
NDVI mean	0.507	-0.130	0.719	0.059	10 m	2017–2025
NDVI slope (per	0.002	-0.160	0.092	0.011	10 m	2017–2025
NDWI mean	0.410	-0.364	0.641	0.083	20 m	2017–2025
NDWI slope	0.003	-0.118	0.085	0.011	20 m	2017–2025
LST mean	32.693	24.176	50.831	2.825	30 m	2017–2025
LST slope	0.350	-2.794	2.550	0.417	30 m	2017–2026
Distance to canals	4724.721	0	41676.203	6775.457	10 m	Static
Canal density	1.136	0	15.756	1.895	10 m	Static
TWI	6.048	-5.841	24.700	7.328	101,74 m	Static
Fire density	0.094	0	6.382	0.337	1 km	2017–2025

Table A4b. Forest loss summary within study area (2017–2024)

Variable	% Area	Total area (km²)	Period
Forest loss	6.59%	1526.5 km²	2017–2024

Values represent pixel-level or raster summary statistics within the study area unless otherwise stated.

Appendix A5

Tree Cover within Peatland Areas, 2000

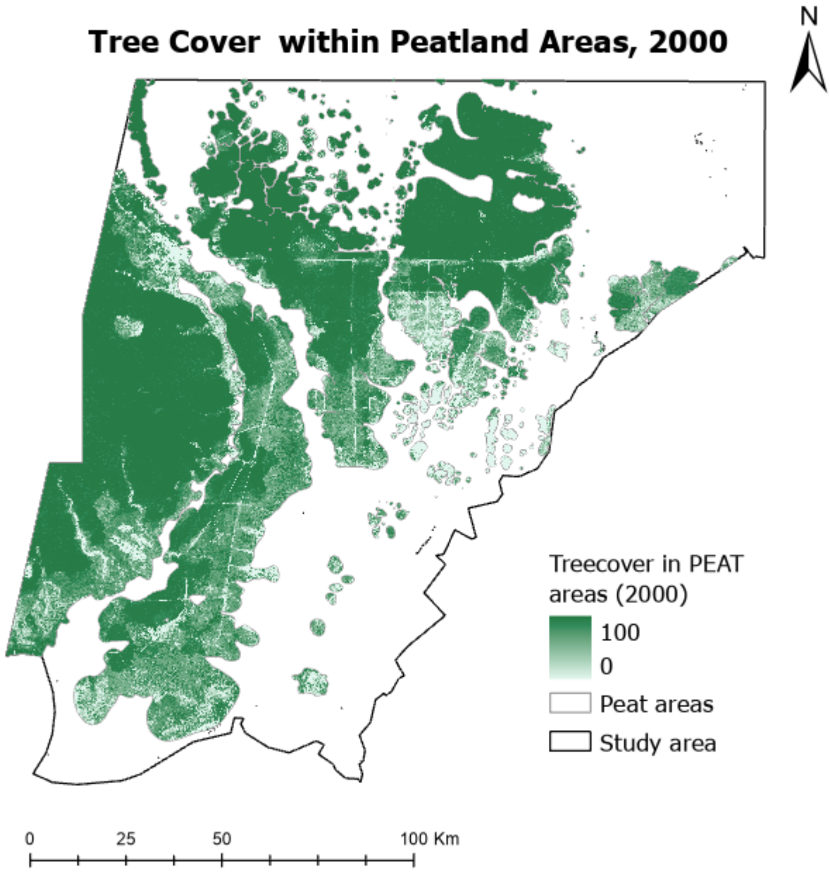

Figure A5. Tree cover within peatland areas in 2000 derived from the Hansen Global Forest Change dataset (Hansen et al., 2013).

The figure illustrates that large portions of the peatland landscape were historically forested prior to subsequent forest loss and land-cover change. This information was used as supporting evidence when interpreting land-cover classes in the 2021 ESA WorldCover dataset.

Appendix A6

Reclassification thresholds and forest-loss classification used for peatland degradation mapping

Table A6. Threshold values used for peatland degradation reclassification

Indicators	Degradation influence		
	High	Moderate	Low
NDVI slope	-0.139 to -0.020	-0.020 to 0.000	0.000 to -0.076
NDWI slope	-0.102 to -0.010	-0.010 to 0.000	0.000 to -0.083
TWI	4.58 to 5	5 to 10	10 to 24.33
Fire density	2 to 6.38	0.5 to 2	0 to 0.5
Forest loss	2017 to 2020	2021 to 2024	No forest loss
Distance to drainage canal	0 to 500 (m)	500 to 2000 (m)	>2000 (m)

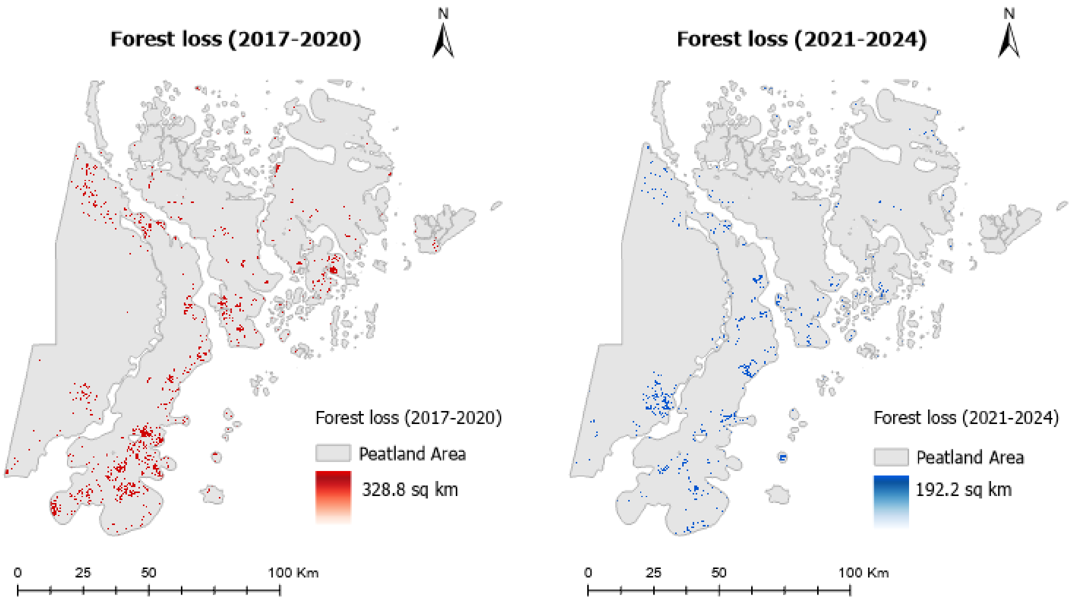

Figure A6. Forest-loss classification used in the integrated peatland degradation analysis

Forest-loss classes were grouped into 2017–2020 and 2021–2024 periods based on mapped forest-loss extent within peatland areas.

Appendix A7

Spatial pattern of maximum NDVI trends for the period 2017–2025

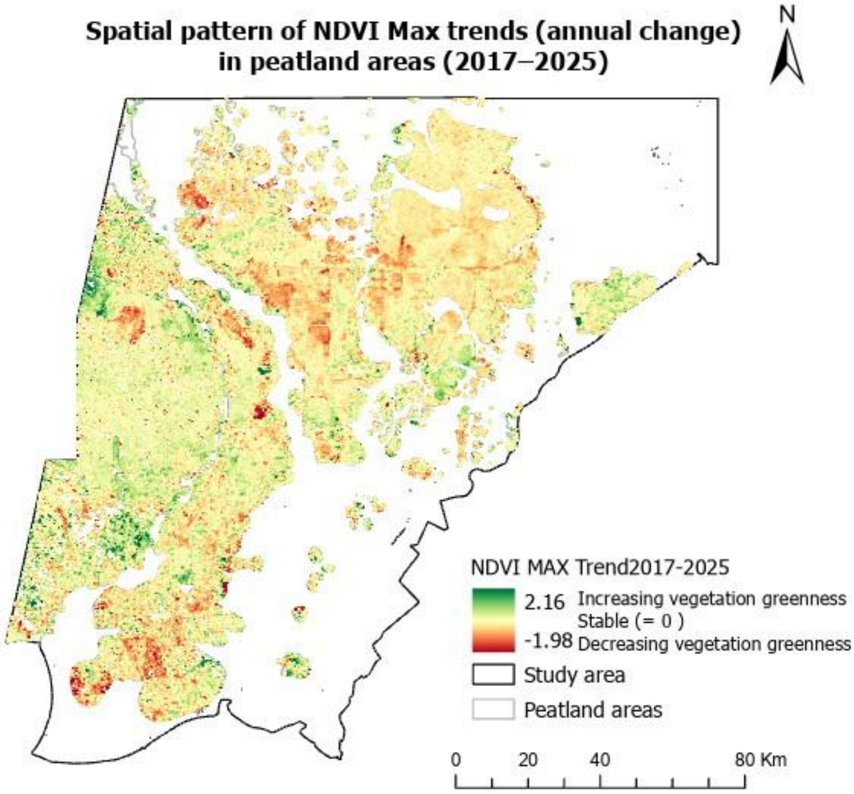

Figure A7. Spatial pattern of maximum NDVI trends for the period 2017–2025, representing peak vegetation greenness reached at least once during the study period.

The maximum NDVI trend values range approximately from −1.98 to 2.16. The values show distinct spatial heterogeneity across the study area. Areas with high maximum NDVI values are unevenly distributed and form distinct spatial patterns that differ from those observed in the mean NDVI and NDVI temporal trend maps.

This indicates that locations capable of achieving high peak vegetation greenness do not necessarily maintain consistently high vegetation conditions over time. The maximum NDVI trend values range approximately from -2.41 to 2.86, reflecting substantial spatial variability in peak vegetation dynamics across the peatland landscape.

Appendix A8

OLS Regression results for NDWI slope (Stage I and Stage II)

Table A8a. OLS diagnostics

Statistic	Value	
	Stage I	Stage II
R^2	0.0470	0.0782
Adjusted R^2	0.0467	0.0778
AIC	-82,964.7810	-83,343.7833
Koenker (BP) statistic	357.7871	722.6975
Moran's I (residual)	0.4424	0.4441

Table A8b. OLS regression coefficient- Stage I

Variable	Coefficient	Std Error	t-value	p-value	VIF
Distance to canals	-0.000000	0.000000	-21.796803	0.000000*	1.24758
Canal density	-0.000033	0.000030	-0.871158	0.464665	1.305014
TWI	-0.000013	0.000020	-0.490987	0.688540	1.105528
Fire density	-0.000082	0.000148	-0.556995	0.690306	1.054457

Table A8c. OLS regression coefficient- Stage II

Variable	Coefficient	Std Error	t-value	p-value	VIF
Distance to canals	-0.000000	0.000000	-25.944702	0.000000*	1.310896
Canal density	0.000103	0.000038	2.703105	0.024590*	1.349535
TWI	0.000022	0.000025	0.879371	0.469726	1.110971
Fire density	0.000784	0.000151	5.185532	0.000282*	1.152051
Forest loss	-0.001158	0.000059	-19.677850	0.000000*	1.330954

Note: * indicates a statistically significant p-value ($p < 0.001$). VIF values close to 1 indicate low multicollinearity.

Note:

R^2 represents the proportion of variance explained by the model, while adjusted R^2 accounts for the number of predictors. AIC evaluates model fit, with lower values indicating better performance. The Koenker (BP) statistic tests for spatial non-stationarity, where significant values indicate spatially varying relationships. Moran's I measure spatial autocorrelation in model residuals, with positive values indicating clustering. The associated z-score indicates the statistical significance of this pattern.

The t-value represents the ratio between the estimated coefficient and its standard error, indicating the strength of the relationship. The p-value indicates the statistical significance of each variable, with lower values representing stronger evidence against the null hypothesis. VIF (Variance Inflation Factor) measures multicollinearity among variables, where values close to 1 indicate low correlation between predictors.

Appendix A9

Spatial variation in the Local Effect of TWI (GWR Stage II)

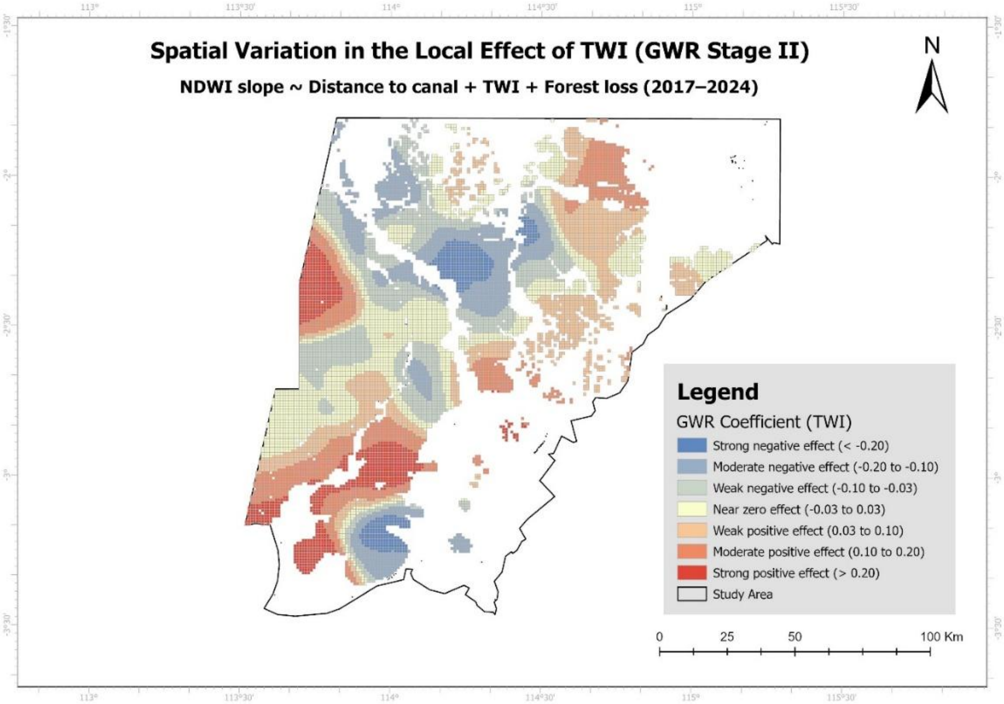

Figure A9. Spatial distribution of GWR Standardized Residual (GWR Stage II)

Series from Lund University

Department of Physical Geography and Ecosystem Science

Master Thesis in Geographical Information Science

1. *Anthony Lawther:* The application of GIS-based binary logistic regression for slope failure susceptibility mapping in the Western Grampian Mountains, Scotland (2008).
2. *Rickard Hansen:* Daily mobility in Grenoble Metropolitan Region, France. Applied GIS methods in time geographical research (2008).
3. *Emil Bayramov:* Environmental monitoring of bio-restoration activities using GIS and Remote Sensing (2009).
4. *Rafael Villarreal Pacheco:* Applications of Geographic Information Systems as an analytical and visualization tool for mass real estate valuation: a case study of Fontibon District, Bogota, Columbia (2009).
5. *Siri Oestreich Waage:* a case study of route solving for oversized transport: The use of GIS functionalities in transport of transformers, as part of maintaining a reliable power infrastructure (2010).
6. *Edgar Pimiento:* Shallow landslide susceptibility – Modelling and validation (2010).
7. *Martina Schäfer:* Near real-time mapping of floodwater mosquito breeding sites using aerial photographs (2010).
8. *August Pieter van Waarden-Nagel:* Land use evaluation to assess the outcome of the programme of rehabilitation measures for the river Rhine in the Netherlands (2010).
9. *Samira Muhammad:* Development and implementation of air quality data mart for Ontario, Canada: A case study of air quality in Ontario using OLAP tool. (2010).
10. *Fredros Oketch Okumu*: Using remotely sensed data to explore spatial and temporal relationships between photosynthetic productivity of vegetation and malaria transmission intensities in selected parts of Africa (2011).
11. *Svajunas Plunge:* Advanced decision support methods for solving diffuse water pollution problems (2011).

12. *Jonathan Higgins:* Monitoring urban growth in greater Lagos: A case study using GIS to monitor the urban growth of Lagos 1990 - 2008 and produce future growth prospects for the city (2011).

13. *Mårten Karlberg:* Mobile Map Client API: Design and Implementation for Android (2011).

14. *Jeanette McBride:* Mapping Chicago area urban tree canopy using color infrared imagery (2011).

15. *Andrew Farina:* Exploring the relationship between land surface temperature and vegetation abundance for urban heat island mitigation in Seville, Spain (2011).

16. *David Kanyari*: Nairobi City Journey Planner: An online and a Mobile Application (2011).

17. *Laura V. Drews:* Multi-criteria GIS analysis for siting of small wind power plants - A case study from Berlin (2012).

18. *Qaisar Nadeem:* Best living neighborhood in the city - A GIS based multi criteria evaluation of ArRiyadh City (2012).

19. *Ahmed Mohamed El Saeid Mustafa:* Development of a photo voltaic building rooftop integration analysis tool for GIS for Dokki District, Cairo, Egypt (2012).

20. *Daniel Patrick Taylor*: Eastern Oyster Aquaculture: Estuarine Remediation via Site Suitability and Spatially Explicit Carrying Capacity Modeling in Virginia's Chesapeake Bay (2013).

21. *Angeleta Oveta Wilson:* A Participatory GIS approach to *unearthing* Manchester's Cultural Heritage '*gold mine'* (2013).

22. *Ola Svensson:* Visibility and Tholos Tombs in the Messenian Landscape: A Comparative Case Study of the Pylian Hinterlands and the Soulima Valley (2013).

23. *Monika Ogden:* Land use impact on water quality in two river systems in South Africa (2013).

24. *Stefan Rova:* A GIS based approach assessing phosphorus load impact on Lake Flaten in Salem, Sweden (2013).

25. *Yann Buhot:* Analysis of the history of landscape changes over a period of 200 years. How can we predict past landscape pattern scenario and the impact on habitat diversity? (2013).

26. *Christina Fotiou:* Evaluating habitat suitability and spectral heterogeneity models to predict weed species presence (2014).
27. *Inese Linuza:* Accuracy Assessment in Glacier Change Analysis (2014).
28. *Agnieszka Griffin:* Domestic energy consumption and social living standards: a GIS analysis within the Greater London Authority area (2014).
29. *Brynja Guðmundsdóttir:* Detection of potential arable land with remote sensing and GIS - A Case Study for Kjósarhreppur (2014).
30. *Oleksandr Nekrasov:* Processing of MODIS Vegetation Indices for analysis of agricultural droughts in the southern Ukraine between the years 2000-2012 (2014).
31. *Sarah Tressel:* Recommendations for a polar Earth science portal in the context of Arctic Spatial Data Infrastructure (2014).
32. *Caroline Gevaert:* Combining Hyperspectral UAV and Multispectral Formosat-2 Imagery for Precision Agriculture Applications (2014).
33. *Salem Jamal-Uddeen:* Using GeoTools to implement the multi-criteria evaluation analysis - weighted linear combination model (2014).
34. *Samanah Seyedi-Shandiz:* Schematic representation of geographical railway network at the Swedish Transport Administration (2014).
35. *Kazi Masel Ullah:* Urban Land-use planning using Geographical Information System and analytical hierarchy process: case study Dhaka City (2014).
36. *Alexia Chang-Wailing Spitteler:* Development of a web application based on MCDA and GIS for the decision support of river and floodplain rehabilitation projects (2014).
37. *Alessandro De Martino:* Geographic accessibility analysis and evaluation of potential changes to the public transportation system in the City of Milan (2014).
38. *Alireza Mollasalehi:* GIS Based Modelling for Fuel Reduction Using Controlled Burn in Australia. Case Study: Logan City, QLD (2015).
39. *Negin A. Sanati:* Chronic Kidney Disease Mortality in Costa Rica; Geographical Distribution, Spatial Analysis and Non-traditional Risk Factors (2015).
40. *Karen McIntyre:* Benthic mapping of the Bluefields Bay fish sanctuary, Jamaica (2015).

41. *Kees van Duijvendijk:* Feasibility of a low-cost weather sensor network for agricultural purposes: A preliminary assessment (2015).

42. *Sebastian Andersson Hylander:* Evaluation of cultural ecosystem services using GIS (2015).

43. *Deborah Bowyer:* Measuring Urban Growth, Urban Form and Accessibility as Indicators of Urban Sprawl in Hamilton, New Zealand (2015).

44. *Stefan Arvidsson:* Relationship between tree species composition and phenology extracted from satellite data in Swedish forests (2015).

45. *Damián Giménez Cruz*: GIS-based optimal localisation of beekeeping in rural Kenya (2016).

46. *Alejandra Narváez Vallejo:* Can the introduction of the topographic indices in LPJ-GUESS improve the spatial representation of environmental variables? (2016).

47. *Anna Lundgren:* Development of a method for mapping the highest coastline in Sweden using breaklines extracted from high resolution digital elevation models (2016).

48. *Oluwatomi Esther Adejoro:* Does location also matter? A spatial analysis of social achievements of young South Australians (2016).

49. *Hristo Dobrev Tomov:* Automated temporal NDVI analysis over the Middle East for the period 1982 - 2010 (2016).

50. *Vincent Muller:* Impact of Security Context on Mobile Clinic Activities A GIS Multi Criteria Evaluation based on an MSF Humanitarian Mission in Cameroon (2016).

51. *Gezahagn Negash Seboka:* Spatial Assessment of NDVI as an Indicator of Desertification in Ethiopia using Remote Sensing and GIS (2016).

52. *Holly Buhler:* Evaluation of Interfacility Medical Transport Journey Times in Southeastern British Columbia. (2016).

53. *Lars Ole Grottenberg*: Assessing the ability to share spatial data between emergency management organisations in the High North (2016).

54. *Sean Grant:* The Right Tree in the Right Place: Using GIS to Maximize the Net Benefits from Urban Forests (2016).

55. *Irshad Jamal:* Multi-Criteria GIS Analysis for School Site Selection in Gorno-Badakhshan Autonomous Oblast, Tajikistan (2016).

56. *Fulgencio Sanmartín:* Wisdom-volkano: A novel tool based on open GIS and time-series visualization to analyse and share volcanic data (2016).

57. *Nezha Acil:* Remote sensing-based monitoring of snow cover dynamics and its influence on vegetation growth in the Middle Atlas Mountains (2016).

58. *Julia Hjalmarsson:* A Weighty Issue: Estimation of Fire Size with Geographically Weighted Logistic Regression (2016).

59. *Mathewos Tamiru Amato:* Using multi-criteria evaluation and GIS for chronic food and nutrition insecurity indicators analysis in Ethiopia (2016).

60. *Karim Alaa El Din Mohamed Soliman El Attar:* Bicycling Suitability in Downtown, Cairo, Egypt (2016).

61. *Gilbert Akol Echelai:* Asset Management: Integrating GIS as a Decision Support Tool in Meter Management in National Water and Sewerage Corporation (2016).

62. *Terje Slinning:* Analytic comparison of multibeam echo soundings (2016).

63. *Gréta Hlín Sveinsdóttir:* GIS-based MCDA for decision support: A framework for wind farm siting in Iceland (2017).

64. *Jonas Sjögren:* Consequences of a flood in Kristianstad, Sweden: A GIS-based analysis of impacts on important societal functions (2017).

65. *Nadine Raska:* 3D geologic subsurface modelling within the Mackenzie Plain, Northwest Territories, Canada (2017).

66. *Panagiotis Symeonidis*: Study of spatial and temporal variation of atmospheric optical parameters and their relation with PM 2.5 concentration over Europe using GIS technologies (2017).

67. *Michaela Bobeck:* A GIS-based Multi-Criteria Decision Analysis of Wind Farm Site Suitability in New South Wales, Australia, from a Sustainable Development Perspective (2017).

68. *Raghdaa Eissa*: Developing a GIS Model for the Assessment of Outdoor Recreational Facilities in New Cities Case Study: Tenth of Ramadan City, Egypt (2017).

69. *Zahra Khais Shahid*: Biofuel plantations and isoprene emissions in Svea and Götaland (2017).

70. *Mirza Amir Liaquat Baig*: Using geographical information systems in epidemiology: Mapping and analyzing occurrence of diarrhea in urban - residential area of Islamabad, Pakistan (2017).

71. *Joakim Jörwall*: Quantitative model of Present and Future well-being in the EU-28: A spatial Multi-Criteria Evaluation of socioeconomic and climatic comfort factors (2017).

72. *Elin Haettner*: Energy Poverty in the Dublin Region: Modelling Geographies of Risk (2017).

73. *Harry Eriksson*: Geochemistry of stream plants and its statistical relations to soil- and bedrock geology, slope directions and till geochemistry. A GIS-analysis of small catchments in northern Sweden (2017).

74. *Daniel Gardevärn:* PPGIS and Public meetings – An evaluation of public participation methods for urban planning (2017).

75. *Kim Friberg:* Sensitivity Analysis and Calibration of Multi Energy Balance Land Surface Model Parameters (2017).

76. *Viktor Svanerud:* Taking the bus to the park? A study of accessibility to green areas in Gothenburg through different modes of transport (2017).

77. *Lisa-Gaye Greene*: Deadly Designs: The Impact of Road Design on Road Crash Patterns along Jamaica's North Coast Highway (2017).

78. *Katarina Jemec Parker*: Spatial and temporal analysis of fecal indicator bacteria concentrations in beach water in San Diego, California (2017).

79. *Angela Kabiru*: An Exploratory Study of Middle Stone Age and Later Stone Age Site Locations in Kenya's Central Rift Valley Using Landscape Analysis: A GIS Approach (2017).

80. *Kristean Björkmann*: Subjective Well-Being and Environment: A GIS-Based Analysis (2018).

81. *Williams Erhunmonmen Ojo*: Measuring spatial accessibility to healthcare for people living with HIV-AIDS in southern Nigeria (2018).

82. *Daniel Assefa*: Developing Data Extraction and Dynamic Data Visualization (Styling) Modules for Web GIS Risk Assessment System (WGRAS). (2018).

83. *Adela Nistora*: Inundation scenarios in a changing climate: assessing potential impacts of sea-level rise on the coast of South-East England (2018).

84. *Marc Seliger*: Thirsty landscapes - Investigating growing irrigation water consumption and potential conservation measures within Utah's largest master-planned community: Daybreak (2018).

85. *Luka Jovičić*: Spatial Data Harmonisation in Regional Context in Accordance with INSPIRE Implementing Rules (2018).

86. *Christina Kourdounouli*: Analysis of Urban Ecosystem Condition Indicators for the Large Urban Zones and City Cores in EU (2018).

87. *Jeremy Azzopardi*: Effect of distance measures and feature representations on distance-based accessibility measures (2018).

88. *Patrick Kabatha*: An open source web GIS tool for analysis and visualization of elephant GPS telemetry data, alongside environmental and anthropogenic variables (2018).

89. *Richard Alphonce Giliba*: Effects of Climate Change on Potential Geographical Distribution of Prunus africana (African cherry) in the Eastern Arc Mountain Forests of Tanzania (2018).

90. *Eiður Kristinn Eiðsson*: Transformation and linking of authoritative multi-scale geodata for the Semantic Web: A case study of Swedish national building data sets (2018).

91. *Niamh Harty*: HOP!: a PGIS and citizen science approach to monitoring the condition of upland paths (2018).

92. *José Estuardo Jara Alvear*: Solar photovoltaic potential to complement hydropower in Ecuador: A GIS-based framework of analysis (2018).

93. *Brendan O'Neill*: Multicriteria Site Suitability for Algal Biofuel Production Facilities (2018).

94. *Roman Spataru*: Spatial-temporal GIS analysis in public health – a case study of polio disease (2018).

95. *Alicja Miodońska*: Assessing evolution of ice caps in Suðurland, Iceland, in years 1986 - 2014, using multispectral satellite imagery (2019).

96. *Dennis Lindell Schettini*: A Spatial Analysis of Homicide Crime's Distribution and Association with Deprivation in Stockholm Between 2010-2017 (2019).

97. *Damiano Vesentini*: The Po Delta Biosphere Reserve: Management challenges and priorities deriving from anthropogenic pressure and sea level rise (2019).

98. *Emilie Arnesten*: Impacts of future sea level rise and high water on roads, railways and environmental objects: a GIS analysis of the potential effects of increasing sea levels and highest projected high water in Scania, Sweden (2019).

99. *Syed Muhammad Amir Raza*: Comparison of geospatial support in RDF stores: Evaluation for ICOS Carbon Portal metadata (2019).

100. *Hemin Tofiq*: Investigating the accuracy of Digital Elevation Models from UAV images in areas with low contrast: A sandy beach as a case study (2019).

101. *Evangelos Vafeiadis*: Exploring the distribution of accessibility by public transport using spatial analysis. A case study for retail concentrations and public hospitals in Athens (2019).

102. *Milan Sekulic*: Multi-Criteria GIS modelling for optimal alignment of roadway by-passes in the Tlokweng Planning Area, Botswana (2019).

103. *Ingrid Piirisaar*: A multi-criteria GIS analysis for siting of utility-scale photovoltaic solar plants in county Kilkenny, Ireland (2019).

104. *Nigel Fox*: Plant phenology and climate change: possible effect on the onset of various wild plant species' first flowering day in the UK (2019).

105. *Gunnar Hesch*: Linking conflict events and cropland development in Afghanistan, 2001 to 2011, using MODIS land cover data and Uppsala Conflict Data Programme (2019).

106. *Elijah Njoku*: Analysis of spatial-temporal pattern of Land Surface Temperature (LST) due to NDVI and elevation in Ilorin, Nigeria (2019).

107. *Katalin Bunyevácz*: Development of a GIS methodology to evaluate informal urban green areas for inclusion in a community governance program (2019).

108. *Paul dos Santos*: Automating synthetic trip data generation for an agent-based simulation of urban mobility (2019).

109. *Robert O' Dwyer*: Land cover changes in Southern Sweden from the mid-Holocene to present day: Insights for ecosystem service assessments (2019).

110. *Daniel Klingmyr*: Global scale patterns and trends in tropospheric NO2 concentrations (2019).

111. *Marwa Farouk Elkabbany*: Sea Level Rise Vulnerability Assessment for Abu Dhabi, United Arab Emirates (2019).

112. *Jip Jan van Zoonen*: Aspects of Error Quantification and Evaluation in Digital Elevation Models for Glacier Surfaces (2020).

113. *Georgios Efthymiou*: The use of bicycles in a mid-sized city – benefits and obstacles identified using a questionnaire and GIS (2020).

114. *Haruna Olayiwola Jimoh*: Assessment of Urban Sprawl in MOWE/IBAFO Axis of Ogun State using GIS Capabilities (2020).

115. *Nikolaos Barmpas Zachariadis*: Development of an iOS, Augmented Reality for disaster management (2020).

116. *Ida Storm*: ICOS Atmospheric Stations: Spatial Characterization of CO2 Footprint Areas and Evaluating the Uncertainties of Modelled CO2 Concentrations (2020).

117. *Alon Zuta*: Evaluation of water stress mapping methods in vineyards using airborne thermal imaging (2020).

118. *Marcus Eriksson*: Evaluating structural landscape development in the municipality Upplands-Bro, using landscape metrics indices (2020).

119. *Ane Rahbek Vierø*: Connectivity for Cyclists? A Network Analysis of Copenhagen's Bike Lanes (2020).

120. *Cecilia Baggini*: Changes in habitat suitability for three declining Anatidae species in saltmarshes on the Mersey estuary, North-West England (2020).

121. *Bakrad Balabanian*: Transportation and Its Effect on Student Performance (2020).

122. *Ali Al Farid*: Knowledge and Data Driven Approaches for Hydrocarbon Microseepage Characterizations: An Application of Satellite Remote Sensing (2020).

123. *Bartlomiej Kolodziejczyk*: Distribution Modelling of Gene Drive-Modified Mosquitoes and Their Effects on Wild Populations (2020).

124. *Alexis Cazorla*: Decreasing organic nitrogen concentrations in European water bodies - links to organic carbon trends and land cover (2020).

125. *Kharid Mwakoba*: Remote sensing analysis of land cover/use conditions of community-based wildlife conservation areas in Tanzania (2021).

126. *Chinatsu Endo*: Remote Sensing Based Pre-Season Yellow Rust Early Warning in Oromia, Ethiopia (2021).

127. *Berit Mohr*: Using remote sensing and land abandonment as a proxy for long-term human out-migration. A Case Study: Al-Hassakeh Governorate, Syria (2021).

128. *Kanchana Nirmali Bandaranayake*: Considering future precipitation in delineation locations for water storage systems - Case study Sri Lanka (2021).

129. *Emma Bylund*: Dynamics of net primary production and food availability in the aftermath of the 2004 and 2007 desert locust outbreaks in Niger and Yemen (2021).

130. *Shawn Pace*: Urban infrastructure inundation risk from permanent sea-level rise scenarios in London (UK), Bangkok (Thailand) and Mumbai (India): A comparative analysis (2021).

131. *Oskar Evert Johansson*: The hydrodynamic impacts of Estuarine Oyster reefs, and the application of drone technology to this study (2021).

132. *Pritam Kumarsingh*: A Case Study to develop and test GIS/SDSS methods to assess the production capacity of a Cocoa Site in Trinidad and Tobago (2021).

133. *Muhammad Imran Khan*: Property Tax Mapping and Assessment using GIS (2021).

134. *Domna Kanari*: Mining geosocial data from Flickr to explore tourism patterns: The case study of Athens (2021).

135. *Mona Tykesson Klubien*: Livestock-MRSA in Danish pig farms (2021).

136. *Ove Njøten*: Comparing radar satellites. Use of Sentinel-1 leads to an increase in oil spill alerts in Norwegian waters (2021).

137. *Panagiotis Patrinos*: Change of heating fuel consumption patterns produced by the economic crisis in Greece (2021).

138. *Lukasz Langowski*: Assessing the suitability of using Sentinel-1A SAR multi-temporal imagery to detect fallow periods between rice crops (2021).

139. *Jonas Tillman*: Perception accuracy and user acceptance of legend designs for opacity data mapping in GIS (2022).

140. *Gabriela Olekszyk*: ALS (Airborne LIDAR) accuracy: Can potential low data quality of ground points be modelled/detected? Case study of 2016 LIDAR capture over Auckland, New Zealand (2022).

141. *Luke Aspland*: Weights of Evidence Predictive Modelling in Archaeology (2022).

142. *Luís Fareleira Gomes*: The influence of climate, population density, tree species and land cover on fire pattern in mainland Portugal (2022).

143. *Andreas Eriksson*: Mapping Fire Salamander (Salamandra salamandra) Habitat Suitability in Baden-Württemberg with Multi-Temporal Sentinel-1 and Sentinel-2 Imagery (2022).

144. *Lisbet Hougaard Baklid*: Geographical expansion rate of a brown bear population in Fennoscandia and the factors explaining the directional variations (2022).

145. *Victoria Persson*: Mussels in deep water with climate change: Spatial distribution of mussel (Mytilus galloprovincialis) growth offshore in the French Mediterranean with respect to climate change scenario RCP 8.5 Long Term and Integrated Multi-Trophic Aquaculture (IMTA) using Dynamic Energy Budget (DEB) modelling (2022).

146. *Benjamin Bernard Fabien Gérard Borgeais*: Implementing a multi-criteria GIS analysis and predictive modelling to locate Upper Palaeolithic decorated caves in the Périgord noir, France (2022).

147. *Bernat Dorado-Guerrero*: Assessing the impact of post-fire restoration interventions using spectral vegetation indices: A case study in El Bruc, Spain (2022).

148. *Ignatius Gabriel Aloysius Maria Perera*: The Influence of Natural Radon Occurrence on the Severity of the COVID-19 Pandemic in Germany: A Spatial Analysis (2022).

149. *Mark Overton*: An Analysis of Spatially-enabled Mobile Decision Support Systems in a Collaborative Decision-Making Environment (2022).

150. *Viggo Lunde*: Analysing methods for visualizing time-series datasets in open-source web mapping (2022).

151. *Johan Viscarra Hansson*: Distribution Analysis of Impatiens glandulifera in Kronoberg County and a Pest Risk Map for Alvesta Municipality (2022).

152. *Vincenzo Poppiti*: GIS and Tourism: Developing strategies for new touristic flows after the Covid-19 pandemic (2022).

153. *Henrik Hagelin*: Wildfire growth modelling in Sweden - A suitability assessment of available data (2023).

154. *Gabriel Romeo Ferriols Pavico*: Where there is road, there is fire (influence): An exploratory study on the influence of roads in the spatial patterns of Swedish wildfires of 2018 (2023).

155. *Colin Robert Potter*: Using a GIS to enable an economic, land use and energy output comparison between small wind powered turbines and large-scale wind farms: the case of Oslo, Norway (2023).

156. *Krystyna Muszel*: Impact of Sea Surface Temperature and Salinity on Phytoplankton blooms phenology in the North Sea (2023).

157. *Tobias Rydlinge*: Urban tree canopy mapping - an open source deep learning approach (2023).

158. *Albert Wellendorf*: Multi-scale Bark Beetle Predictions Using Machine Learning (2023).

159. *Manolis Papadakis*: Use of Satellite Remote Sensing for Detecting Archaeological Features: An Example from Ancient Corinth, Greece (2023).

160. *Konstantinos Sourlamtas*: Developing a Geographical Information System for a water and sewer network, for monitoring, identification and leak repair - Case study: Municipal Water Company of Naoussa, Greece (2023).

161. *Xiaoming Wang*: Identification of restoration hotspots in landscape-scale green infrastructure planning based on model-predicted connectivity forest (2023).

162. *Sarah Sienaert*: Usability of Sentinel-1 C-band VV and VH SAR data for the detection of flooded oil palm (2023).

163. *Katarina Ekeroot*: Uncovering the spatial relationships between Covid-19 vaccine coverage and local politics in Sweden (2023).

164. *Nikolaos Kouskoulis*: Exploring patterns in risk factors for bark beetle attack during outbreaks triggered by drought stress with harvester data on attacked trees: A case study in Southeastern Sweden (2023).

165. *Jonas Almén*: Geographic polarization and clustering of partisan voting: A local-level analysis of Stockholm Municipality (2023).

166. *Sara Sharon Jones*: Tree species impact on Forest Fire Spread Susceptibility in Sweden (2023).

167. *Takura Matswetu*: Towards a Geographic Information Systems and Data-Driven Integration Management. Studying holistic integration through spatial accessibility of services in Tampere, Finland. (2023).

168. *Duncan Jones*: Investigating the influence of the tidal regime on harbour porpoise *Phocoena phocoena* distribution in Mount’s Bay, Cornwall (2023).

169. *Jason Craig Joubert*: A comparison of remote sensed semi-arid grassland vegetation anomalies detected using MODIS and Sentinel-3, with anomalies in ground-based eddy covariance flux measurements (2023).

170. *Anastasia Sarelli*: Land cover classification using machine-learning techniques applied to fused multi-modal satellite imagery and time series data (2024).

171. *Athanasios Senteles*: Integrating Local Knowledge into the Spatial Analysis of Wind Power: The case study of Northern Tzoumerka, Greece (2024).

172. *Rebecca Borg:* Using GIS and satellite data to assess access of green area for children living in growing cities (2024).

173. *Panagiotis–Dimitrios Tsachageas*: Multicriteria Evaluation in Real Estate Land-use Suitability Analysis: The case of Volos, Greece (2024).

174. *Hugo Nilsson*: Inferring lane-level topology of signalised intersections from aerial imagery and OpenStreetMap using deep learning (2024).

175. *Pavlos Alexantonakis*: Estimating lake water volume fluctuations using Sentinel-2 and ICESat-2 remote sensing data (2024).

176. *Karl-Martin Wigen*: Physical barriers and where to find them (2024).

177. *Martin Storsnes*: Temporal RX-algorithm performance on Sentinel-2 images (2024).

178. *Saulė Gabrielė Petraitytė*: The Relation Between Covid-19 Vaccination and Voting Trends in Lithuania: A Spatial Analysis (2024).

179. *Pedro Martinez Duran*: Olive yield forecasting from remote sensing and climate datasets in the Jaen province (Spain) (2024).

180. *Josefine Kynde Hämberg*: Proximity to Urban Green Spaces for Older Adults in Specific Housings - a Case Study of Malmö, Sweden (2024).

181. *Max Bengtsson*: A Site Selection of An Energy Island in the North Sea: Optimal Location in an Ecological and an Economic Scenario Using a Multicriteria Decision Analysis (MCDA) (2024).

182. *Anna Börmann*: Assessing Great Britain as a relocation site for the threatened Iberian Lynx in a changing climate (2024).

183. *Josephine Roosli*: Flood Risk Assessment for the Kävlinge River for Present and Future Climate Scenarios using HEC-RAS Rain-on-Grid (2024).

184. *Seán Flanagan*: Spatiotemporal dynamics of E-scooter sharing ridership and their associations with the built environment: A Swedish comparative study (2024).

185. *Wouter Vorsters*: Assessing the Impact of Combined Sewer Overflow on the Habitat of Lampetra planeri: A Case Study in Flanders, Belgium (2025).

186. *Kathleen Macdonald*: Cetacean strandings on the Scottish coast: coastal accessibility factors lead to underreporting (2025).

187. *Athanasios Emmanouil Mourampetzis*: Navigating the Shadows: A Comparative Analysis of SAR and Optical Imagery for Detecting (Dark) Vessels (2025).

188. *Nizam-ud-Din*: Spatial Land Records System using Geospatial Techniques: a case study of a Mid-Sized Village in Pakistan (2025).

189. *Nedim Nasic Kjellgren*: Linked Geodata: Improving Rooftop Photovoltaic Production Estimates through BIM-GIS Integration using Semantic Web Technologies (2025).

190. *Vedrana Pretkovic*: Spatio-temporal vegetation changes in the Pacific-Chocó region of Colombia during the conflict and post-conflict periods (2025).

191. *Evelina Bengtsson*: A Socioeconomic Dimension of Crime: A Spatial Study of Firearm-related Violence in Malmö (2025).

192. *Martynas Bielinis*: Application of C-band Radar Interferometry for Dune Monitoring in the Curonian Spit (2025).

193. *Paulina Magdalena Rieke*: Case study of the benefits of BIM and GIS solutions used on a live infrastructure project (2025).

194. *Alina Schärer*: Evaluating the Impact of Urban Green Spaces and Vegetation Characteristics on Land Surface Temperature Across Swiss Cities Using Machine Learning (2025).

195. *Paul Stewart:* Where is wild in Glasgow's Southside? A test of the applicability of relative wildness mapping to suburban Scotland (2025).

196. *Georgios Fylakis:* Spatiotemporal analysis of the integration between shared e-scooters and public transport: Case studies in Oslo and Stockholm (2025).

197. *Andreas Klasson*: Generating 3D building models according to Swedish building specification using footprints and airborne laser scanning (2025).

198. *Agaton Järemo Lawin*: The spread of Japanese knotweed in Scania: Invasion suitability prediction using species distribution modelling (2025).

199. *Jesse Stewart:* Contextualizing the Geographic Influence on Infantry Manoeuvrability in a Historical Battlefield Using GIS: A Case Study of the Canadian Corps in the Second Battle of Passchendaele, First World War (2025).

200. *Oskar Vejkdal Thorsberg*: Automatic geometry extraction in digital building permits: A case study using BIM and NS Building (2025).

201. *Spyridon Gerafentis*: Impact of the COVID-19 “Lockdown” on Air Quality in Athens (2025).

202. *Symeon Andriotis*: Political Violence in Athens, Greece (2008-2024): A Machine Learning Approach for Predictive Modelling of Spatial Risk Patterns (2025).

203. *Simon Westman*: Detecting Structurally Old Scots Pine: A Crown-Metric Approach Using National ALS and LIFT Enrichment (2026).

204. *Freja Randeris Kristoffersen*: Satellite-Derived Bathymetry of Danish Coastal Waters Using Machine Learning with Sentinel-2 and ICESat-2 data (2026).

205. *Markus Honkanen*: Securitas Per Scientiam: GIS-MCDA of Civil Defence Shelter Distribution Efficiency in the Helsinki Capital Region (2026).

206. *Amanda Carolina Santos Motta*: Visualization Tools for Simulation Results Based on 3D City Models: An Urban Planner-Focused Study (2026).

207. *Gintars Krumins*: Mapping forest felling activities in Latvia from Sentinel-2 satellite imagery using machine learning (2026).

208. *Jenny Berntsson*: Using Multi-criteria GIS analysis in nature conservation planning in Lilla Edet municipality (2026).

209. *Sebastian Daland*: Flood impacts on road accessibility and buildings in Gothenburg during a 100-year rainfall event (2026).

210. *Polyxeni Karapanagiotidou*: GIS-based Multi-Criteria Decision Analysis (MCDA) framework for Flood Risk Assessment in the Thermi Basin (2026).

211. *Nour Abdulmagid A. Bensaid*: Urban Expansion and its Relation to the Urban Heat Island Effect: A Case Study of Tripoli, Libya (2026).

212. *Iris Krohn*: Compound Extreme Events in Hamburg, Germany: A Flood Risk Assessment (2026).

213. *Johan Wahlberg*: Towards Data-Centric Geospatial Applications: A Knowledge Graph Approach to Road Maintenance in Stockholm, Sweden (2026).

214. *Athanasios Fyntanidis*: Towards Data-Centric Geospatial Applications: Machine Learning–Driven Assessment of Urban Heat Island Intensity in Athens: Integrating Remote Sensing, Landscape Metrics, and Green Infrastructure for Climate-Resilient Urban Planning (2026).

215. *J.C.W. van Diest*: Detecting Spatial Impacts of Violence through Remote Sensing: A Case Study of Conflict-Affected Regions in Central Mali (2026).

216. *Ingrid Martha Kintu*: Monitoring Landslide Disturbance and Forest Recovery in Afromontane Landscapes: The Case of Nyungwe Forest Reserve, Rwanda (2026).

217. *Reneé Clarencia Hägglund*: Environmental Determinants of Peatland Degradation in Central Kalimantan: A GIS-Based Remote Sensing Analysis (2026).